STUDIES OF PULSATING CARBON STARS

A Thesis
Submitted For The Degree Of
Doctor Of Philosophy In The Faculty Of Science
BANGALORE UNIVERSITY

By

A.V.RAVEENDRAN

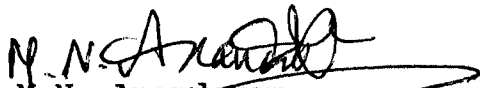INDIAN INSTITUTE OF ASTROPHYSICS
BANGALORE
INDIA

OCTOBER 1989

DECLARATION

I hereby declare that the matter contained in this thesis is the result of the investigations carried out by me in the Indian Institute of Astrophysics, Bangalore and The Department of Physics, Bangalore University, Bangalore, under the supervisions of Prof. N. Kameswara Rao and Dr. M.N. Anandaram. This work has not been submitted for the award of any degree, Diploma, associateship, fellowship, etc. of any University or Institute.

Raveendran

(A.V. Raveendran)

Candidate

N. Kameswara Rao

Supervisor

M.N. Anandaram

Supervisor

Bangalore - 34

23 Oct 1989

Acknowledgements

Summary

The present work was begun with the goal of understanding the formation and properties of circumstellar dust envelopes around carbon-rich objects, especially those belonging to the RV Tauri group of variables. A study of dust envelopes would provide valuable information not only on the mass loss from the objects but also on the nature of interstellar grains because of their probable origin in circumstellar envelopes. Both multiwavelength polarimetry and infrared photometry serve as the most useful observational tools for such an investigation.

The thesis essentially contains, (i) broadband multiwavelength (UBVRI) polarimetry of a sample of carbon-rich objects belonging to the different variability types — cepheids, RV Tauri stars and red variables - and its analysis, (ii) extensive two colour (BV) photometry of the RV Tauri star AR Pup, (iii) an interpretation of the InfraRed Astronomy Satellite data of RV Tauri stars, and (iv) a discussion of some theoretical aspects of polarization produced by circumstellar dust envelopes. It has been divided into six chapters and each into several sections and subsections.

In the first chapter brief descriptions of the observational characteristics of the different variability classes are given. Short accounts of the mechanisms which cause the instabilities and the mass loss observed in these objects are also presented. The instrumentation used for the observations, and the method of observations and data reduction are discussed in the second and third chapters, respectively.

The data, analysis and results are presented in the fourth chapter which has two parts; part A deals with the cepheids and RV Tauri stars, and part B with the red carbon stars. The list of programme stars for polarimetry contained 2 carbon cepheids (RU Cam and V553 Cen), 4 carbon RV Tauri stars (AR

Pup, RU Cen, SX Cen and AC Her) and 12 red carbon stars (VX And, UU Aur, T Cae, Y CVn, U Hya, Y Hya, R Lep, RY Mon, W Ori, Y Per, RT Pup and X Vel). Out of these objects, polarimetric observations have been reported in the literature only for RU Cam, AC Her, R Lep, Y CVn, Y Per, W Ori and Y Hya, and except for R Lep, multiwavelength observations have been reported for none of them. A considerable part of the available 102-cm telescope time was devoted to observe AR Pup since it was found to show exceptionally large and highly time dependent polarization. The amplitude of polarization in U band was found to be ~14.6%, the highest ever observed in any late-type star.

The IRAS Point Source Catalogue, which gives the fluxes at far Infrared wavelengths – 12, 25, 60 and 100μm – provides a good database for a systematic study of the composition and formation of circumstellar dust; an interpretation of the IRAS data on RV Tauri stars is presented in the fifth chapter. In the same chapter a discussion of the possible polarization mechanisms operating in the objects considered, and a few computational polarization models of circumstellar envelope using Mie theory under single scattering approximation are also presented.

Finally, in the last chapter the conclusions are summarized, and the further investigations needed to answer some of the related problems are discussed.

The equations, tables and figures are numbered sequentially in each chapter, and the corresponding chapter number is prefixed whenever a reference is made to them in any other chapter. The related publications and literature cited are listed at the end.

Contents

I. INTRODUCTION

1. Pulsating stars

Pulsating stars form a subset of a wider class of intrinsic variables, wherein the causes of the variability rest entirely within the stars themselves. Apart from the light variability, other observed properties such as spectral type or colour and radial velocity also vary. It has been well-established that the variables are not abnormal stars but represent merely normal stages of evolution which every star must pass through if started with similar initial characteristics; the investigation of these objects promises a deeper insight into the structure and evolution of stars than the study of their nonvariable counterparts.

Some of the observational properties of the best recognized and physically significant groups of pulsating stars, taken from Kukarkin et al. (1969), are given in Table 1 and their location in the Hertzsprung-Russell diagram, which is a plot of the intrinsic luminosity L (or absolute visual magnitude M_v) against the corresponding surface temperature (or spectral type), is shown in Figure 1. It is clear from the figure that the different types of variables occupy well-defined regions in the H-R diagram.

2. Carbon-rich objects among pulsating stars

The existence of carbon-rich objects, whose spectra display strong bands of C_2 and other molecules of carbon like CH and CN, was first noted by Angelo Secchi in 1868 and ever since has posed several astrophysical problems. Carbon variables do not form a homogeneous group; various physical groups covering a large range in temperature and luminosity - cepheids, RV

1

Observational characteristics of the pulsating variables.

Variable star type	Designation	Range of periods	Characteristic period	Population type	Range of spectral types	Absolute Magnitude
RR Lyrae	RR_{ab}, RR_c	0.05 - 1.2 d	0.5 d	II	A - F	0.0 to 0.5
Classical Cepheids	$C\delta$	1 - 70 d	5 - 10 d	I	F - K	-0.5 to -6
W Virginis stars	CW	1 - 70 d	12 - 20 d	II	F - G	0 to -3
RV Tauri stars	RV_a, RV_b	30 - 150 d	70 - 80 d	II	F - K	-3 to -5
Yellow semiregular variables	SR_d	30 - 150 d	70 - 80 d	II	F - K	0 to -3
Red semiregular variables	SR_a, SR_b, SR_c	30 - 1000 d	100 - 200 d	I and II	M, C, S	-1 to -3
Long period variables	M	80 - 1000 d	200 - 300 d	I and II	Me, Ce, Se	+1 to -2
β Cephei (β CMa) star	βC	0.1 - 0.6 d	0.2 d	I	B0 - B3	-3.5 to -4.5
Dwarf Cepheids and Delta Scuti stars	RR_s and δ Sct	0.04 - 0.2 d	0.1 d	I	A - F	+2 to +3

Table 1

2
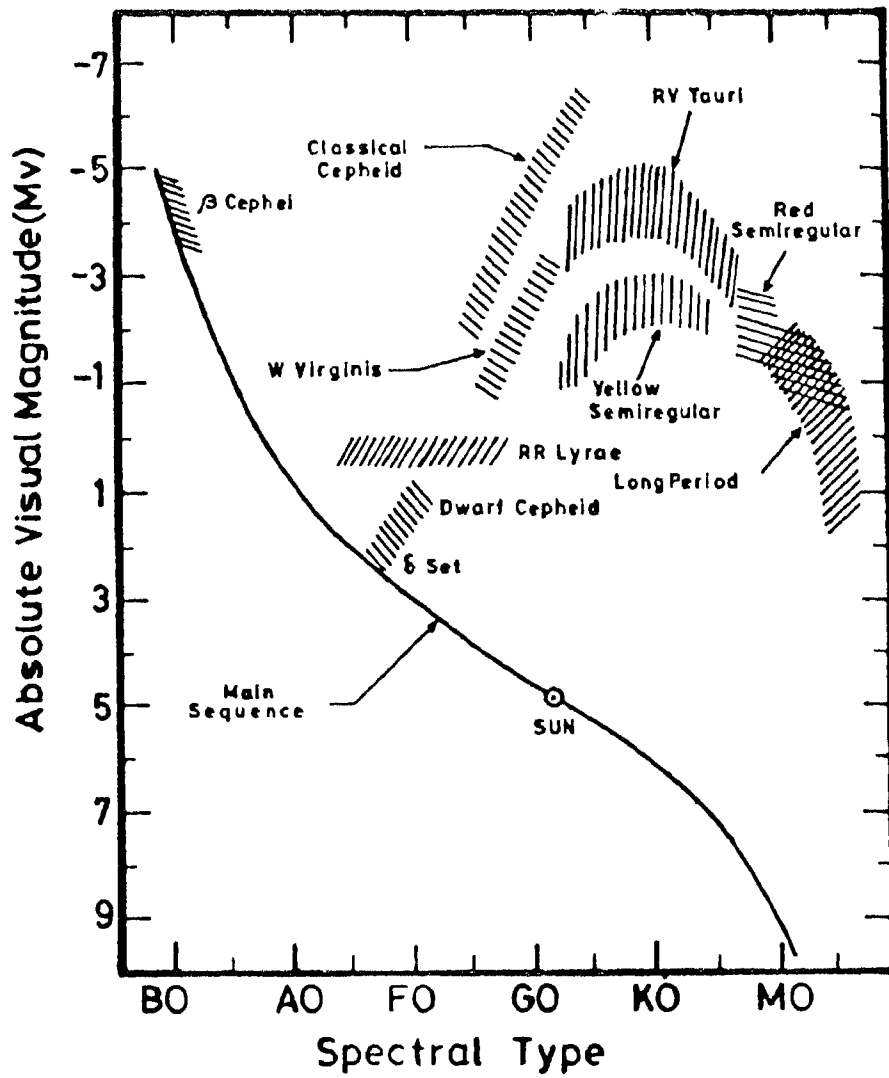
Locations of the various groups of pulsating stars in the H-R diagram.

Figure 1

Tauri stars and red variables - are found among them; these are briefly described below. Comprehensive presentations of the observational properties of the various groups of pulsating stars are given in Kukarkin (1975). In addition to the above three variability classes there is a group of peculiar carbon-rich and hydrogen deficient objects, known as R Coronae Borealis stars, which show pulsational characteristics superposed on the more dominant, large amplitude, irregular variations (Alexander et al. 1972; Raveendran, Ashoka & Kameswara Rao 1986).

2.1. Cepheids

Cepheids are easily distinguished from the rest of the intrinsic variables by their least irregularities in periods and shapes of light curves. Based on the nature of light curves, spectral characteristics and radial velocity variations, two different sub-classes are recognized.

(a) Classical cepheids (Cδ) : These comprise the most nearly homogeneous type of pulsating stars with strictly periodic light curves. They obey a definite period-luminosity relation discovered by Leavitt (Pickering 1912) and which subsequently became the most powerful tool in the determination of the distance scale of the universe. The period-luminosity relation of classical cepheids is probably even universal (Sandage & Tammann 1968). They are confined to the spiral arms of the galaxy and are often found in young open clusters. The radial velocity curves are continuous and mirror reflections of their light curves.

(b) W Virginis stars (CW) : These objects share the period and spectral range of the classical cepheids but are distinguished from the latter by their kinematics and galactic distribution. They are found in the spherical component of the galaxy and more frequently in globular clusters and do not follow the well-defined relationship between the shape of the light curve and the length of its period shown by their classical counterparts. W Virginis stars are considered to

4

belong to Population II which comprises old and metal-poor objects. The radial velocity curves are not continuous; the discontinuity occurs near the steep part of the ascending branch of the light curve. W Virginis variables also obey a period-luminosity relation, approximately parallel and about 1.5 mag below that of the classical cepheids.

The few carbon-rich objects, which are presently known among the W Virginis stars, show large irregularities in their light curves, both in the period and amplitude, and hence Lloyd Evans (1983) has suggested that there is a possible connection between the extreme irregularities and the occurrence of over-abundance of carbon.

2.2. RV Tauri stars

RV Tauri stars are rare yellow supergiants which constitute an interesting and little understood class of pulsators. The principal characteristics of the RV Tauri stars are (Payne-Gaposchkin, Brenton & Gaposchkin 1943) : (i) spectral types lie in the range F-K, (ii) light curves exhibit alternating deep and shallow minima which may interchange occasionally, and (iii) period between two consecutive deep minima lies in the range 30-150 days. The light curves are more of cyclic than of strictly periodic nature. The first spectroscopic survey of RV Tauri stars was made by Rosino (1951) who distinguished two groups of objects depending on the appearance of TiO bands and the behaviour of hydrogen lines. Later, Preston et al. (1963) identified three spectroscopic subgroups and designated them as group A, B and C. But for the appearance of TiO bands during deep minima, all group A objects have spectral features corresponding to types G or K, whereas those belonging to B and C show large discrepancies between spectral types based on Ca II lines and that based on hydrogen lines. Presence of strong CN bands between secondary and primary light maxima differentiate group B stars from group C. Objects of group A are metal-rich, and of C are weak-lined and metal-poor; group B objects are also metal-poor, but show carbon enhancements (Preston et al. 1963;

5

Lloyd Evans 1974; Dawson 1979; Baird 1981). Kukarkin et al. (1969) have subdivided RV Tauri stars into two classes, RVa and RVb, on the basis of their light curves; the former shows a constant mean brightness and the latter a cyclically varying mean brightness.

2.3. Red variables

The group of red variables of spectral classes M, C and S constitutes the most numerous type of variable star. Stars of spectral class M (oxygen-rich) display very intense bands of oxides of Ti, Sc and V, whereas the spectra of stars of class S are dominated by the bands of oxides of Zr, Y and Ba. Bands of carbon compounds (CN, C_2 and CH) predominate the spectra of C-type (carbon-rich) objects. Rarely, objects of intermediate spectra (CS and MS) are also observed.

Red variables have been divided into several subgroups – long period variables (Mira-type stars, denoted by M), semiregular variables (SRa, SRb and SRc) and irregular variables (L, Lb and Lc). Mira-type variables show emission lines of hydrogen balmer series, silicon and iron which appear during the rising part of the light curve and become very intense at the light maximum. The intensity of the emission lines decreases with decreasing brightness and disappear entirely at the light minimum. The light curves of red variables show appreciable changes both in the amplitude and period. But, in the case of Miras and to a certain extent in the case of SRa-type objects, a mean period can be defined. SRa variables share several common features with the Miras. Many of them exhibit bright emission lines and they differ from the long period variables only in their lower light amplitudes. There is a well-defined deficiency of stars with light amplitudes of 2-3 mag in the visual and photographic regions, indicating that the subdivision into types SRa (amplitudes < 2.5 mag) and M (amplitudes > 2.5 mag) is physically significant (Payne-Gaposchkin 1954).

Semiregular variables of SRb-type have light cycles of

different lengths and it is often impossible to predict the epochs of maximum and minimum. Irregular variables are characterized by slow luminosity variations with no signs of periodicity. In general, both SRb and L-type objects do not show any emission lines in their spectra. Ikaunieks (1975) has suggested that a part of an evolutionary sequence, constant-L-SR-M-SR-L-constant, probably exists.

3. Cause of variability

Pulsation as a cause for stellar variability was first established by Shapley (1914) to account for the observed characteristics of cepheids. From detailed calculations, now it is clear that the thermo-nuclear reactions near the centre make no important direct contribution to the driving of pulsation and that the main excitation mechanism is the envelope ionisation mechanism which modulates the flux flowing through the stellar envelope, as a consequence of pressure and temperature dependent opacities (Cox 1974). In the case of cepheids, the pulsation is attributed to the presence of He II ionisation zone in the atmosphere at a critical depth, sufficiently shallow that the pulsation energy is large enough to move the material between the ionisation zone and the surface appreciably. The presence of He I ionisation, H I ionisation and H_2 molecular dissociation zones in the outer envelopes at critical depths are considered to be the important physical mechanisms causing the observed instability in RV Tauri stars and red variables (Strohmeier 1972). The present understanding of the basic cause and nature of stellar pulsation is in fairly satisfactory state and the gaps that exist in our understanding of the this subject are mainly due to the complexity of the phenomena involved (Cox 1974).

4. A brief sketch of stellar evolution

In what follows the most important stages in the evolution of a star are outlined (initial mass in the range 1-8 M$\odot$);

7

needless to mention, the details depend on both its initial mass and chemical composition. Comprehensive reviews of results of several evolutionary model calculations are presented by Iben (1967, 1974) and Iben & Renzini (1983).

Major changes that occur in the interior of a star during the course of its evolution are always accompanied by changes in the two physical parameters, luminosity and effective temperature, which are derived observationally with comparatively less difficulty. The evolutionary sequence of a star can be conveniently described in terms of its position in the conventional H-R diagram or its equivalent, colour-magnitude diagram; its main branches are schematically shown in Figure 2.

When the first nuclear reactions - hydrogen burning into helium - commence in the core, the gravitational contraction halts and the star settles itself as a main sequence object, its position along the sequence being determined largely by its mass. Since hydrogen is the most abundant fuel, the star stays as a main sequence object for a considerable part of its life. The first ascent along the red giant branch occurs when a critical fraction (in the range, 10-13% of the initial mass) of hydrogen is exhausted in the core. The site of nuclear energy production then shifts to a thick hydrogen shell surrounding the core. Meanwhile, the core, whose mass increases as a result of further hydrogen burning in the shell, contracts and heats up. The ascent along the red giant branch is terminated when helium is ignited in the stellar core and the star descends to the horizontal branch; the exact location depends on the total mass of the star and its initial chemical composition. The star in this stage of evolution has core-helium and shell-hydrogen burning as the sources of nuclear energy production.

When helium is exhausted in the core (by burning into carbon and oxygen) helium burning is established in a thick shell and hydrogen continues to burn in an overlying thin shell. The inert carbon-oxygen core, whose mass steadily

8
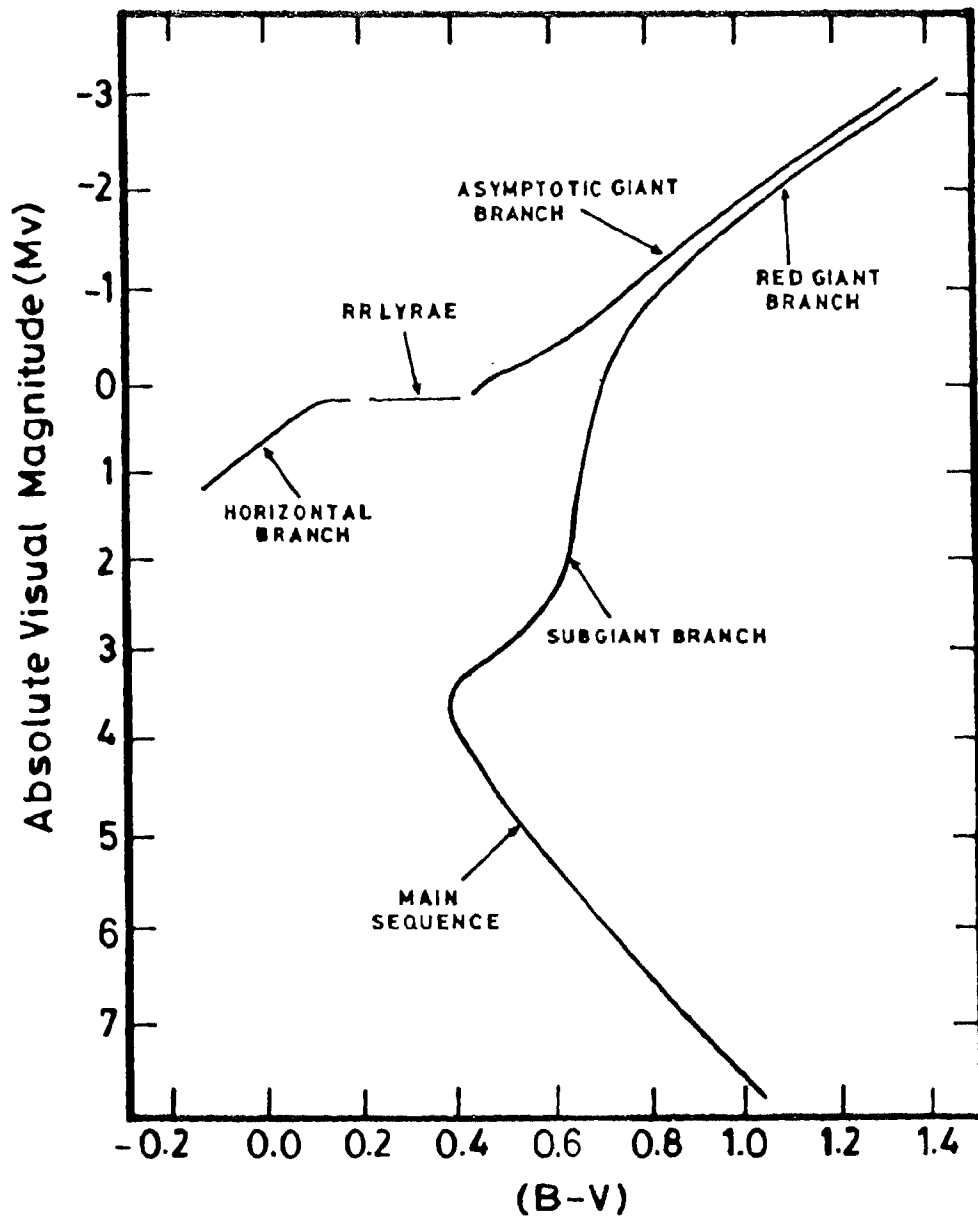
Locations of the various branches in the colour-magnitude diagram.

Figure 2

9

increases, continues to contract. Outwardly, the star evolves upward in the H-R diagram along the asymptotic giant branch; several types of instability occur while burning hydrogen in one shell and helium in another. During carbon-burning and all subsequent nuclear-burning (which occur in high mass objects) phases the evolution is so fast that the possibility of finding a real star passing through such phases is remote (Iben 1977). Hence, most of the available evolutionary model calculations concentrate on the periods of hydrogen- and helium-burning.

As the star moves along the asymptotic giant branch, the envelope mass above the hydrogen-burning shell decreases both as a consequence of burning at the base and mass loss at the surface, and the star may eventually eject a major part of its hydrogen envelope marking the termination of the asymptotic giant phase and the remnant evolves towards its final white dwarf status.

More massive objects have a quite different evolutionary history; they approach the red giant branch only at very advanced stages of nuclear evolution in their cores.

5. Evolutionary status of the objects under study

From Figure 1, it is seen that RV Tauri objects along with the W Virginis stars and red variables form a near-continuous sequence, normally referred to as the 'Great sequence' (Payne-Gaposchkin & Gaposchkin 1938). As one goes from the left to the right end of the sequence, the period of pulsation increases from about a day to more than two years; the absolute luminosity peaks around the positions of RV Tauri stars. Rosino (1951, 1980) has suggested that RV Tauri stars are the natural continuation to longer periods of the W Virginis objects and that probably a single period-luminosity relation exists for the group comprising W Virginis stars, RV Tauri variables and the yellow semiregular variables in globular clusters. Low masses (< 1 M⊙) are indicated for RV

10

Tauri stars if one tries to resolve the discrepancy between the absolute magnitudes given by the period-luminosity relation and the spectroscopic luminosity class, in favour of the former which is more accurate (Barnes & DuPuy 1975). All RV Tauri stars are presumably going through the same stage of evolution and the photospheric enhancement of carbon in some objects may be due to their slightly different masses (Baird 1981) (or slightly different mixing efficiencies ?).

Evolutionary model calculations identify the short period, less luminous, Population II cepheids as stars with small envelope masses (~ 0.02 $M_{\odot}$) undergoing blueward excursions from the asymptotic giant branch due to readjustments between the hydrogen and helium-burning shell luminosities following the exhaustion of helium core and the more luminous Population II cepheids as those undergoing blueward loops from the asymptotic giant branch in response to helium shell flashes or finally evolving to the blue as a result of hydrogen-burning shell nearing the surface (Gingold 1974); if the horizontal branch mass is relatively large, when the objects undergo their final movement from the tip of the asymptotic giant branch, they will be at relatively high luminosities and spend a considerable amount of time at positions occupied by RV Tauri stars in the H-R diagram (Gingold 1974, 1976).

Making use of the data on the members of the metal-poor globular cluster ω Cen and Kapteyn's star group to establish the positions of RV Tauri stars, Eggen (1986) has concluded that these are low mass objects undergoing post-asymptotic giant branch evolution. Recently, Jura (1986) has arrived at a similar conclusion; from an analysis of the IRAS data and the number density of RV Tauri objects in the solar neighbourhood, he has suggested that they have just evolved from the phases of rapid mass loss and are in transition from asymptotic giant branch to white dwarfs.

In the literature the term carbon stars normally refers to the carbon-rich red giants and supergiants, and the carbon-rich cepheids and RV Tauri stars are referred to as

peculiar or special carbon stars since their photospheres show evidences of oxygen (Bidelman 1956; Wallerstein 1973); the same terminologies are followed throughout here. The substantial range in the absolute magnitudes, the spread in population types and the observed low number density of red carbon stars indicate that many stars evolve through the carbon star phase for a short fraction of their life time as red giants (Wallerstein 1973; Alksne & Ikaunieks 1981). Surface abundance anomalies correlate well with the nuclear properties and predicted products of nuclear reactions in stellar interiors and according to the present theoretical understanding carbon stars are asymptotic giant branch objects in double shell burning phase (Iben & Renzini 1983; Lambert 1988).

The anomalies in the observed surface abundance are interpreted as due to the dredging up of material that has experienced nuclear processing in stellar interior. During thermal pulses that occur in asymptotic giant branch stars, as a result of instabilities in the helium and hydrogen burning shells, the principal product of incomplete helium burning in the convective shell is ^{12}C (Iben & Renzini 1983). In more massive stars (with core mass > 0.75 M$\odot$) the mixing occurs when the base of the convective hydrogen-rich envelope extends inward; but the problem of mixing in low mass objects with core mass $\leq$ 0.6 M$\odot$ is still not clearly understood (Iben 1987). According to Schwarzschild & Harm (1967), the convective helium burning shell can reach the hydrogen-rich envelope after several relaxation cycles that occur during the helium shell flashes, thus mixing the hot carbon-rich interior with the hydrogen. This may be the mechanism which produces over-abundance of carbon in Type II cepheids (and possibly in RV Tauri stars also) (Lloyd Evans, Wisse & Wisse 1972).

In the frame work of the dredge up theory, every star has to pass through an S-type phase (C/O $\approx$ 1) before becoming a carbon star (C/O > 1) from an initial M-type star (C/O < 1) and the time scale involved is ~ 10^5 years (Iben 1987).

12

Willems & de Jong (1986) have reported the identification of 9.8 and 18μm silicate features, typical of objects with oxygen-rich environments, in the spectra of 9 out of a sample of 304 carbon stars for which low resolution spectra were obtained by the InfraRed Astronomy Satellite. Recently, they (Willems & de Jong 1988) have interpreted this in terms of a very low transition time of ~ 10 years from the oxygen-rich to carbon-rich phase and have suggested that the theory of asymptotic giant branch evolution needs revision. Further, they have remarked that such a small time-scale would imply an envelope mass much smaller than usually considered in theoretical model calculations. It is possible that the apparent paradox is due to the binary nature of these rare objects (Little-Marenin 1986; Bidelman 1988, private communication).

6. Motivation for the study

RV Tauri stars are known to possess infrared radiation far in excess of their black-body continuum, presumably, due to the re-radiation of the absorbed stellar light by the dust grains present in their extended circumstellar envelopes (Gehrz & Woolf 1970; Gehrz 1972; Gehrz & Ney 1972).

Observations show a considerable individuality in the nature of infrared spectra in the 2-22μm interval. Gehrz (1972) and Gehrz & Ney (1972) have suggested that metallic silicates are a major constituent of dust around oxygen-rich RV Tauri stars while an unidentified material has condensed around the carbon-rich object AC Her. However, Lloyd Evans (1974) has found that some of the objects (AR Pup, SX Cen and IW Car) which Gehrz (1972) and Gehrz & Ney (1972) considered to be oxygen-rich on the basis of their infrared energy distribution are actually carbon-rich, and hence suggested that the AC Her-type spectrum also possibly contains the silicate emission superposed on a continuum produced at lower dust temperatures than in the oxygen-rich cases.

13

Although W Virginis objects show a number of similarities to RV Tauri stars at optical wavelengths, in general they have no infrared excess (Gehrz & Woolf 1970; Gehrz & Hackwell 1974).

The existence of cool circumstellar material around many late-type giant stars has also been established as a result of extensive observations (Gillett, Merrill & Stein 1971; Neugebauer, Becklin & Hyland 1971; Woolf 1973). The strong 9.8 and 18μm emissions characteristic of silicate grains appear in M-type objects, whereas, apart from a resonance feature of silicon carbide (SiC) near 11μm, the infrared spectra of carbon stars are generally featureless and are presumed to be due to graphite grains. The dust grains comprise a relatively small fraction of the total mass of the circumstellar envelope; the major gaseous component is seen in the emission lines of a number of molecules. A review of the properties of circumstellar envelopes around late-type giants is given by Zuckerman (1980).

The late-type giants (spectral types M, S and C) occupy that part of the H-R diagram where the evolutionary model calculations lose track of the future course because of significant mass loss which substantially influence the ultimate fate of stars. The magnitude of mass loss cannot be calculated at present theoretically from first principles and can only be ascertained by an analysis of observational features.

Gilman (1972) has shown that under conditions relevant to circumstellar envelopes, the dust grains are adequately momentum coupled to the surrounding co-existing gas, and hence the radiation pressure acting on the grains can drive mass loss. The other mechanism usually being suggested for the observed mass loss is the ejection of material by atmospheric shocks associated with either pulsational or dynamical instability. Jones, Ney & Stein (1981) have presented arguments to show that the above two mechanisms are probably

14

mutually coupled in pulsating stars which under favourable conditions enhance the mass loss. The correlation between the infrared excess and the period, found by Degioia-Eastwood et al. (1981) for a sample of Mira variables, indicates a possible connection between the pulsation and mass loss which has since been substantiated by further studies (Jura 1986a; Willson 1987).

In any case it is certain that the circumstellar grains are involved directly in mass loss in late-type stars, underlining the importance of the study of the dust envelopes surrounding these objects. Mass loss from the evolved stars is a major source of freshly made elements replenishing the interstellar medium. Further, circumstellar envelopes are the potential sites for the production of the interstellar grains.

Information on the physical mechanism responsible for mass loss can be derived from a study of the radial and azimuthal distribution of material in the circumstellar envelope. If mass loss is via steady dust-driven stellar wind, one would expect the shape of the envelope to be spherical with a uniform density distribution that varies as the inverse square of the radial distance. Non-radial pulsations or rotation of the star may lead to non-spherical dust envelopes and a nonuniform density profile may result from mass ejection by either periodic atmospheric shocks or in episodic violent events.

The present work was undertaken with the goal of understanding the formation and properties of dust envelopes around carbon-rich objects, especially those belonging to the RV Tauri group of variables. The main observational tools for the study of dust envelopes are multiband infrared photometry and polarimetry – the first provides information on the absorption and emission characteristics and the second on their scattering properties. It is true that the problem of deriving physical parameters is essentially an inverse problem. However, detailed modeling of the observations may lead to important clues on the nature of dust grains.

7. Observational material

Many late-type variables exhibit intrinsic linear polarization which often varies quasi-periodically (Dyck 1968; Kruszewski, Gehrels & Serkowski 1968; Dyck & Jennings 1971; Dyck & Sanford 1971; Serkowski 1971; Shawl 1975). Dyck et al. (1971) have reported that the intrinsic polarization in the visual region of a wide variety of cool objects are related to their corresponding infrared excess at 11μm and they have suggested that polarization and infrared excess are related through the scattering and absorption optical depths of a circumstellar cloud of solid particles; however, from an extended series of infrared observations of objects with large variation in polarization, Forrest, Gillett & Stein (1975) have concluded that the relationship is not that direct.

Photospheric effects can also give rise to polarization (Harrington 1969; Coyne & McLean 1979). But, in a majority of cases, the observed continuum polarization is consistent with the scattering of stellar radiation by dust grains (Kruszewski, Gehrels & Serkowski 1968; Dyck & Sanford 1971; Shawl 1975; Landstreet & Angel 1977).

In general, RV Tauri and carbon stars have received comparatively less attention polarimetrically. Multiwavelength observations are important in determining the specific mechanism which produces the polarization; it would provide important information not only on the nature and sizes of the grains responsible but also on their distribution in the envelope, if dust scattering is the main mechanism operative.

A study of the variation of polarization and its wavelength dependence would throw light on the process of formation and evolution of circumstellar dust clouds. To know of any correlation between the changes that occur in polarization and other observed properties, especially light, would be of immense help in interpreting the polarimetric data meaningfully. Hence, a list of carbon-rich pulsating stars

16

belonging to different variability types was drawn up for multiwavelength polarimetric observations and near-simultaneous photometry.

The InfraRed Astronomy Satellite (IRAS) Point Source Catalogue, which gives the fluxes at far infrared wavelengths - 12, 25, 60 and 100μm -, and the catalogue of Low Resolution Spectra between 7 and 23μm have since been published (Beichman et al. 1985; Olnon & Raimond 1986); they provide a good database for a systematic study of the composition and formation of circumstellar dust.

II. INSTRUMENTATION

1. Photometer

A schematic layout of the photoelectric photometer, a conventional single channel instrument, used for the observations is given in Figure 1. The wide angle eyepiece has a field of about 45 arcmin. A 60 arcsec diaphragm was used throughout for the observations. The following filters were used: B (1mm BG12 + 2mm GG13) and V (corning 3384). The essential purpose of the Fabry lens is to reduce the problems associated with the nonuniform sensitivity across the surface of the photocathode by spreading the starlight over an appreciable area (Cox & Sinnott 1977). An uncooled RCA 1P21 photomultiplier kept at 900 V was used for the entire observations. The output from the photomultiplier was amplified to a convenient level by the d.c. amplifier described below and then registered using a Brown recorder made by Minneapolis-Honeywell.

2. D.C. amplifier

In astronomical photometry the most commonly used detector is the photomultiplier tube because of its capability to respond to extremely weak light signals without adding appreciable noise. For each photon detected at the photocathode of the tube an electron is released, which is then multiplied by the secondary emissions from a series of dynodes before being collected at the anode. Though the gain thus achieved in a photomultiplier is very large (typically, ~ 10^6), because of low flux of photons the output current would be extremely small. Hence, it is necessary to amplify the output from the photomultiplier by external circuitry before it can be measured easily and reliably.
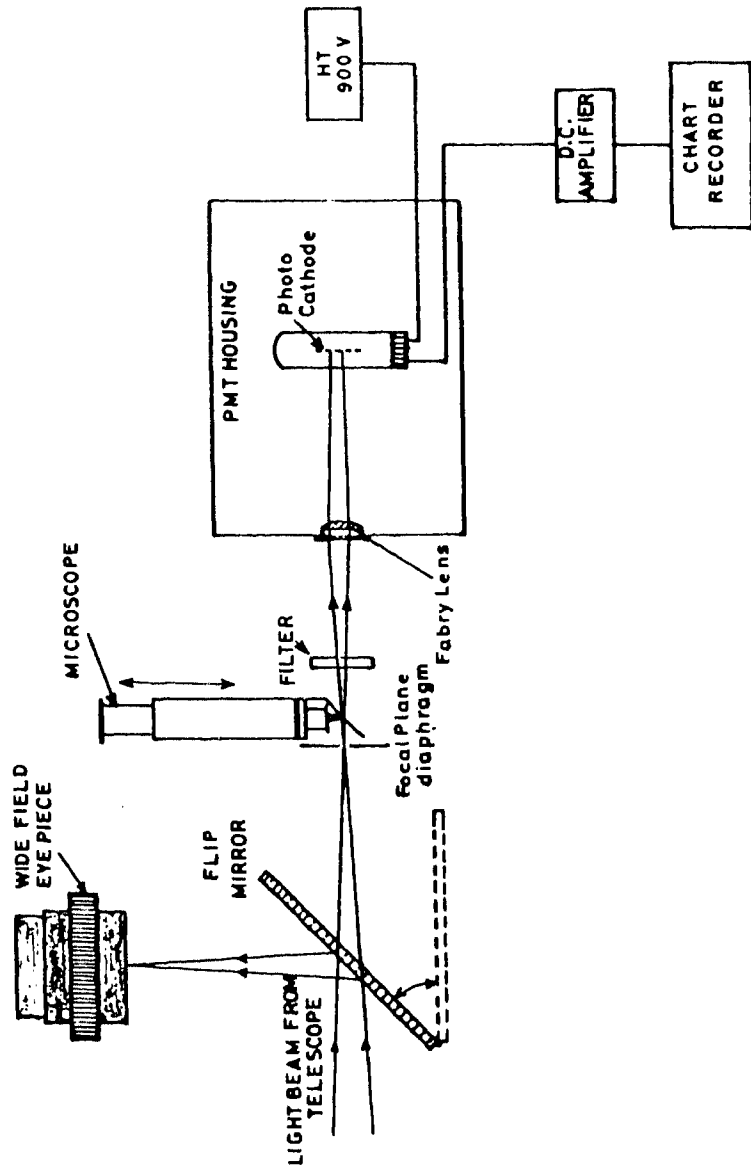
A schematic layout of the photoelectric photometer

Figure 1

19

There are two modes of measuring photomultiplier output produced by the photons from celestial sources. At very high time resolutions (< 1m sec), the anode current can be resolved into individual bursts which can produce sharp voltage pulses across a suitable load resistor. In the pulse counting mode, these pulses are amplified, shaped and then discriminated against low level noise pulses before being counted finally. In the alternative conventional d.c. method, the average anode current is directly amplified to a conveniently measurable value (1 mA) and then registered using a strip chart recorder. In this mode of operation, the most important electronic unit is a current amplifier. The photomultiplier output is linear over a wide range of input light flux (cf. Stebbins, Whitford & Johnson 1950). Hence, to match the performance of photomultipliers, it is imperative that the amplifier used in astronomical photometry is also highly linear with a good gain stability over a wide range of input signals; this has to be achieved against unfavourable conditions normally existing on the open observing floor with a large variation in temperature and humidity that occur during the course of a night as well as during different seasons.

The basic requirements of a good current amplifier used for photoelectric photometry are (Oliver 1975): (i) a very stable gain, (ii) a short warm up time, (iii) a low output drift after warm up, (iv) a low noise, (v) a wide range of gain settings, (vi) a stable calibration, (vii) a variety of output time constants, and (viii) insensitivity to misuse.

While working at the telescope it is convenient to have half magnitude gain steps. The commercially available amplifiers seldom meet all the requirements needed for accurate astronomical photometry, and hence a current amplifier has been built using available modern electronic components.

2.1. Circuit description

The design has been primarily based on that given by Oliver

20

(1975) because of its simplicity, employment of a few discrete components, high reliability and ease of maintenance. The important circuit elements of the d.c. amplifier are schematically represented in Figure 2. It has two stages, a basic amplifier stage, and a buffer and time constant stage. The key component of the basic amplifier stage is a varactor bridge op amp (Analog Devices Model 310J) which has a low bias current ($\sim 10^{-14}$ A) and a very high input impedance ($\sim 10^{14}$ Ω), making it ideal for measurement of low current signals. The negative feed back through the resistor Rf ensures that the input terminal is at virtual ground, and hence the anode of the photomultiplier is always at the ground potential. This is essential for a linear tube response because any variation in the anode potential may cause nonlinearity (Young 1974). Coarse gain steps are achieved by selecting different values of the feed back resistor Rf. The second stage (built around an Analog Devices Model 118K op amp) has a unit voltage gain, and the fine gain adjustments are made by selecting the input to this stage through the output voltage divider of the basic amplifier unit. Different time constants of integration are obtained by selecting the capacitor Ct connected in the feed back loop of the buffer stage.

Three additional features, which make the amplifier unit more flexible in use, have been included in the circuit given by Oliver (1975). Some of the commercially available strip chart recorders, like the one used at the 34-cm telescope do not have facilities for the adjustment of zero level externally. If the photomultiplier is refrigerated or the observations are made at low amplitude gains (for bright objects), the sky deflections will be very small, almost at the lower limit of the recorder pen movement, especially during the dark moon periods. It is always desirable to keep the zero point of measurement slightly above the lower limit for a better reading accuracy. Changes were incorporated in the circuit so that the zero reference on the recorder chart can be adjusted at will. A voltage divider was introduced at
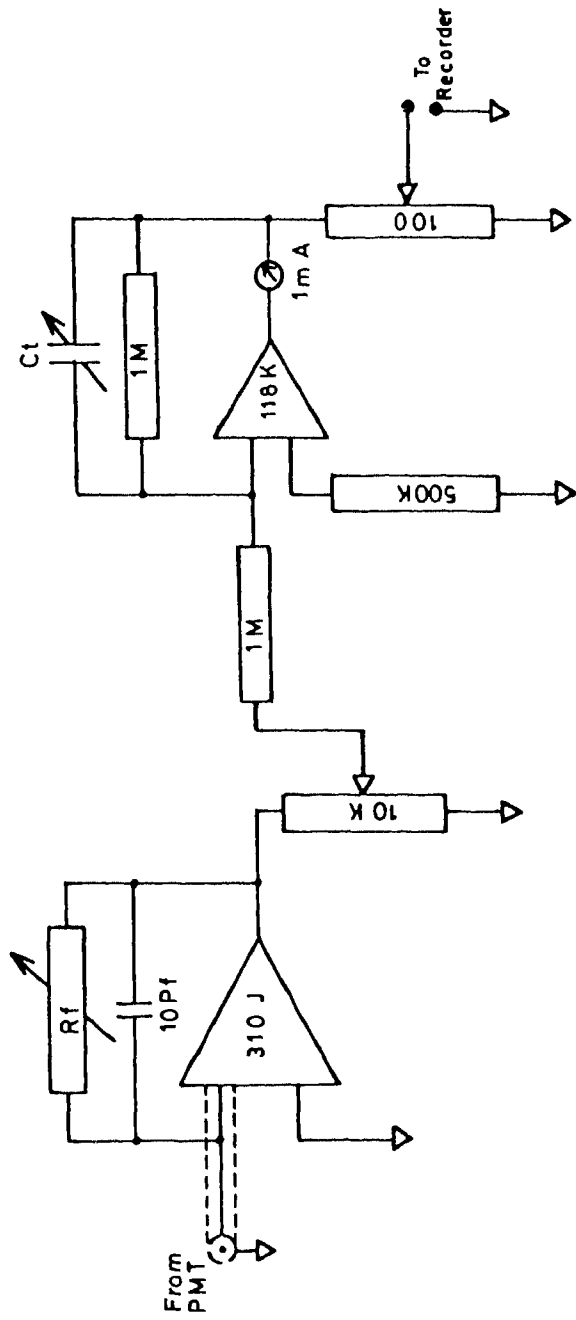
A schematic representation of the d.c. amplifier.

Figure 2

22

the output end of the amplifier so that a range of output voltages are available. Further, a provision was made to change the polarity of the current passing through the meter to make the unit a more general purpose electrometer.

For a long-term gain stability, it is very essential that the resistors used in the circuit have very low temperature coefficients. All the resistors up to the value of 1 MΩ, used in the circuit, are of metal-film with temperature coefficients of 25 ppm and are accurate to 0.05%. The high megohm carbon resistors with tolerance values of 1% are in glass encapsulation for longer stable life. Attention to insulation is extremely important while working with low current signals ($\sim 10^{-10}$ A). It is highly essential that the contacts of the selector switches are proper and absolutely clean for the repeatability of the gain calibration. Hence, in the construction of the amplifier ceramic selector switches with silver coated contacts were used to achieve the above requirements. When the amplifier is used with the zero adjustments, because of the passive nature of the related circuit, the variations in power supply may cause significant drift problems and so it is imperative to have a well-regulated power supply. The modular power supply (Analog Devices Model 904E) used has line and load regulations of 0.02% each, and a temperature coefficient of 0.015%.

2.2. Performance

The amplifier was installed at the 34-cm reflector of Vainu Bappu Observatory in 1987 January and since then extensively used for photoelectric photometry; its performance is discussed below.

2.2.1. GAIN CALIBRATION

Regular calibration of the gain steps is very important in the d.c. technique since the accuracy of photometry depends partly on the accurate calibration of the gain ratios of the various steps; it is done with the help of the built-in current source.

23

Calibration of the half-magnitude steps are done first. The feed-back resistor Rf corresponding to the first coarse gain step of the amplifier is a metal-film resistor (100 KΩ, 0.05%). While calibrating fine gain steps, coarse gain is set to this step because the stable and precise resistor establishes the calibration stability of the half-magnitude steps. Fine gain is then set to step 2 and the current source is adjusted to give a near full scale deflection ($\sim$ 95%) on the recorder chart. After tracing for about 30 sec, the fine gain is reduced by one step (i.e., to step 1) and again tracing is done. The zero-point reading is obtained each time by grounding the amplifier input by using the mode selection switch. The ratio of the two readings gives the gain ratio. Normally, this is expressed in the magnitude form

$$\Delta m = -2.5 \log (d_1/d_2),$$

where d_1 and d_2 are the two corresponding deflections on the recorder chart. The procedure is repeated for every fine gain step.

The coarse gain step calibration is done with respect to the already known fine gain steps. To start with, the coarse and fine gain steps are set to 1 and 11, respectively; the corresponding amplifier gain setting is denoted by 1(11). The current source is then adjusted to give a near full scale deflection. The fine gain setting is next reduced to 6 and coarse gain is increased to 2, and the tracing is again obtained. The zero-point reading is taken as mentioned before. The ratio of the two readings, adjusted to the known change in the half-magnitude gain setting from 11 to 6, gives the gain difference between the coarse steps 2 and 1. The procedure is then repeated by comparing pairs of readings corresponding to the amplifier gain settings 1(11),2(6); 2(6),3(1); 2(11),3(6); etc.

Table 1 contains the magnitude differences between the fine gain steps, available in the amplifier, obtained on several occasions during 1987-88 period and Table 2 the results of

24

Fine gain magnitude difference.

		Gain steps								
Date	2-1	3-2	4-3	5-4	6-5	7-6	8-7	9-8	10-9	11-10
1987 Feb 26	0.499	0.499	0.499	0.499	0.498	0.499	0.500	0.500	0.499	0.504
1987 Mar 21	0.495	0.496	0.495	0.495	0.495	0.497	0.495	0.495	0.496	0.498
1988 Jan 16	0.494	0.494	0.494	0.495	0.496	0.496	0.495	0.495	0.496	0.502
1988 Feb 12	0.499	0.499	0.499	0.498	0.498	0.500	0.499	0.498	0.499	0.504
1988 Mar 9	0.499	0.501	0.499	0.499	0.500	0.499	0.498	0.496	0.500	0.504

Table 1

25

Coarse gain calibration. The number outside the bracket indicates the coarse gain step and that inside the fine gain step.

Date	Magnitude difference					
	1(6)-2(1)	1(11)-2(6)	2(6)-3(1)	2(11)-3(6)	3(6)-4(1)	3(11)-4(6)
1987 Feb 26	-	+0.002	-0.002	-	+0.006	+0.006
1987 Mar 28	-	+0.008	-0.007	+0.000	+0.002	+0.006
1988 Jan 16	+0.002	+0.003	-0.006	-0.005	+0.003	+0.006
1988 Feb 12	-	+0.004	-0.008	-0.006	-0.003	+0.008
1988 Mar 9	+0.001	+0.003	-0.007	-0.004	+0.003	+0.006

Table 2

26

coarse gain calibration. Due to an uncertainty Δd in the readout from the chart, the expected error in the magnitude calibration is given by

$$\Delta m = 1.086 \ \Delta d \ (d_1^{-2} + d_2^{-2})^{1/2},$$

where d_1 and d_2 are the deflections corresponding to the steps being compared. In the fine gain calibration, $d_1 \sim 95\%$ and $d_2 \sim 60\%$, whereas in the coarse gain calibration both d_1 and d_2 are $\sim 95\%$. With $\Delta d \sim 0.2\%$, the expected uncertainties in the two cases are 0.004 mag and 0.003 mag, respectively. It is to be noted that the values given in Tables 1 and 2 are well within the expected uncertainties, indicating an excellent repeatability of the gain differences. Further, the fine gain magnitude differences are within the errors of exactly 0.500 mag, consistent with the very low tolerance values of the metal-film resistors used.

2.2.2. LINEARITY

On 19 February 1987 night fifteen stars in Pleiades cluster – which lie in the 2.87–12.02 mag interval – were observed with the 34-cm telescope for the purpose of checking the linearity of the amplifier. The advantages of using a cluster for such a study come from the following: (i) the uncertainty in the atmospheric extinction coefficient will have negligible effect on the results obtained, and (ii) a cluster will contain stars with a wide range in magnitudes. The limit on the brighter side was set by the brightest star in the cluster (η Tauri, V = 2.87 mag). The detector was an uncooled RCA 1P21 tube operated at 900 V and the dark current was $\sim$ 3 nA. A 12.0 mag star was giving an output current of 0.5 nA, about a sixth of the ambient dark current. Stars fainter than 12.02 mag could not be observed because the dark current fluctuation was introducing significant error in the measurement. The results of observations are plotted in Figure 3, and it is quite evident that in the magnitude interval considered (2.87–12.02 mag) the amplifier has an excellent linear response (slope = 0.998 ± 0.002)
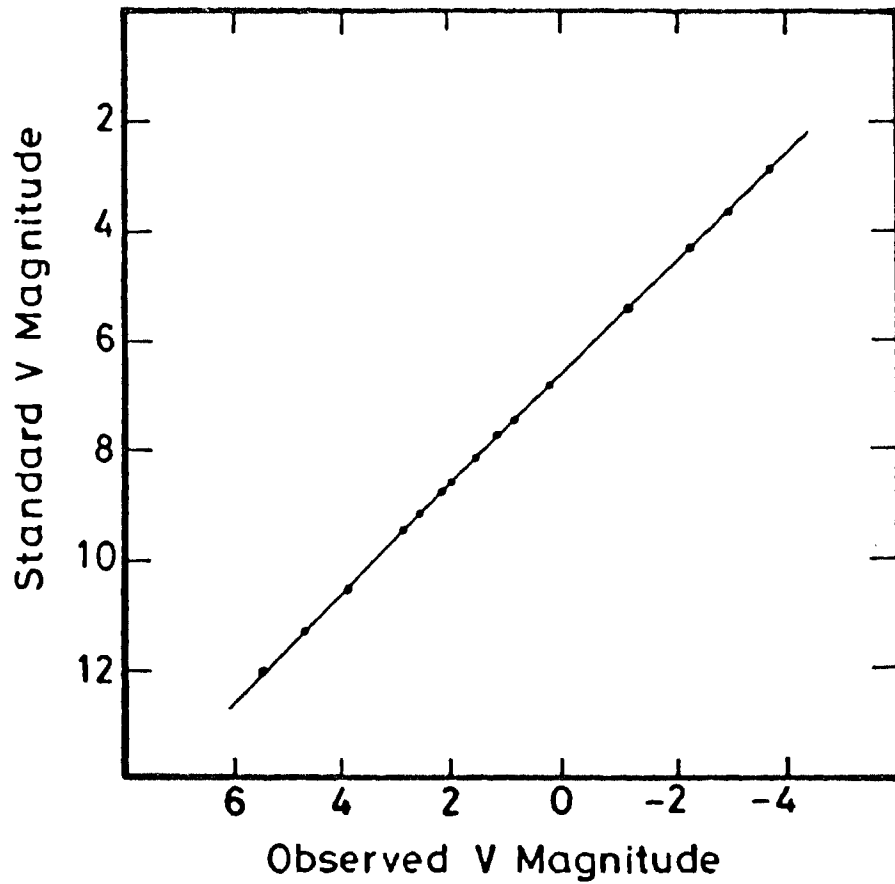
Plot of standard V magnitudes of Pleiades stars against the corresponding atmospheric extinction-corrected observed magnitudes. Corrections for the differences in the (B-V) colours of the stars have also been applied from the known system transformation coefficients.

Figure 3

For variable star photometry it is desirable to have the brightness of comparison stars very similar to that of the variable. But, in practice it will not be always possible to choose such comparison stars. Hence, to get a near full scale deflection on the recorder chart, it becomes a necessity to change the amplifier gain. If the amplifier sensitivity affects the comparison and variable stars differently, the advantage of the differential star photometry is lost.

HD 66559 and HD 65723 were observed as comparison and check stars of the RV Tauri star AR Puppis during 1986-87 (16 nights) and 1987-88 (14 nights) observing seasons (section IVA-1.1.) The V magnitudes of these stars differ by ~ 1.5, and hence a change in the amplifier gain was necessary while observing them. Figure 4 shows the plot of the differences in V of HD 65723 and HD 66559 obtained against the corresponding Julian days of observation. The mean differential magnitudes, -1.366±0.002 and -1.359±0.003, obtained during the two seasons are well within the observational uncertainties, indicating an excellent repeatability of differential measurements.

3. Polarimeter

3.1. Stokes parameters

The most convenient way to describe the state of polarization of a beam of light, particularly in scattering problems, is to use the four Stokes parameters defined as

$$I = \ <E_{0x}^2> + <E_{0y}^2>$$

$$Q = \ <E_{0x}^2> - <E_{0y}^2>$$

$$U = \ <2\ E_{0x}\ E_{0y}\ \cos\delta>$$

$$V = \ <2\ E_{0x}\ E_{0y}\ \sin\delta>,$$

where E_{0x} and E_{0y} are amplitudes of the components of electric vector E_0 in two orthogonal planes xz and yz, and δ is the
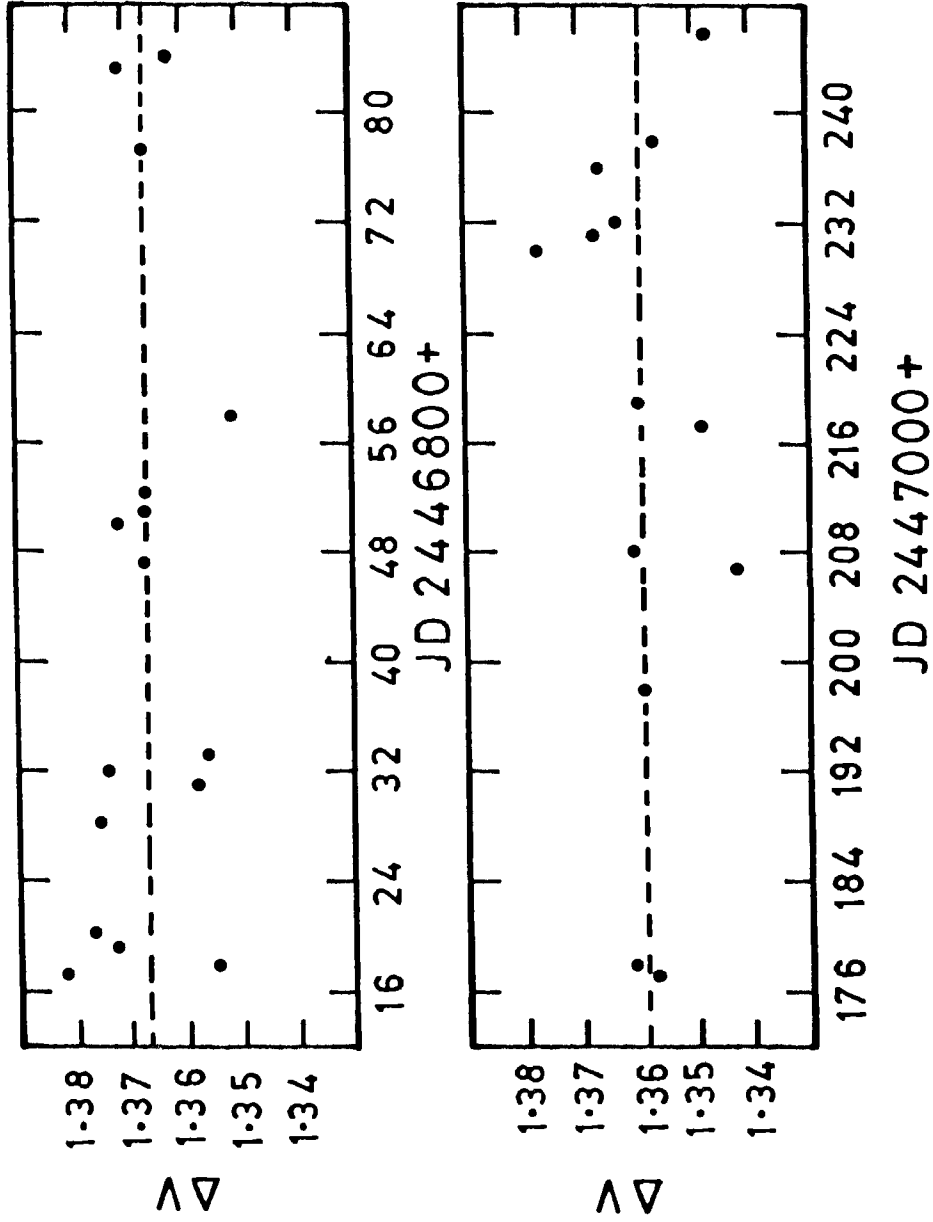
Plot of the differential magnitudes of HD 65723 with respect to HD 66559 against the corresponding Julian days of observation.

Figure 4

30

phase difference between the x- and y- vibrations. If E_0 makes an angle θ (usually, called the position angle of polarization) with the x-axis, then

$$E_{0x} = E_0 \cos\theta$$

$$E_{0y} = E_0 \sin\theta.$$

The Stokes parameters can be re-written as

$$I = <E_{0x}^2 + E_{0y}^2> = <E_0^2>$$

$$Q = I <\cos2\theta>$$

$$U = I <\sin2\theta \cos\delta>$$

$$V = I <\sin2\theta \sin\delta>.$$

The most general form of polarization is partially elliptical polarization. If χ is the angle between the major axis of the ellipse traced by the end point of electric vector and the x-axis of the coordinate system, then

$$\tan2\chi = \tan2\theta \cos\delta \qquad \qquad ....(1)$$

and the square of the ratio (r) of minor and major axes is given by (Gerrard & Burch 1975)

$$r^2 = \{1-(1-\sin^2 2\theta \sin^2\delta)^{1/2}\} \, / \, \{1+(1-\sin^2 2\theta \sin^2\delta)^{1/2}\}.$$
$$\qquad\qquad\qquad\qquad\qquad\qquad\qquad ....(2)$$

Denoting r by $\tan\beta$ and making use of relations (1) and (2)

$$I = E_0^2$$

$$Q = I <\cos2\chi \cos2\beta>$$

$$U = I <\sin2\chi \cos2\beta> \qquad\qquad ....(3)$$

$$V = I <\sin2\beta>.$$

It is fairly obvious from equations (3) that for any beam of light, according to the chosen reference axes the parameters Q and U take on particular values, whereas the other two remain

independent. In other words, the three quantities I, (Q^2+U^2), and V are invariant under rotation of the reference axes. For a celestial object, the equatorial coordinate system provides a convenient system of reference axes, with the x-axis in the direction of north, y- in the direction of east and z- in the direction of line of sight. The direction of vibration of the electric vector (position angle θ) is measured eastward from the direction of north, and the degree of polarization is given by

$$P = (Q^2 + U^2 + V^2)^{1/2} / I.$$

The Stokes parameters can be written in terms of the degree of linear polarization p, position angle θ and the degree of circular polarization q as

I (intensity)

$Q = Ip \cos2\theta$

$U = Ip \sin2\theta$

$V = Iq,$

with $p = (Q^2+U^2)^{1/2}/I$ and $q = V/I$. For partially plane polarized light, $V = 0$.

3.2. The PRL-instrument

Linear polarization measurements of the programme stars were made using the PRL-polarimeter (Deshpande et al. 1985). A schematic layout of the instrument is shown in Figure 5. In astronomical polarimetry the main sources of error are of atmospheric origin, the scintillation and seeing. Atmospheric scintillation is the amplitude modulation of starlight as a result of lateral displacement of rays caused by turbulent strata, very high in the atmosphere. A Wollaston prism is used as the analyser, and so the two beams with mutually perpendicular planes of polarization can be measured simultaneously. Because air is not birefringent, the scintillation noise pattern is same for all planes of

32
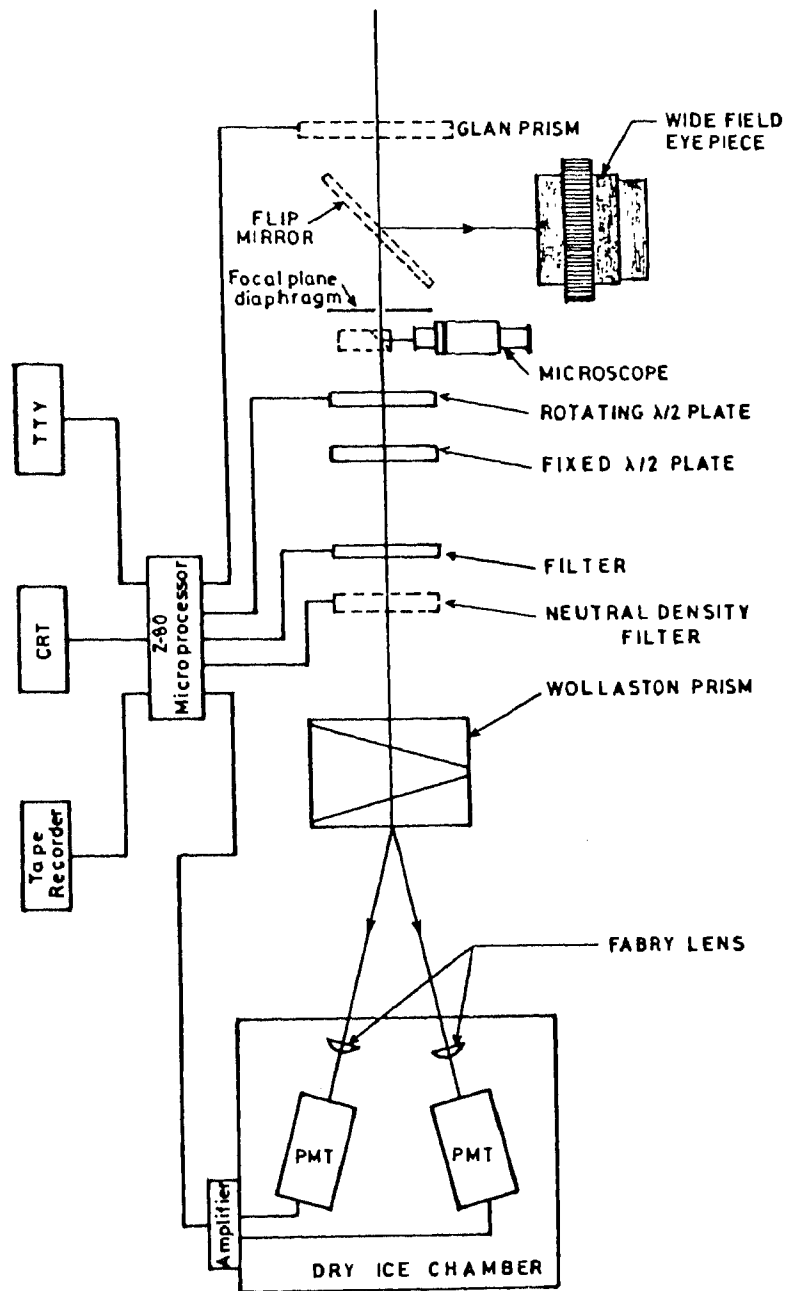
A schematic layout of the PRL-polarimeter

Figure 5

polarization, and hence by taking ratio of the two beams it can be essentially eliminated. This procedure also helps to reduce the errors caused by any variation in atmospheric transparency (Hiltner 1962). The simultaneous measurements of the two beams further ensures that the incident radiation is fully utilized, thereby reducing the observation time required to build up the desired signal to noise ratio.

Sensitivity across the surfaces of photocathodes is nonuniform. Hence, the measurements are impaired by atmospheric seeing, which is the smearing and wandering of telescopic images caused by refractive deflection of starlight as it passes through turbulent lower atmospheric strata. Another factor which has a similar harmful effect on polarimetric accuracy is the imperfections in telescope guiding. To a certain extent, the errors caused by these two sources can be minimized by the use of Fabry lenses in front of detectors (Cox & Sinnott 1977). Young (see Serkowski 1974) has shown that the errors of atmospheric origin can be diminished by a sinusoidal modulation of the light with a frequency that is larger than a critical value which depends on the telescope aperture. For a 100-cm telescope, the critical frequency is ~ 10 Hz. The PRL-polarimeter works on rapid modulation of the signal, and it is achieved by the rotation of a superachromatic half-wave plate. The main disadvantage of using such a plate, made by cementing three achromatic plates of quartz and magnesium flouride (Pancharatnam 1955), is the wavelength dependence of position angle of its effective optical axis. This would render difficulties in the accurate determination of position angle of polarization, because when wide spectral bands are used corrections that depend on the spectral energy distribution of the observed object must be applied to the measured position angle. Such an inconvenience is avoided by introducing another stationary identical Pancharatnam plate between the rotating plate and analyser (Frecker & Serkowski 1976). The intensity (I') of the transmitted light by two half-wave plates followed

by the analyser depends only on the Stokes parameters I, Q and U of the incident light and the angle (ψ) between the effective optical axes of the two half-wave plates, and is given by (Serkowski 1974)

$$I' = 1/2 \ (\ I \pm Q \ \cos4\psi \pm U \ \sin4\psi \ ).$$

The upper signs represent the case with the principal plane of analyser at position angle $0°$ and the lower signs that at $90°$. The rotation frequency of the first half-wave plate is 10.41 Hz, and because of the 4ψ factor the actual modulation frequency is four times this. The Glan-Taylor prism, which can be inserted in the beam of light, is for the purpose of checking the instrument for 100% polarization. The acquisition and on-line processing of the data are done using a microcomputer built around a Z-80 microprocessor.

The detector used during the 1984-85 season was a dry ice cooled RCA 31034A photomultiplier and that used during the 1985-86 and 1986-87 seasons was a thermoelectrically cooled EMI 9864B tube. The following filter combinations (Landolt 1983) were used: U (corning 9863 + liquid $CuSO_4$), B (2mm GG385 + 2mm BG 18 + 2mm BG12), V (2mm GG495 + 2mm BG18), R (2mm KG3 + 2mm OG570) and I (3mm RG715 + 1mm RG780). The effective wavelengths of the above filter combinations are approximately at 0.36, 0.44, 0.55, 0.70 and 0.90μm.

By flipping the plane mirror to a $45°$ position in the telescope beam, the star field can be identified by using the wide angle eye-piece provided. Different sizes of focal plane diaphragms are available, and a 16 arcsec diaphragm was used throughout for observations. The centring of the star is checked by pushing the right-angled prism in the telescope beam to reflect the light into the high power microscope.

III. OBSERVATIONS AND DATA REDUCTION

1. BV photometry

Observations were made with the 34-cm reflector of Vainu
Bappu Observatory, Kavalur. A typical sequence of observations
of a star was the following: star plus sky in filter V, sky in
V, star plus sky in B and sky in B. During the observations,
if the photometric quality of the sky was found to be
inferior, the sequence was repeated in the reverse order for
standard stars. The sequence, comparison-variable-check star,
was repeated at least four times during each night of
observation, essentially, to bring down the errors caused by
variations in sky transparency and poor telescope tracking. On
a few nights, the check star was not observed, and hence the
truncated sequence, comparison-variable, was followed.

Each time à star deflection was taken, the amplifier gain
was adjusted to get a deflection of more than 60% on the chart
recorder, and it was traced for more than a minute (speed ~
3/4-inch/min). The amplifier gain steps and the corresponding
mean time of observation were noted down on the chart itself.

1.1. System magnitude and colour

The combination of the telescope, filter and light detector
defines its own set of magnitude and colours, normally
referred to as the observer's system quantities. The
deflections (d) read from the chart were first corrected for
the corresponding sky background and then converted to system
magnitude using

$$m = -2.5 \log d.$$

All the values thus obtained were then brought to the same
arbitrary amplifier gain step, coarse gain=3 and fine gain=6.

The calibration of the amplifier gain steps adopted for the reduction of the data is given in Table 1. From the system magnitudes v and b (through filters V and B), the system colour (b-v) was calculated for each object observed.

1.2. Extinction correction

From the mean time of observation through V and B filters, the airmass X through which the object was observed, was obtained using the expression (Hardie 1962)

$$X = secz-0.0018167(secz-1)-0.002875(secz-1)^2 -0.0008083(secz-1)^3.$$

secz was calculated from the known hour angle (h), declination (δ) of the object and the latitude of the place $(\phi=12°34'32''$, for Kavalur) using

$$secz = (sin\phi \ sin\delta + cos\phi \ cos\delta \ cosh)^{-1}.$$

The magnitude (v_0) and $(b-v)_0$ corrected for the atmospheric extinction can be obtained from

$$v_0 = v-\{ k_v + k_v'(b-v) \} X \qquad ....(1)$$

$$(b-v)_0=(b-v) - \{ k_{bv}+ k_{bv}'(b-v) \}X, \qquad ....(2)$$

where k_v and k_v' are the first and second order magnitude extinction coefficients, and k_{bv} and k_{bv}' are the corresponding quantities for the (b-v) colour. The second order coefficient in yellow band (V) is negligible (Hardie 1962), and hence equation (1) reduces to

$$v_0= v - k_v X. \qquad ....(3)$$

The slope of the line obtained by plotting the observed v magnitude against the corresponding airmass gives the extinction coefficient k_v.

In the upper panel of Figure 1 the v magnitudes obtained on a few nights during the 1986-87 season are plotted against the corresponding airmasses. The slopes (k_v) of the lines derived using least square technique are indicated inside the

37

Adopted amplifier calibration.

| | Gain steps | Magnitude difference | |
		1986-87	1987-88
a)	Fine gain		
	11 - 10	0.502	0.503
	10 - 9	0.499	0.498
	9 - 8	0.499	0.496
	8 - 7	0.499	0.497
	7 - 6	0.498	0.498
	6 - 5	0.498	0.498
	5 - 4	0.499	0.497
	4 - 3	0.499	0.497
	3 - 2	0.499	0.498
	2 - 1	0.499	0.497
b)	Coarse gain		
	4 - 3	2.492	2.486
	3 - 2	2.497	2.496
	2 - 1	2.494	2.487

Table 1
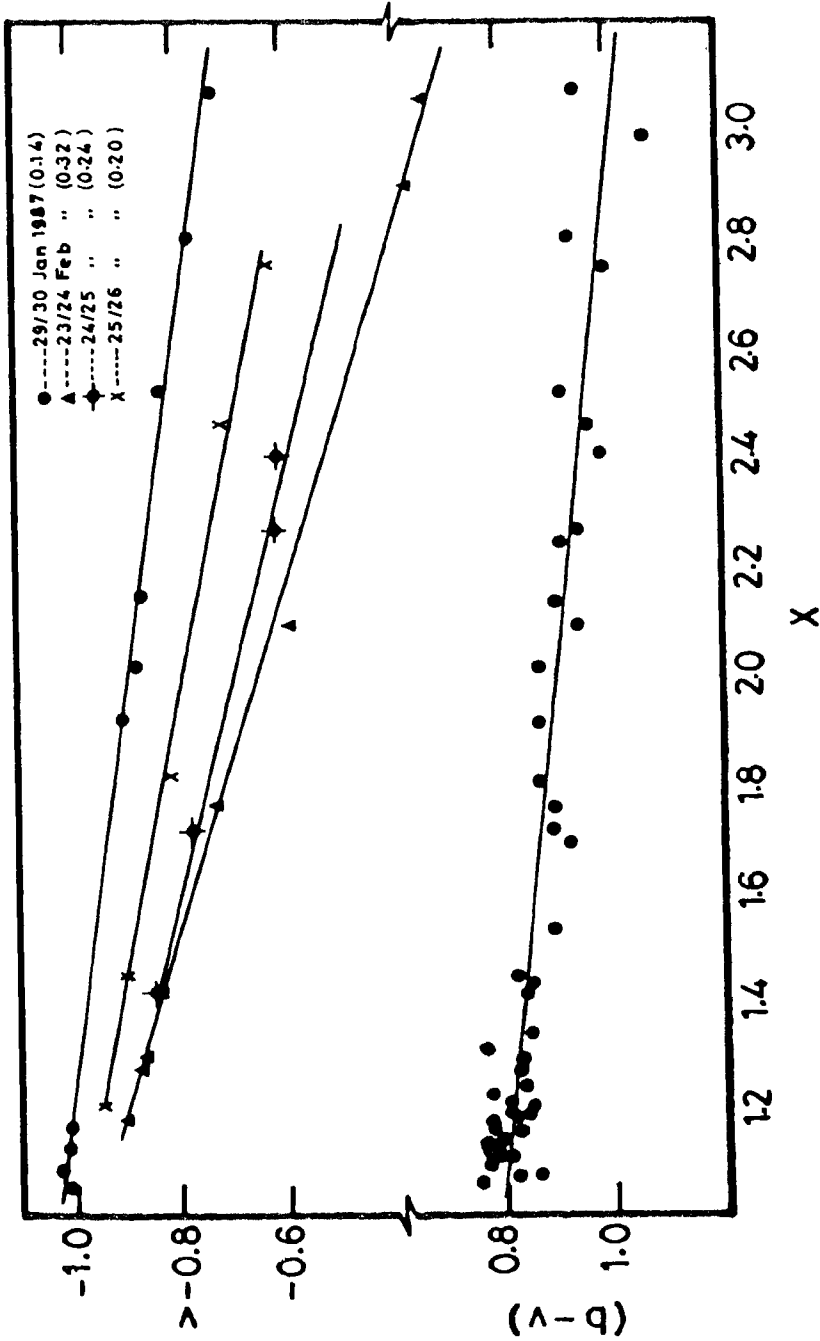
Figure 1

Observations of 62 Ari (G5III). The upper panel contains the plots of v magnitudes against the corresponding airmasses. The values of k_v derived are indicated inside the brackets against the dates of observation.

brackets. Clearly, k_v varies from night to night, and the observed values at Kavalur usually lie in the range 0.14-0.34. On many nights, on which the programme stars were observed, it was not possible to determine the extinction coefficients due to several reasons, the presence of intermittent clouds being one of them. Hence, for consistency mean extinction coefficients were used for the data reduction.

In variable star photometry, all the measurements are made differentially with respect to a close-by comparison at a nearly identical airmass. In terms of the differences, equation (3) can be written as

$$\Delta v_0 = \Delta v - k \; \Delta X. \qquad \qquad \ldots . (4)$$

The mean differences in the airmasses of the variable and comparison at the times of observation normally do not exceed 0.02; for example, in the case of AR Pup (section IVA-1.1.) it never exceeded 0.01. A maximum uncertainty of ~ 0.1 in k_v will effect the magnitude difference by less than 0.002 mag which is negligible compared to other sources of errors. Hence, the use of an average value for k_v in place of the particular night's extinction coefficient would not introduce any significant error in the results of differential photometry.

According to equation (4), k_v can be obtained by observing the difference in magnitudes of two nonvariable stars through a range of differential airmasses. This procedure can be advantageously used to determine a mean extinction coefficient representing an entire observing season by combining several nights' data, because it essentially removes the effects due to any variation in the zero-point of magnitude that arises from the changes in several parameters, like, H.T. voltages, reflectivity of the telescope optics, transmittance of the various optical components in the photometer, etc. Similarly, if there are two or more observations of a standard star on any single night, data obtained on several nights can be combined to derive a mean value of k_v. In this case equation (3) reduces to

$$k_v \Delta X = \Delta v.$$

Figure 2 shows a plot of the differential v magnitudes of 10 Tau (V=4.28, F8V) with respect to 62 Ari (V=5.54, G5III), obtained on several nights during 1986-87 observing season, against the corresponding differences in airmasses, and Figure 3, a similar plot of the differences in v magnitudes of 10 Tau obtained during 1987-88 season; least square fits to the data yielded k_v=0.23±0.01 and k_v=0.22±0.01, respectively.

The values of k_v assumed for the reduction of the data obtained during 1986-87 and 1987-88 seasons are given in Table 2.

In differential photometry, equation (2) becomes

$$\Delta(b-v)_0 = \Delta(b-v) - k_{bv}\Delta X - k_{bv}'\Delta(b-v)\Delta X.$$

The second order term k_{bv}' has a value in the range -0.02 to -0.04 (Hardie 1962). Usually, the chosen comparison star will have a colour very similar to that of the variable. This, together with $\Delta X < 0.02$ (as explained before), makes the contribution by the second order term negligibly small. So, the second order term has been completely neglected in the data reduction, and the following equation was used

$$\Delta(b-v)_0 = \Delta(b-v) - k_{bv}\Delta X. \qquad \dots\dots(5)$$

Unlike the magnitude extinction coefficient, the colour extinction coefficient does not vary significantly from night to night (see Oke 1965). Hence, as in the case of differential magnitudes, use of mean k_{bv} will not introduce any appreciable error in the differential colour.

The (b-v) values of 62 Ari obtained during the 1986-87 season and that of 10 Tau obtained during 1987-88 season are plotted in Figures 1 (bottom panel) and 4, against the corresponding airmasses; the respective slopes (k_{bv}) are 0.11±0.01 and 0.13±0.01. A few other objects were also observed for the determination of k_{bv}, and the values adopted
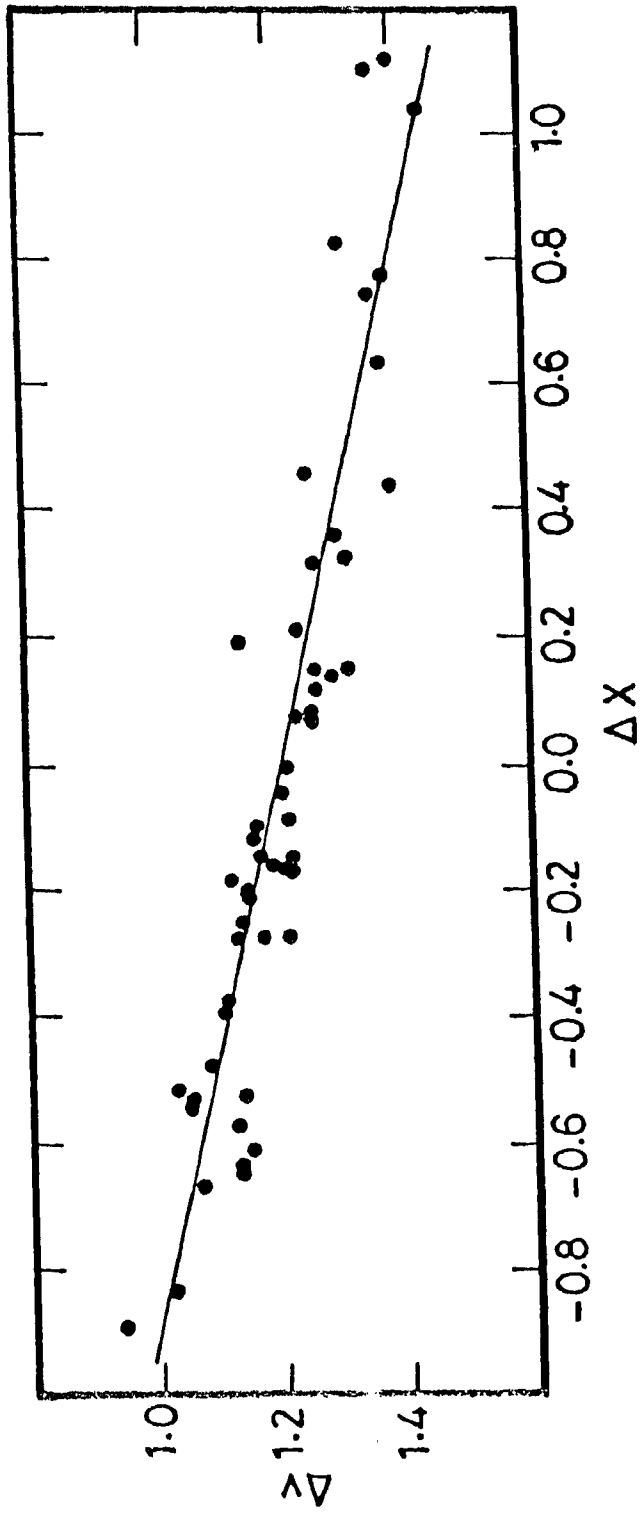
Plot of the differential magnitudes of 62 Ari with respect to 10 Tau obtained during 1986-87 season against the corresponding differential airmasses.

Figure 2

42
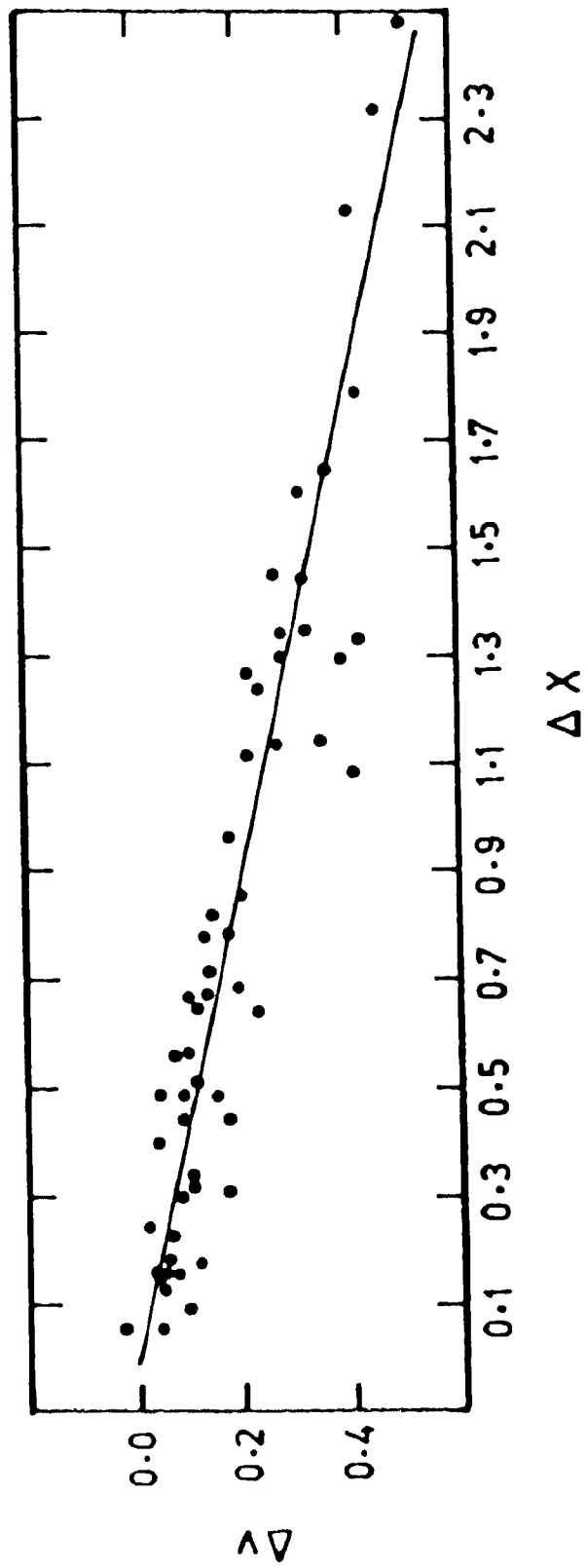
Plot of the difference in magnitudes against the corresponding difference in air-masses of 10 Tau obtained during 1987-88 season.

Figure 3

Extinction and system coefficients.

Quantity	Season	
	1986-87	1987-88
k_v	0.23	0.22
k_{bv}	0.15	0.12
μ	0.987 ± 0.006	1.037 ± 0.005
ζ_{bv}	0.490 ± 0.002	0.282 ± 0.003
ϵ	0.021 ± 0.003	0.042 ± 0.004

Table 2
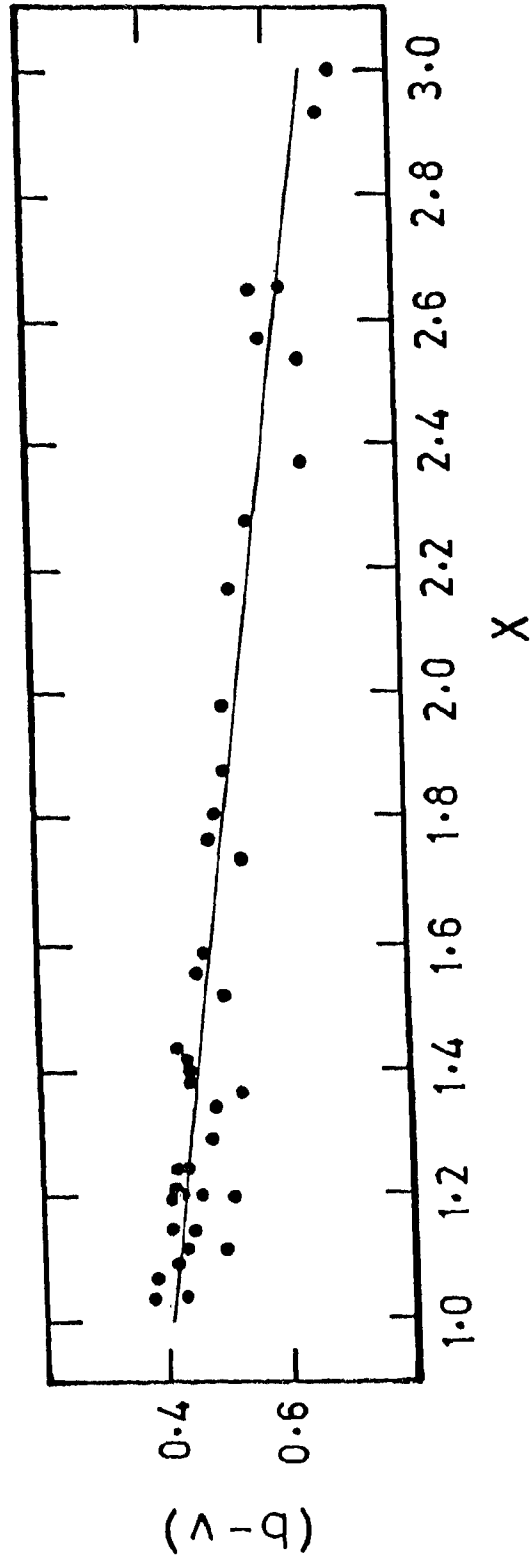
Plot of (b-v)colours of 10 Tau against the corresponding air-
masses obtained during 1987-88 season.

Figure 4

are given in Table 2. With a maximum possible uncertainty of ~ 0.05 in k_{bv}, the error in the differential colour is only 0.0005 mag.

1.3. System calibration

The system magnitude and colour obtained were next transformed to the standard UBV system (Johnson 1963), which was achieved by observing a number of stars with well-defined standard UBV values and deriving the system transformation coefficients using the following relations (Hardie 1962):

$$(B-V) = \mu(b-v)_0 + \zeta_{bv} \qquad \ldots\ldots(6)$$

$$V = v_0 + \varepsilon(B-V) + \zeta_v \qquad \ldots\ldots(7)$$

The transformation coefficients μ, ζ_{bv} and ε do not vary significantly during a particular observing season, whereas the magnitude zero-point term ζ_v might change appreciably from night to night. An accurate knowledge of the extinction coefficient is essential for an adequate determination of ζ_v. Mean values of μ and ζ_{bv}, representing an entire season, can be obtained by combining standard stars' data obtained on several nights spread over the whole observing season. But ε will have to be determined using a particular night's data, and then a suitable average value can be derived by consolidating the values obtained on several nights during the observing season.

During both 1986-87 and 1987-88 seasons several stars in Praesepe cluster were observed on six good photometric nights each. The stars were selected from the list given by Henden and Kaitchuck (1982). In Figures 5 and 6, the standard (B-V) values of the objects observed are plotted against their corresponding system $(b-v)_0$ values. The values of μ and ζ_{bv} obtained using least square technique are given in Table 2.

The individual night's observations are plotted in Figures 7 and 8 with $(V-v_0)$ along the y-axis and the corresponding (B-V) values along the x-axis. The slope (ε) of the line in each case, derived again using least square technique, is
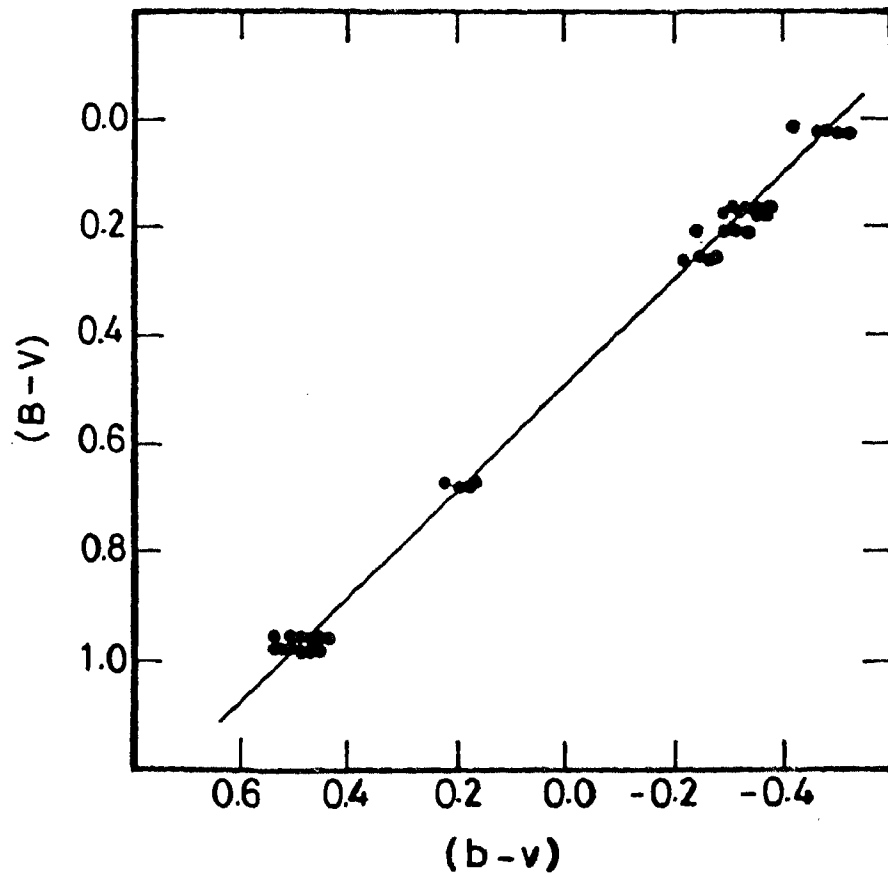
46

Determination of μ and $\mathcal{S}_{bv}$. Plot of (B-V) values against the corresponding extinction corrected (b-V) colours of Praesepe stars obtained on six nights during 1986-87 season.

Figure 5
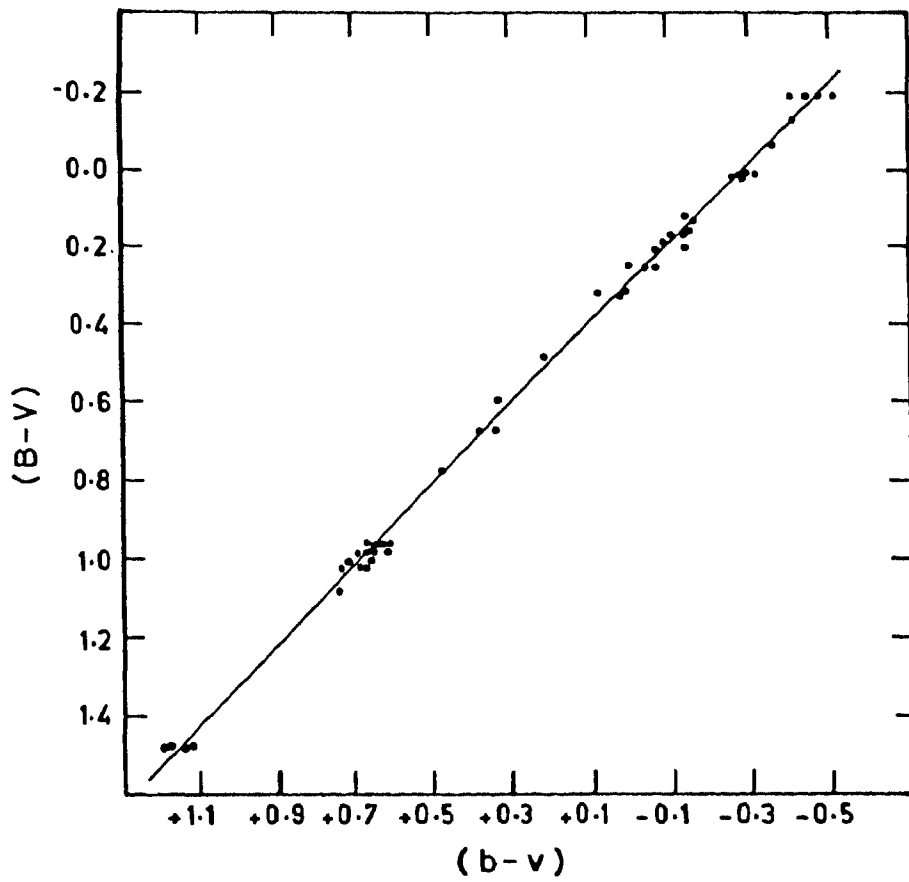
Determination of μ and $\mathfrak{S}_{bv}$. Plot of (B-V) values against the corresponding extinction corrected (b-v) colours of several standard stars observed during 1987-88 season.

Figure 6

Determination of ε plots of (V-v) values of Praesepe stars obtained during 1986-87 season against the corresponding (B-V) colours. The values inside the brackets give slopes (ε) derived using least square technique.

Figure 7

49
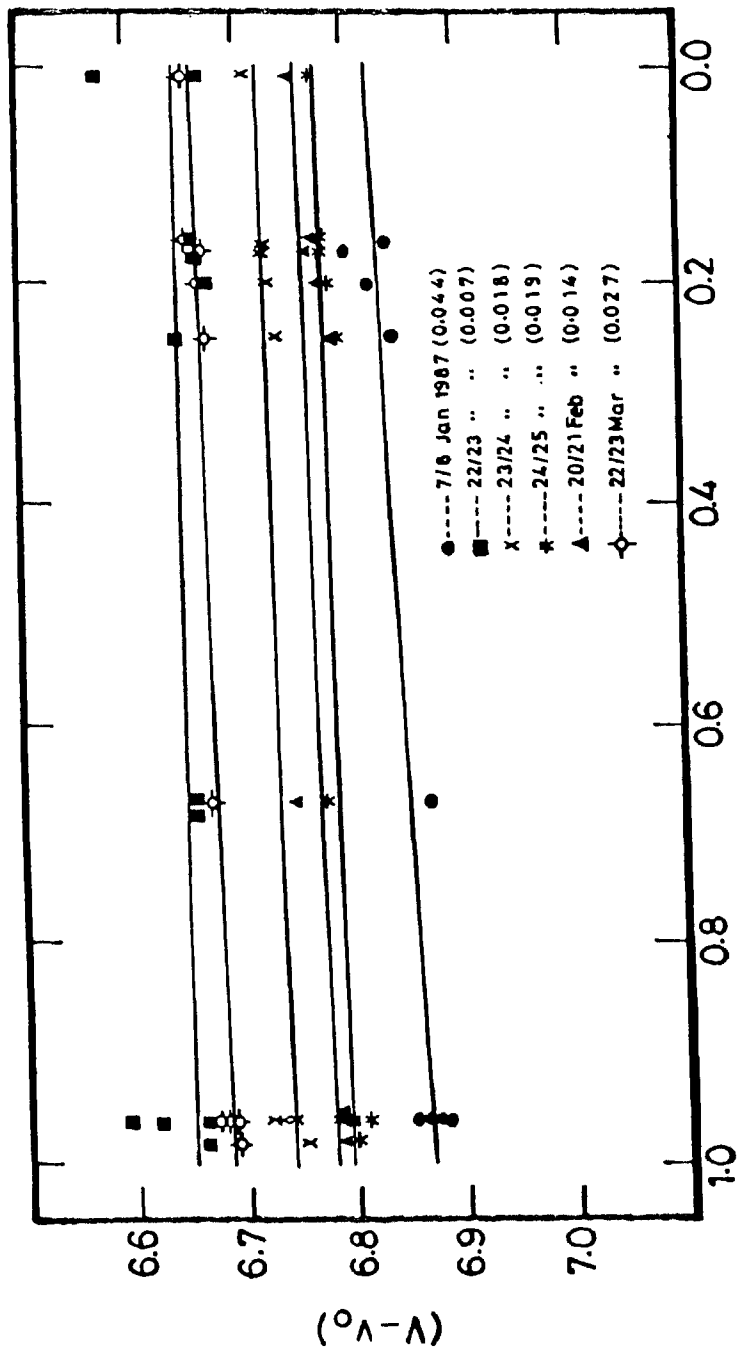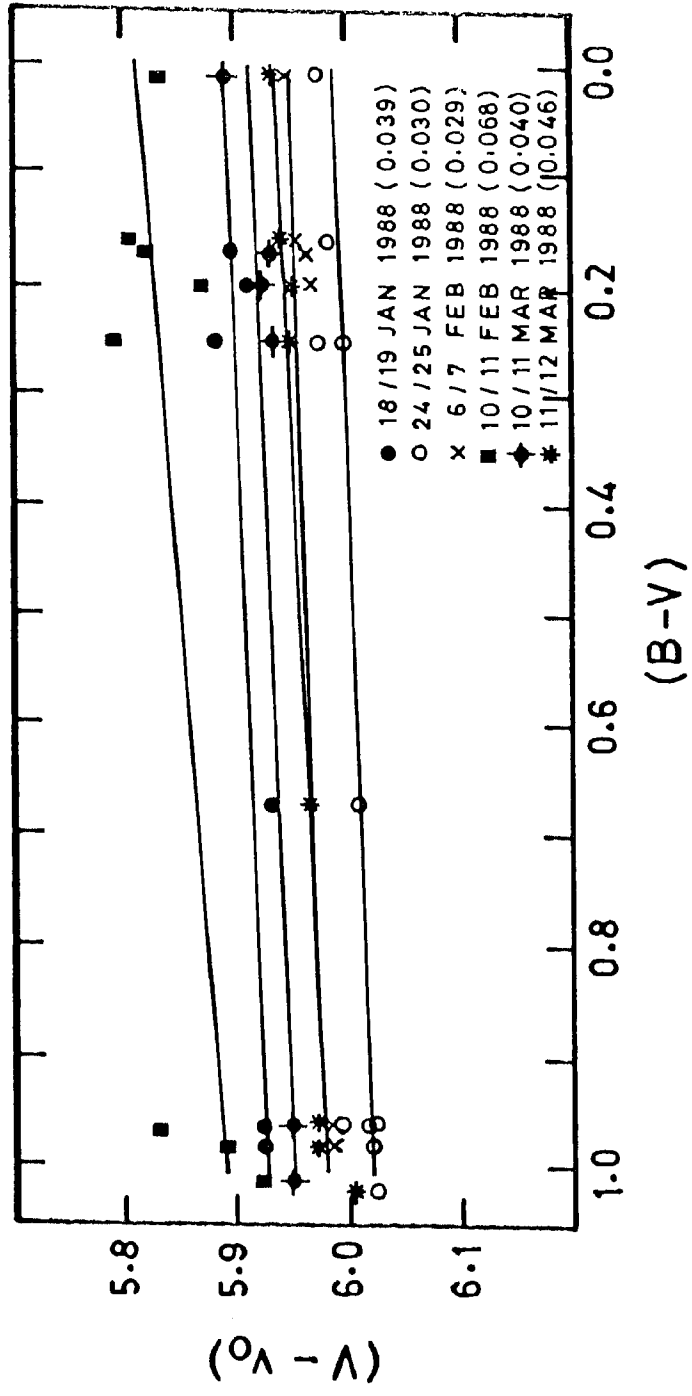
Determination of ϵ. Plots of $(V - v_0)$ values of Praesepe stars obtained during 1987-88 season against the corresponding $(B-V)$ colours. The values inside the brackets give slopes (ϵ) derived using least square technique.

Figure 8

indicated inside the brackets against the respective date. The final adopted mean values for the two observing seasons are also given in Table 2.

1.4. Standard differential quantities

As already mentioned, in variable star photometry all the measurements are done with respect to a nearby comparison. Equations (6) and (7) can be written using differences as

$$\Delta(B-V) = \mu \; \Delta(b-v)_0$$

$$\Delta V = \Delta v_0 + \varepsilon \; \Delta(B-V).$$

If σ_μ and $\sigma_{\Delta bv}$ are the probable errors in μ and $\Delta(b-v)_0$, the error in $\Delta(B-V)$ is given by

$$\sigma_{\Delta BV} = (\; \Delta(b-v)_0^2 \; \sigma_\mu^2 + \mu^2 \; \sigma_{\Delta bv}^2 \;)^{1/2}. \qquad \ldots (8)$$

Similarly, if $\sigma_{\Delta v}$ and σ_ε are the probable errors in Δv_0 and ε, probable error in ΔV is given by

$$\sigma_{\Delta v} = (\; \sigma_{\Delta v}^2 + \varepsilon^2 \sigma_{\Delta BV}^2 + \Delta(B-V)^2 \sigma_\varepsilon^2 \;)^{1/2}. \qquad \ldots (9)$$

The only unknowns in the above expressions are $\sigma_{\Delta v}$ and $\sigma_{\Delta bv}$. Usually, along with the comparison one more nonvariable, called the check star, is also observed and the probable errors in Δv_0 and $\Delta(b-v)_0$ are calculated from the standard deviations in the observed differential magnitudes and colours of the comparison and check stars. These quantities, evaluated from the data for an entire season, include the uncertainties in several parameters like the extinction coefficients, gain step calibrations, etc, involved in the reduction of the data.

The differential magnitudes and colours of the variable can be directly converted to magnitudes and colours if standard UBV values are available for either the comparison or check star. Otherwise, another nearby nonvariable with well determined UBV values should be observed differentially with respect to the comparison on a couple of nights. Using the mean differential magnitude and colour thus determined, the

51

standard magnitude and colour of the comparison can be calculated. These values in turn can be used to convert the differential magnitudes and colours of variable star to magnitudes and colours.

2. Polarimetry

The 102-cm reflector of Vainu Bappu Observatory was used for observations of all stars except AC Her which was observed with an almost identical telescope of Utter Pradesh State Observatory, Naini Tal.

The observing procedure with the PRL-polarimeter is as follows. After selecting the desired filter, the sky background adjacent to the programme star is first measured by integrating the sampled data for a particular pre-specified time interval (typically, 60 sec), depending upon the sky transparency conditions and the brightness of the object in the wavelength band considered. The measurements are next repeated on the required object after centring it in the diaphragm. The data reduction program is automatically activated at the end of integration, and the computer calculates and prints out the time of observation, percentage of linear polarization (P%), its probable error (ε_p), position angle of polarization (θ°) and the magnitude(m). Before a least square solution for the Stokes parameters is made, the sky background is subtracted. The parameter I is essentially the brightness of the source, and hence it is converted to magnitude which is printed. To bring down the errors due to photon statistics to a desired level, the above procedure is repeated several times (typically, 5 to 6 times). A zero-point correction, determined by observing polarimetric standards (Serkowski 1974) is applied to the calculated position angle before printing. The probable error in the computed position angle is estimated using (Treanor 1962)

$$\varepsilon_\theta = 28.5^\circ \ \varepsilon_p \ P^{-1}.$$

3. UBVRI photometry

The magnitudes in different filters obtained with the polarimeter can be used to form the colours of the observed object in the natural system and subsequently transformed to a standard photometric system. For this purpose a few UBVRI standards (Iriarte et al. 1965) were also observed during each observing season. The relations (6) and (7), when written in more general forms, yield

$$C_2 = \mu\, C_1 + \zeta_c$$
$$m_2 = m_1 + \varepsilon\, C_2 + \zeta_m, \qquad \qquad \dots\dots(10)$$

where C_1 and m_1 are the colour and magnitude of an object measured in the natural system, and C_2 and m_2 are the corresponding quantities in the standard system.

The system coefficients μ, ζ_c, ε and ζ_m are determined empirically from the standard star data. The (U-B), (B-V), (V-R) and (R-I) colours of the observed standard stars are plotted in Figures 9-12, against their corresponding atmospheric extinction corrected system colours $(u-b)_0$, $(b-v)_0$, $(v-r)_0$ and $(r-i)_0$. Since the available telescope time was limited and the stress was more on obtaining polarimetric data, it was not possible to pay much attention to photometric accuracy; no atmospheric extinction coefficients could be obtained, thereby making it necessary to use the available mean values for Kavalur: $k_v=0.25$, $k_{ub}=0.35$, $k_{bv}=0.21$, $k_{vr}=0.08$ and $k_{ri}=0.03$ for both 1984-85 and 1985-86 seasons, and $k_v=0.21$, $k_{ub}=0.35$, $k_{bv}=0.15$, $k_{vr}=0.08$ and $k_{ri}=0.03$ for 1986-87 season.

The straight lines drawn in Figures 9-12 represent the least square solutions, and the derived coefficients (Table 3) were used to transform the system colours of the programme stars to the standard UBVRI. The probable errors in the colour determination are given inside the brackets in the respective

53
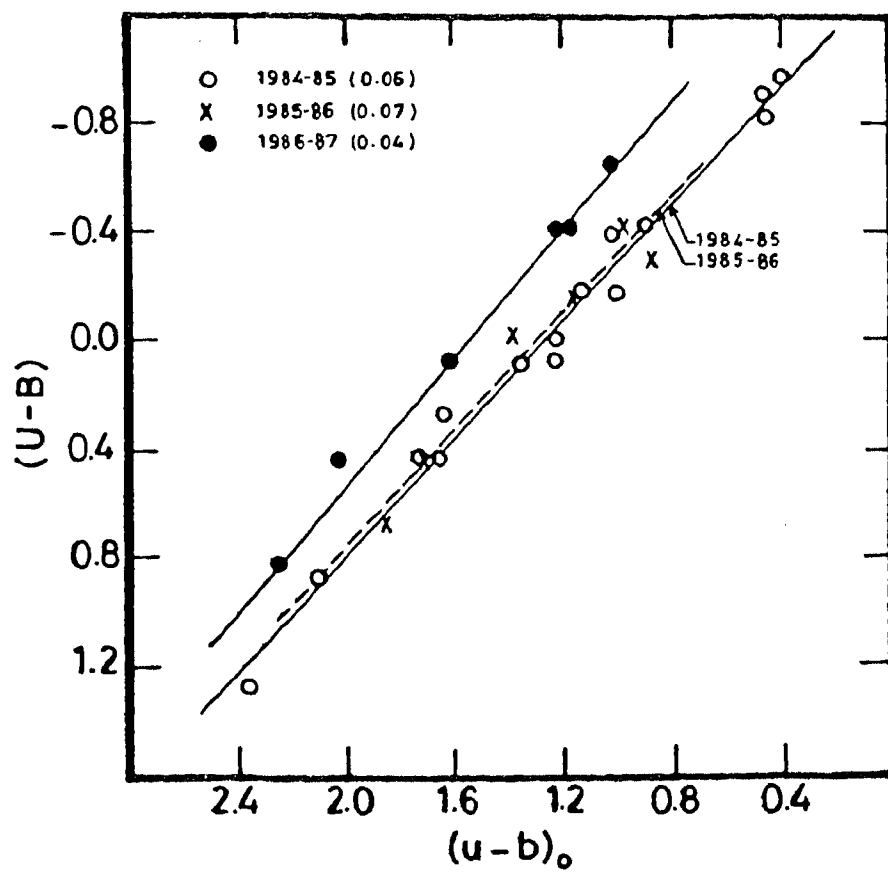
System calibration. Plots of (U-B) values of standard stars against the extinction-corrected system (u-b) values obtained during 1984-85, 1985-86 and 1986-87 seasons. The values inside the brackets indicate the probable errors in the colour determination.

Figure 9
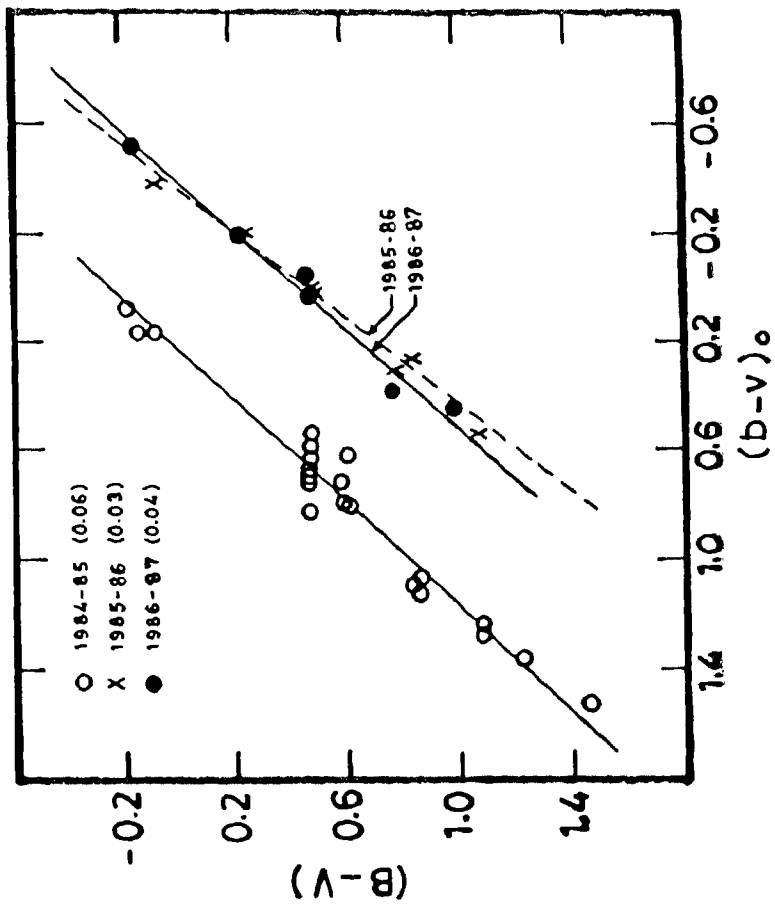
System calibration. Plots of (B-V) values of standard stars against the extinction-corrected system (b-v) values obtained during 1984-85, 1985-86 and 1986-87 seasons. The values inside the brackets indicate the probable errors in the colour determination.

Figure 10

55

Figure 11
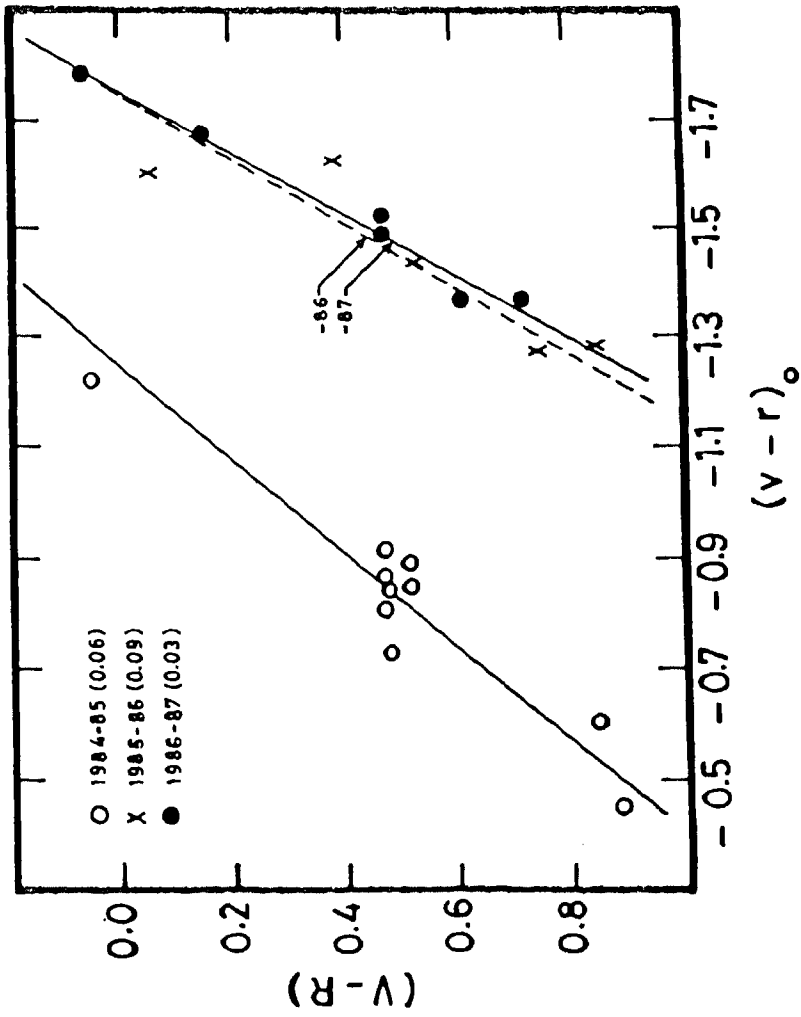
System calibration. Plots of (V-R) values of standard stars against the extinction-corrected system (v-r) values obtained during 1984-85, 1985-86 and 1986-87 seasons. The values inside the brackets indicate the probable errors in the colour determination.
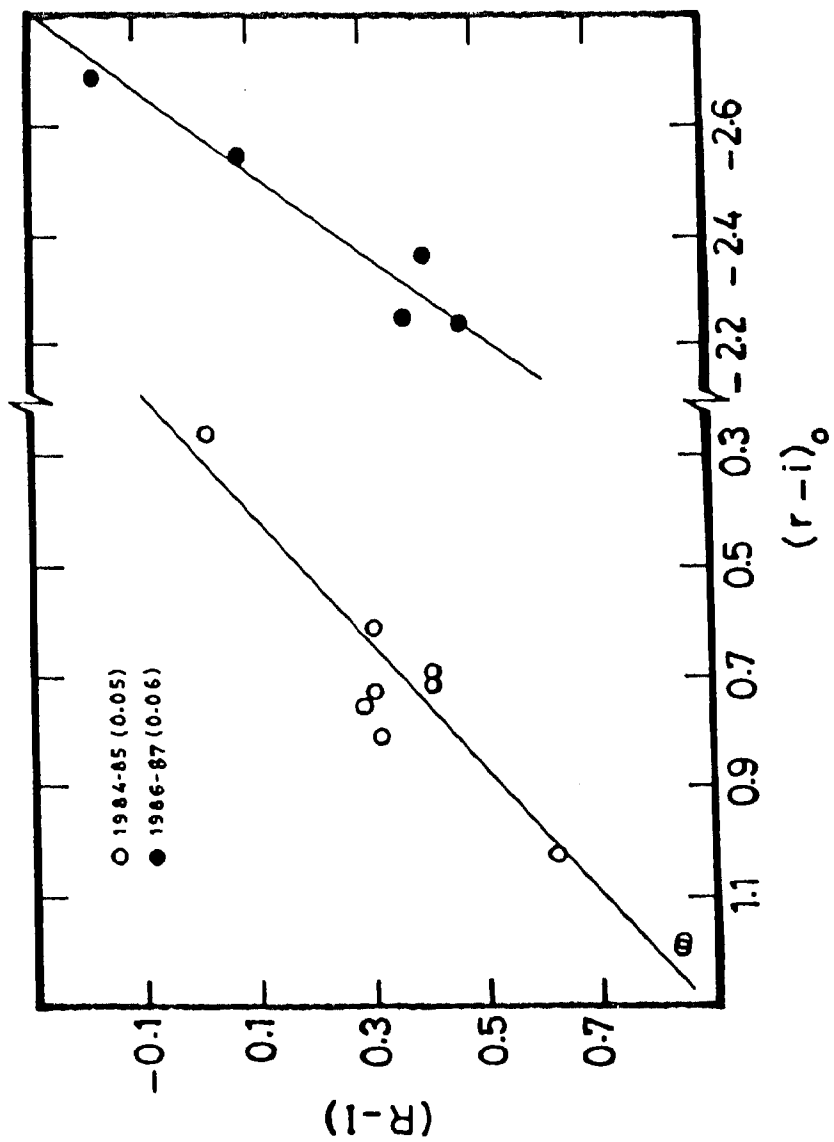
System calibration. Plots of (R-I) values of standard stars against the extinction-corrected system (r-i) values obtained during 1984-85 and 1986-87 seasons. The values inside the brackets indicate the probable errors in the colour determination.

Figure 12

57

Colour transformation coefficients of PRL – polarimeter.

Colour	Season					
	1984-85		1985-86		1986-87	
	Slope	Zero point	Slope	Zero point	Slope	Zero point
U - B	1.070	-1.351	1.059	-1.368	1.143	-1.788
B - V	1.053	-0.237	1.244	+0.468.	1.102	+0.433
V - R	1.191	+1.490	1.660	+2.909	1.743	+3.067
R - I	0.886	-0.268	-	-	1.354	+3.508

Table 3

figures. The comparatively large errors are mainly due to the prevalent poor sky conditions.

As already mentioned, the zero-point term ζ_m in the magnitude transformation is a troublesome parameter to determine because any uncertainty in the adopted extinction coefficient k_m will be directly reflected on it. For V magnitude the colour C_2 that appears in the magnitude (m) transformation relation is (B-V). Only a very limited number of standard stars could be observed during any night of observation, and hence it was not possible to determine ε using any single night's data. So, the following procedure was adopted to estimate ε during each season separately by combining several nights' data. Averaging equation (10) over the number of stars observed on any particular night,

$$\zeta_V = \overline{V - v_0} - \varepsilon \overline{(B-V)},$$

and the transformation equation becomes

$$V - v_0 - \overline{V - v_0} = \varepsilon \{ (B-V) - \overline{(B-V)} \}.$$

Using least square technique, the values, $\varepsilon = -0.16 \pm 0.03$ and $\varepsilon = -0.17 \pm 0.11$, were obtained for 1984-85 and 1986-87 seasons. The reason for such large errors in the determination of ε is the use of mean extinction coefficients k_V in place of the individual night's value. The procedure outlined above would yield a reliable estimation of ε only if standard star data is available on several nights. For this reason, it was not possible to derive ε for 1985-86 season. Since the same set of filters and detectors were used during both 1985-86 and 1986-87, $\varepsilon = 0.17$ was assumed for 1985-86 also. The mean value of ε thus estimated was then used to determine the zero-point of magnitude ζ_V from the photometric standard star data on each night of programme star observation.

IV. DATA, ANALYSIS AND RESULTS

A) CEPHEIDS AND RV TAURI STARS

Some of the observational characteristics of the programme stars taken from Kukarkin et al. (1969) are given in Table 1. All the four RV Tauri stars have been detected by IRAS at 12, 25 and 60μm passbands, and barring SX Cen even at 100μm (Beichman et al. 1985). Both of the cepheids do not appear in the IRAS Point Source Catalogue. RU Cam has been found to show an excess in the near infrared (Gehrz & Woolf 1970), and hence a mild excess in the far infrared below the detection limit of the IRAS cannot be precluded for it. The near infrared data for V553 Cen is not available.

Polarimetric observations have been reported in the literature only for two of the objects - RU Cam and AC Her - given in Table 1; however, both of them do not have any multiwavelength observations. A major part of the available 102-cm telescope time was devoted to observe AR Pup since it was found to show exceptionally large and highly variable polarization. Further, it was closely monitored photometrically in B and V bands with the 34-cm telescope during two seasons.

The results of observations of the individual objects are presented and discussed below.

1. AR Puppis

Light variability of AR Pup (CD-36°4137) was discovered by O'Leary and it was subsequently classified as an RV Tauri-type star by the Harvard investigators (Payne-Gaposchkin, Brenton & Gaposchkin 1943). The long series of photographic observations obtained by them during the years 1900-42 indicates that AR Pup exhibits significant irregularities both in the period and

Basic data on the cepheids and RV Tauri stars.

Star Name	Galactic latitude	Variability type	Period (days)	Spectral type
RU Cam	+28	CW	22.1	K0 - R2
RU Cen	+17	RV	64.7	Fpe
SX Cen	+13	RVb	32.9	F5
V 553 Cen	+25	CW	2.1	G5pI-III
AC Her	+14	RVa	75.5	F2Ib-K4e
AR Pup	-03	RVb	75.0	$cF_0 - cF_8$

Table 1

shape of the light curve. Two consecutive deep minima in the
light curve of AR Pup are separated on an average by about 75
days, and its mean brightness varies with a period around 1200
days. No detailed study on the spectral variation of AR Pup
during its pulsational cycle exists in the literature;
however, it is evident from the two old Harvard plates
(spectral type cF0 and cF8) that the spectral variation is
quite appreciable during the light cycle. It is worth noting
that the latter of the two spectra was obtained near a light
maximum.

During a spectroscopic survey of RV Tauri and yellow
semiregular variables, Rosino (1951) obtained a single
spectrum of AR Pup and pointed out the presence of strong CH
bands. Because the infrared spectrum showed emission features
at 10 and $18\mu m$, Gehrz & Ney (1972), probably unaware of
Rosino's observations, suggested that AR Pup is similar to
oxygen-rich RV Tauri stars. Later, Lloyd Evans (1974)
confirmed the presence of strong CH and CN bands in the
optical spectrum of AR Pup and classified it as a
spectroscopic group B star on the system of Preston et al.
(1963). The presence of the $10\mu m$ emission feature has been
confirmed by the IRAS spectra obtained in the $7-23\mu m$ region
(Olnon & Raimond 1986).

1.1. BV photometry

Altogether, during 1986-87 and 1987-88 seasons, photometric
observations of AR Pup were obtained on 63 nights in B and V
bands. All the observations were made differentially with
respect to the comparison HD 66559 (CD-35°4134, spectral type
G0). As a check on the constancy of the comparison, HD 65723
(CD-36°4067, spectral type G5) was also observed on several
nights during both the seasons. The differential magnitudes
and colours of the comparison star with respect to the check
star, in the sense, HD 66559-HD 65723, thus obtained during
the two observing runs are given in Table 2. The values are
well within the errors of observations, indicating the
constancy of both the comparison and check stars.

62

Differential magnitudes and colours of HD 66559 with respect to HD 65723. Number of nights on which observations were made is given inside the bracket against the corresponding quantity.

Season	ΔV	$\Delta(B-V)$
1987	1.366 ±0.002 (16)	-0.056 ±0.003 (15)
1988	1.359 ±0.003 (14)	-0.057 ±0.002 (14)
mean	1.363 ±0.002	-0.056 ±0.003

Table 2

With V=7.01 and (B-V)=0.98 for HD 65723 (Nicolet 1978), the mean values of the present differential measurements yield V=8.373±0.002 and (B-V)=0.924±0.003 for HD 66559. These values were used to convert the differential magnitudes and colours of AR Pup to V and (B-V) which are given in Table 3. The quoted probable errors of differential magnitude and colour are estimated from the dispersions in the corresponding comparison star minus check star quantities. Each value given in Table 3 is a mean of 4 to 6 independent observations.

1.1.1. LIGHT CURVES

The data given in Table 3 is plotted in Figures 1 and 2. Clearly, the V light curves show considerable variation. Figure 1, which contains the plot of the observations obtained during 1986-87 shows two minima differing in depth by only 0.05 mag and separated by around 37.8 days. The total amplitudes in V and (B-V) are 0.52 mag and 0.32 mag, respectively. Observations obtained during 1987-88 (Figure 2) show a shallow minimum (close to JD 2447180) of short duration. The prominent minima, separated by around 37 days, are of nearly equal depths. The first minimum is very broad, lasting over eight days. The total amplitudes in V and (B-V), 0.43 mag and 0.27 mag, respectively, are only slightly smaller than those of the previous season. The mean light level ((max+min)/2) during 1987-88 is brighter by about 0.13 mag.

1.1.2. BEHAVIOUR OF (B-V)

In the upper panel of Figure 3, the V magnitudes given in Table 3 and that listed by Eggen (1986) are plotted after visually aligning the centres of well-observed light minima in each case along the time axis.

The narrow band (b-y) listed by Eggen are converted to (B-V) using the relation :

$$(B-V) = 1.772 \ (b-y) - 0.087 \qquad \ldots . (1)$$

The above relation was derived using the (B-V) and (b-y) data of bright Ia and Ib supergiants, taken from Astronomical

JD 2440000+	V	(B-V)
6816.271	9.417±0.009	0.877±0.011
17.293	9.448	0.905
18.231	9.489	0.876
19.235	9.505	0.890
20.230	9.535	0.894
21.219	9.581	0.869
22.287	9.577	0.850
26.301	9.496	0.751
27.340	9.445	0.679
28.202	9.373	0.698
29.186	9.327	0.670
34.173	9.248	0.634
35.182	9.242	0.681
36.178	9.242	0.695
44.227	9.199	0.798
45.284	9.219	-
46.191	9.223	0.876
47.168	9.272	0.857
50.241	9.367	0.886
51.220	9.391	0.905
52.215	9.424	0.910
53.205	9.459	0.917
57.190	9.598	0.946
58.184	9.617	0.933
59.260	9.639	0.897
60.160	9.643	0.909
61.157	9.613	0.881
62.171	9.594	0.843
68.109	9.294	0.652
77.097	9.125	0.759
83.106	9.148	0.831
84.104	9.158	0.835
92.108	9.334	0.835
7157.273	9.246±0.010	0.826±0.009
77.354	9.147	0.645
78.262	9.175	0.660
79.232	9.209	0.701
80.313	9.207	0.746

Table 3

JD 2440000+	V	(B-V)
7184.260	9.151	0.776
85.230	9.125	0.820
96.243	9.403	0.902
97.254	9.456	-
98.182	9.489	0.917
7200.206	9.542	0.835
01.214	9.544	0.886
02.207	9.569	0.846
03.228	9.542	-
04.249	9.538	-
05.186	9.571	0.711
07.298	9.546	0.701
08.235	9.532	0.667
17.147	9.227	0.736
18.147	9.234	0.711
19.167	9.209	0.764
30.137	9.300	0.776
31.162	9.322	0.779
32.170	9.347	0.788
33.164	9.362	0.808
38.133	9.486	0.791
39.116	9.506	0.761
46.114	9.424	0.654
47.103	9.319	0.654
51.106	9.341	0.656

Table 3 (cont'd)
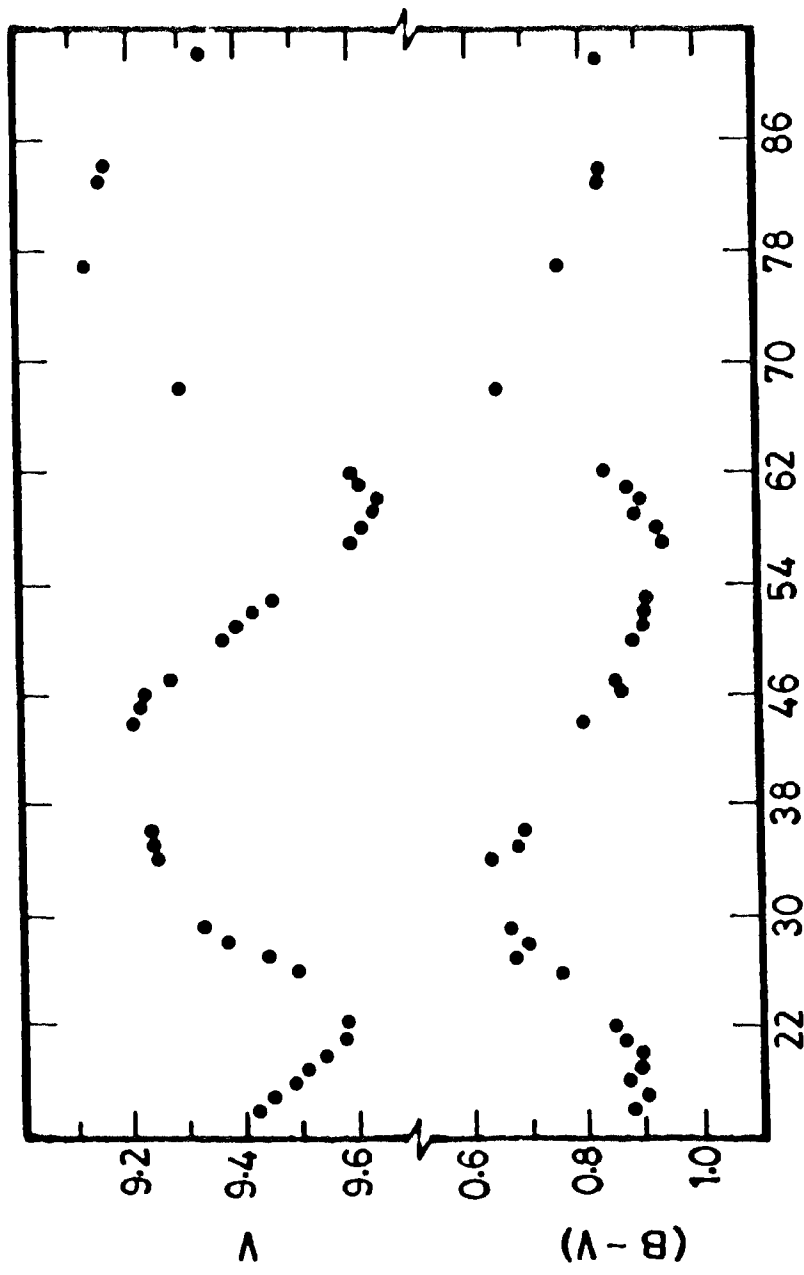
V and (B-V) curves of AR Pup obtained during 1986-87 season.

Figure 1
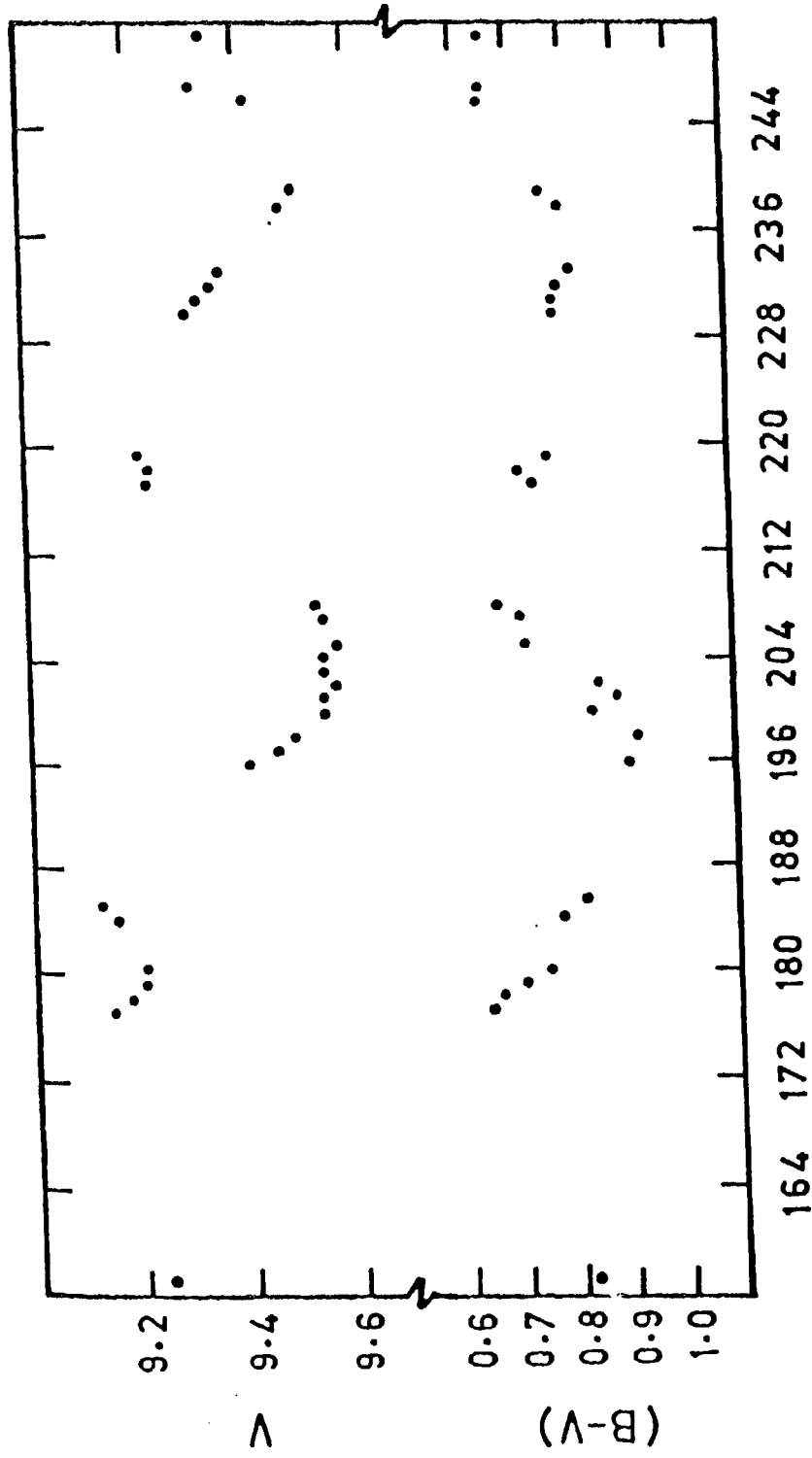
V and (B-V) curves of AR Pup obtained during 1987-88 season.

Figure 2

68
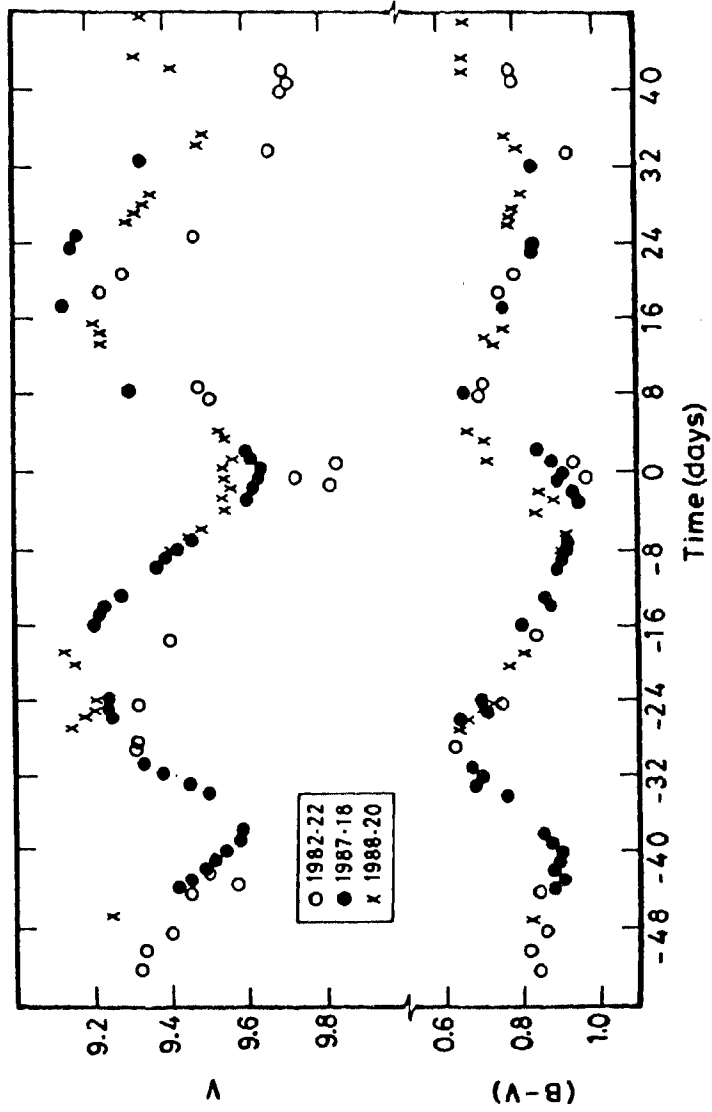
Figure 3

The combined V and (B-V) curves of AR Pup obtained after sliding them along the time axis so as to align the centres of well-defined minima. The mean epochs of the light curves are indicated.

69

Almanac for 1988. The (B-V) values thus derived (with a maximum uncertainty of 0.05 mag) and those given in Table 3 are plotted in the bottom panel of Figure 3, with the same shift along the time axis as applied to the V observations.

It is remarkable that the large variability seen in the V light curve does not seem to be reflected on the (B-V) variation. A similar behaviour has been found in the case of AC Her by Cardelli (1985). The most significant difference between the variation of (B-V) shown by the two objects is that in AC Her the period of variation is fairly stable, whereas in AR Pup it is not. More photometric observations are needed to ascertain the systematic pattern in the behaviour of (B-V) relative to the light variation.

Preston et al. (1963) have found that, in all RV Tauri stars observed by them, (B-V) leads the V light. They have reported that the phase shift between V and (B-V) curves is nearly independent of phase for spectroscopic group A objects, whereas it is much larger at secondary maxima and minima than at primary maxima and minima for group B and C objects. In view of the very limited sample they had at hand to differentiate between the behaviours of the various spectroscopic groups, it is difficult to attach much significance to the above finding.

In the case of AR Pup, sometimes, it is hard to distinguish a primary minimum from a secondary minimum or to fix the time of a maximum (Figures 1 and 2). Therefore, the evaluation of the phase shifts in V and (B-V) curves at different phases becomes highly subjective. But it is safe to conclude that an overall phase shift of about $0.^{P}1$ (assuming a 75.0 day period) exists between the two. From Figure 3 it is clear that (B-V) attains its bluest value during the ascending branch of the light curve, about $0.^{P}1$ after a light minimum.

1.2. AAVSO data

The only available information on the light variation around the times of the polarimetric observations obtained during 1984-85 and 1985-86 seasons is the visual estimates of

brightness by the American Association of Variable Star Observers, and hence it was acquired (Mattei 1986, private communication). Because of the limited number of observations and the inherent scatter in the visual estimates, the data do not define the particular photometric cycles during which the polarimetric measurements were made.

In order to construct the most probable mean light curves for the period under consideration, a truncated Fourier series

$$m_i = a_0 + \sum_{n=1}^{N} \{ a_n \cos(2\pi n t_i / P) + b_n \sin(2\pi n t_i / P) \}$$

was used to represent the visual data. Here m_i represents the observation obtained at time t_i, P is the period of light variation, and a_0, a_ns and b_ns are the Fourier coefficients.

The times of minima estimated from the AAVSO data for the interval JD 2445999-6253 satisfy a 75±1 day period. Further, the present photometry and that obtained by Eggen (Figure 3) indicate that for short stretches of data (probably, 2-3 cycles) a 75.0 day period holds good. So the period was assumed to be P=75.0 day, and separate mean light curves were computed for the AAVSO data obtained during JD 2445999-6253 and JD 2446352-568 using least square technique for different values of N. It is found that for N=2 (i.e., with the first and second harmonics), the condition of goodness of fit

$$G = \{ \sum_{i=1}^{M} (m_{io} - m_{ic})^2 / (M - N) \}^{1/2}$$

is a minimum. Here m_{io} and m_{ic} are the ith observed and computed values and M is the total number of observations.

Since the visual estimates show a large spread, the observations were arranged in order of increasing phases and three point running averages were taken. The results are presented in Figures 4 and 5 along with the computed mean light curves using the first and second harmonics. JD 2445050.0 was taken as the initial epoch.
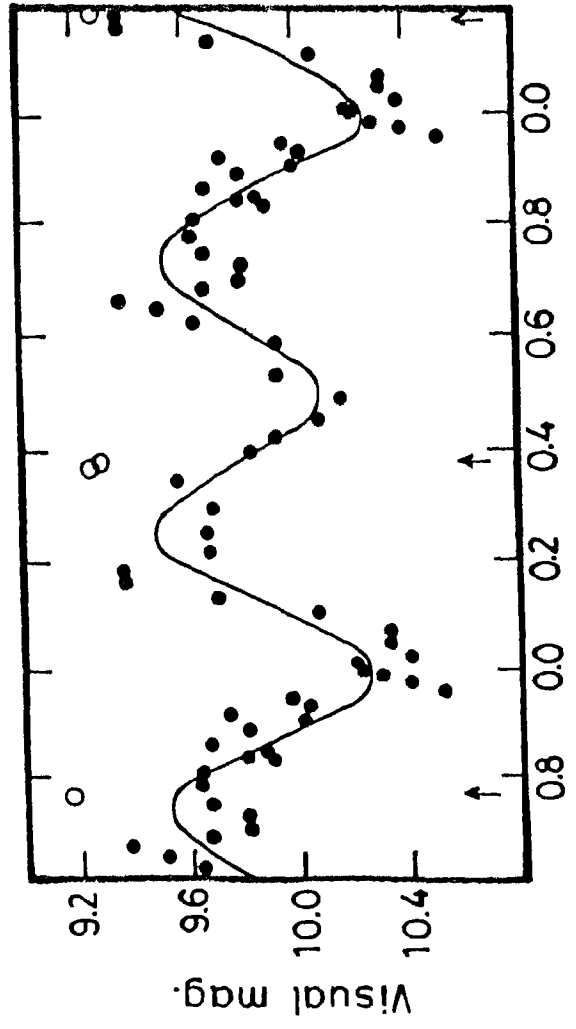
71

Figure 4

Plot of the mean light curve and three point running averages (filled circles) of AR Pup computed from AAVSO data for the interval JD 2445999-6253 after folding over a 75.0 day period. JD 2445050.0 was taken as the initial epoch. The open circles are the V magnitudes obtained with the PRL-instrument. The arrows indicate the phases of polarimetric observations.
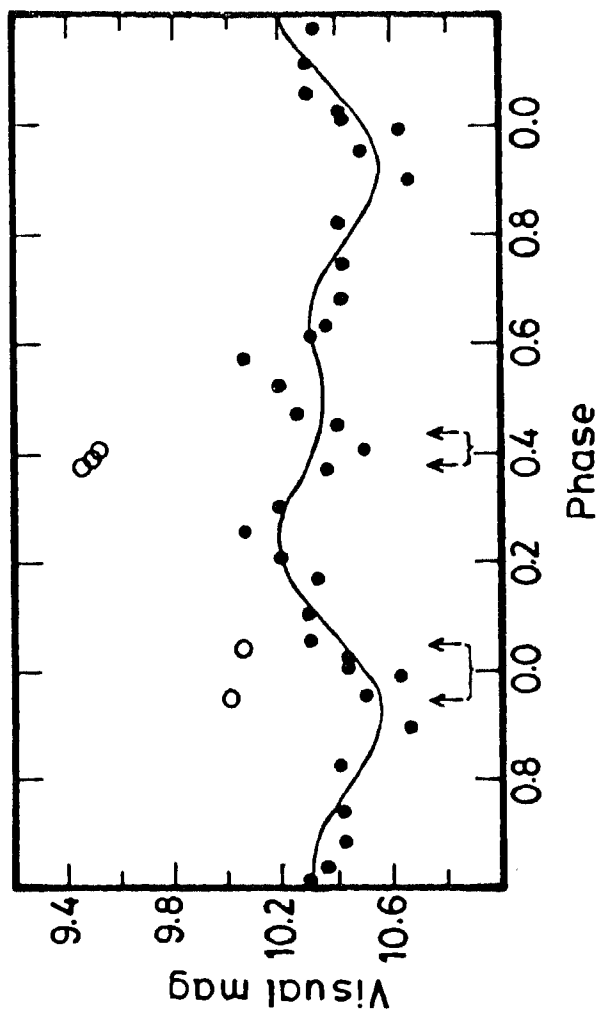
Plot of the mean light curve and three point running averages (filled circles) of AR Pup computed from AAVSO data for the interval JD 2446352-568 after folding over a 75.0 day period. JD 2445050.0 was taken as the initial epoch. The open circles are the V magnitudes obtained with the PRL-instrument. The arrows indicate the phases of polarimetric observations.

Figure 5

73

Figures 4 and 5 clearly bring out the changes that largely occur in the light curves of AR Pup in a few photometric cycles. It is evident from these figures that the mean brightness of AR Pup is variable and the amplitude of the 75 day period light variation is larger when the star has a higher mean brightness; these characteristics are typical of an RV Tauri star of group b (Tsesevich 1975).

1.3. Period of light variation

It is obvious from the photographic data presented by Payne-Gaposchkin, Brenton & Gaposchkin (1943) that AR Pup shows significant departure from the mean period of 75 days. Photoelectrically, AR Pup is not a well-observed star. Table 4 contains the times of light minima determined from the observations of Eggen (1986), AAVSO visual estimates (Figures 4 and 5) and the present data (Figures 1 and 2). No distinction between a primary and a secondary minima was made because, as can be seen from Figures 1-5, sometimes, it is even difficult to differentiate between the two. Times of minima determined from the AAVSO data are more uncertain because of the inherent error in the brightness estimation. The times of minima are converted to phases using the ephemeris

$$JD = 2445050.0 + 75\overset{P}{.}0 \ E.$$

In Figure 6, the phases thus computed are plotted against the corresponding cycle count. The non-linear behaviour of the phase of light minimum with cycle count is a clear indication of a variable period for AR Pup. The two minima are separated by 37 to 38 days.

1.4. Polarimetry

AR Pup was observed polarimetrically on one night each in November and December 1984, and February 1985 in UBVRI bands, on 7 nights during February-March 1986 in UBVR bands, and on six nights during January-March 1987 in UBVRI bands. Linear polarization (P%), position angle ($\theta°$) and the errors in their

Recent epochs of light minima of AR Pup.

No	Light minimum JD 2440000+	Source
1.	5050	Eggen (1986)
2.	5089	"
3.	6025	AAVSO
4.	6062	"
5.	6469	"
6.	6823	present study
7.	6860	"
8.	7204	"
9.	7242	"

Table 4

75
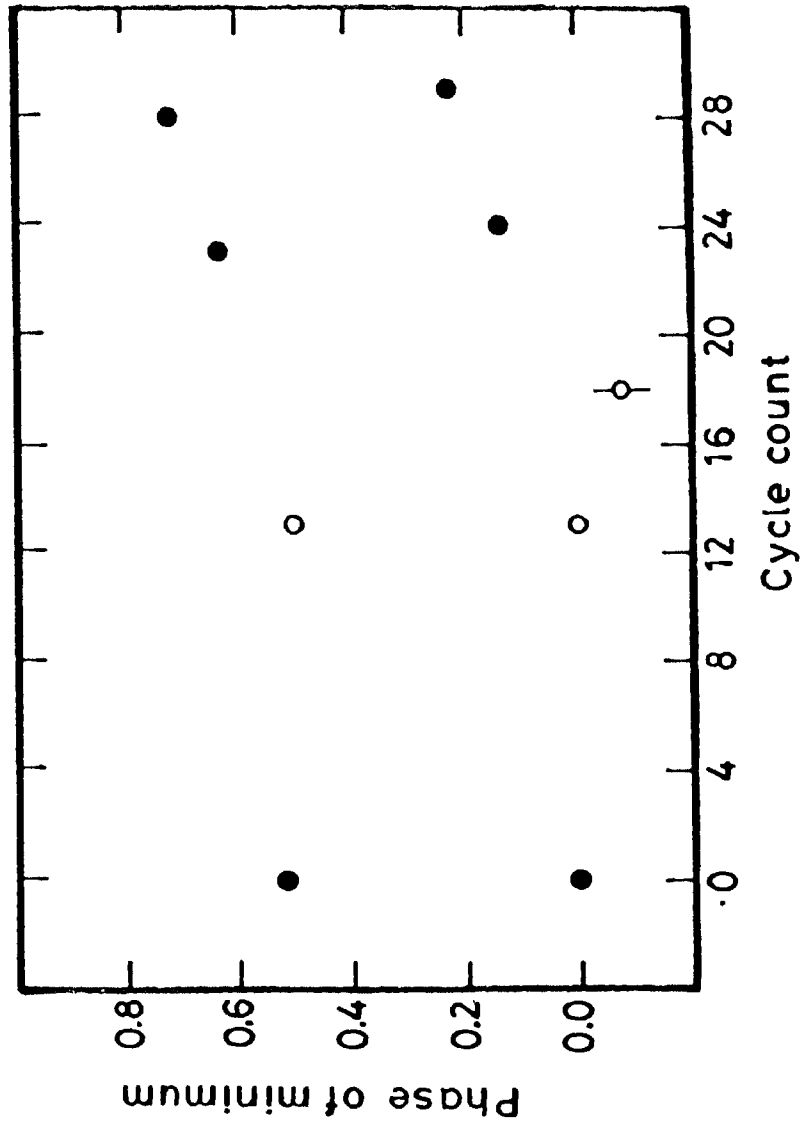
Figure 6

Plot of the phases of light minima of AR Pup against the respective cycle count. Open circles represent AAVSO data. The uncertainty in the phases are less than the size of the circles except in one case where it is explicitly indicated.

UBVRI polarimetry of AR Pup.

JD 2446000+	U		B		V		R		I	
	P%	θ	P%	θ	P%	θ	P%	θ	P%	θ
007.44	0.5±0.4	68±23	0.7±0.1	130±5	1.5±0.1	123±2	2.1±0.1	127±2	2.6±0.1	131±1
053.35	6.5±0.3	95±1	5.6±0.1	104±1	5.1±0.1	107±0	4.6±0.1	112±1	4.2±0.1	119±1
114.28	4.7±0.4	116±2	5.4±0.2	118±1	5.2±0.1	122±1	5.2±0.1	118±1	5.0±0.1	118±1
471.27	9.9±0.4	92±1	8.7±0.2	97±1	7.1±0.1	98±0	6.3±0.1	101±0	-	-
472.27	10.8±0.2	94±1	9.0±0.1	97±0	7.5±0.1	100±0	-	-	-	-
478.17	14.6±0.3	98±1	12.2±0.1	100±0	9.5±0.1	101±0	8.3±0.1	105±0	-	-
503.20	6.4±0.2	80±1	5.9±0.1	87±0	5.3±0.1	96±0	4.6±0.1	99±1	-	-
504.20	5.9±0.2	77±1	6.0±0.1	86±0	5.5±0.1	95±0	4.9±0.1	98±1	-	-
505.18	5.9±0.2	75±1	5.8±0.1	84±0	5.6±0.1	90±0	4.9±0.1	95±1	-	-
508.16	6.1±0.6	75±3	5.8±0.1	85±1	5.6±0.1	93±0	5.1±0.2	100±2	-	-

Table 5

77

JD 2446000+	U		B		V		R		I	
	P%	θ°	P%	θ°	P%	θ°	P%	θ°	P%	θ°
826.24	2.2±0.2	120±2	2.4±0.1	114±1	2.5±0.0	117±0	2.9±0.1	122±1	2.9±0.2	130±2
827.20	1.8±0.2	94±3	1.5±0.0	96±1	1.4±0.1	96±1	1.2±0.1	100±2	2.1±0.3	111±4
844.18	7.8±0.3	97±1	7.0±0.1	102±0	5.2±0.1	106±0	4.6±0.1	118±1	4.0±0.3	116±2
845.22	9.1±0.3	106±1	6.8±0.1	118±0	5.4±0.1	121±0	4.9±0.1	125±1	4.1±0.4	133±3
861.25	5.8±0.3	84±1	4.6±0.1	96±1	3.5±0.1	103±0	3.1±0.1	104±1	3.0±0.4	120±4
862.19	5.2±0.2	90±1	4.8±0.1	94±0	3.5±0.1	103±1	3.0±0.1	110±1	2.3±0.4	108±5

Table 5 (cont'd)

measurements are given in Table 5 along with the corresponding Julian day of observation, and are plotted in Figures 7-9 against the respective inverse of the wavelength of observation. The Julian day of observation is also mentioned against each curve for easy reference.

1.4.1. INTERSTELLAR COMPONENT OF POLARIZATION

No attempt was made to derive the interstellar component of polarization by observing nearby stars; but an upper limit on the interstellar component can be obtained from the colour excess E(B-V), since reddening is an essential condition for the production of interstellar polarization (Schmidt 1958a). Observations of several stars in UBVRI bands by Coyne, Gehrels & Serkowski (1974) and Serkowski, Mathewson & Ford (1975) show that for each direction considered the interstellar linear polarization reaches a maximum P_{max} at some wavelength λ_{max}; but the scaled-down polarization (P/P_{max}) is a well-defined function of the scaled-down wavelength (λ/λ_{max}). Though value of P_{max} is poorly correlated with E(B-V), the maximum possible value for the interstellar component is given by

$$P_{max}(\%) \leq 9.0 \ E(B-V). \qquad \qquad ....(2)$$

Although the values of λ_{max} show a large range, in the direction where there is no dense cloud, it is represented fairly well by the relation

$$\lambda_{max}(\mu) = 0.555 - 0.03 \ E(B-V). \qquad \qquad ....(3)$$

The above two empirical results were obtained by Serkowski, Mathewson & Ford (1975).

The E(B-V)=0.04 mag, quoted by Dawson (1979) for AR Pup, gives a value of $P_{max} \leq 0.34\%$, peaking in V band, and it is comparable to the errors of observation. The above estimation is consistent with the fact that on one occasion, namely JD 2446007.44, the polarization observed in U band was very close to zero. It is evident that the contribution from the interstellar component is negligible and the observed

Plot of linear polarization (P%) and position angle (θ') of AR Pup against the inverse of the effective wavelength of observation. The Julian days of observation, after omitting the first four digits 2446, are indicated.
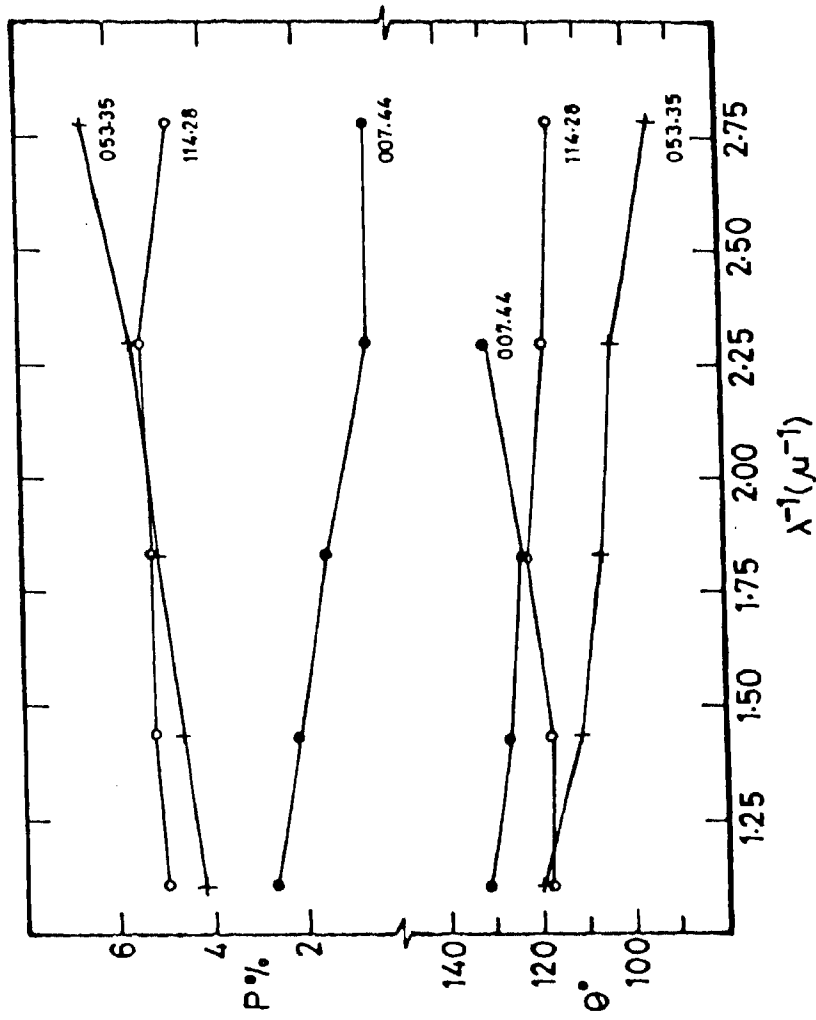
Figure 7
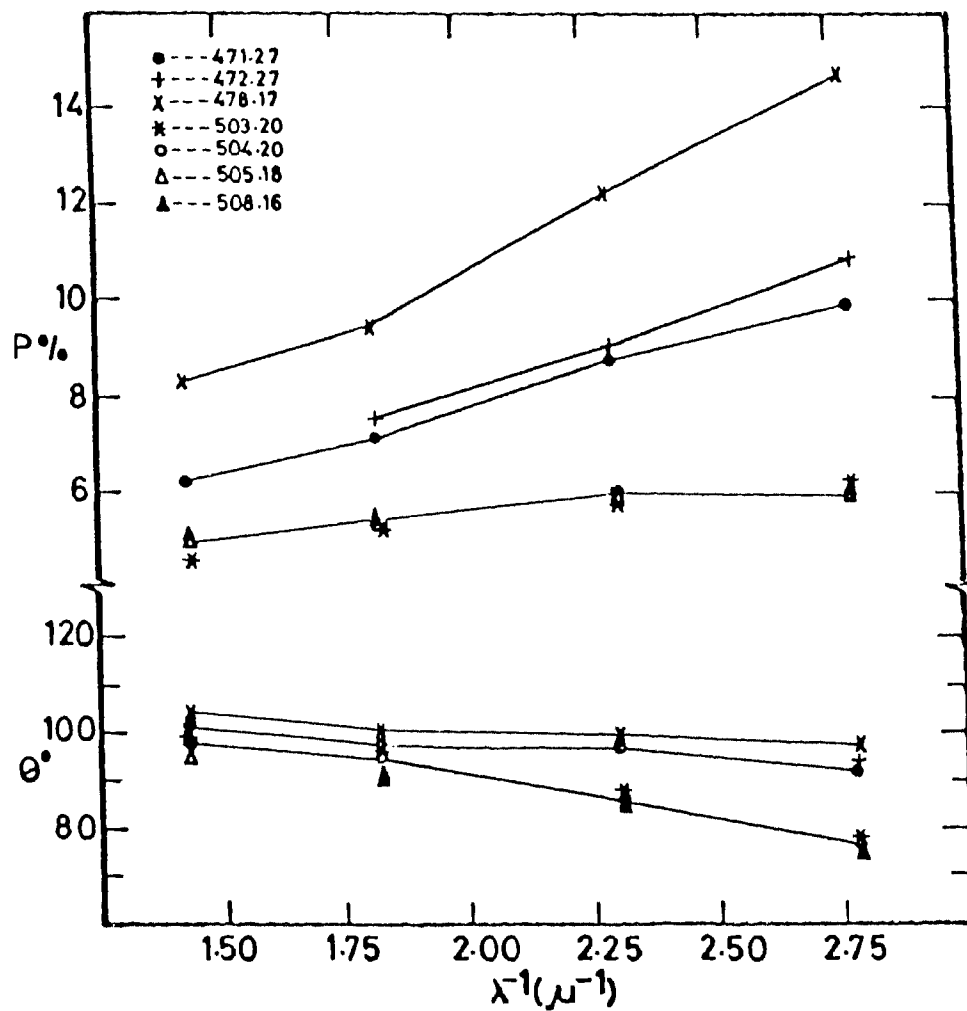
Plot of linear polarization (P%) and position angle ($\theta°$) of AR Pup against the inverse of the effective wavelength of observation. The Julian days of observation, after omitting the first four digits 2446, are indicated.

Figure 8

Plot of linear polarization (P%) and position angle (θ°) of AR Pup against the inverse of the effective wavelength of observation. The Julian days of observation, after omitting the first four digits 2446, are indicated.

Figure 9

82

quantities are intrinsic to the star.

1.4.2. POLARIZATION-LIGHT CURVE CONNECTION

It is clear from Figures 7-9 that drastic changes occur both in the amount and wavelength dependence of polarization over very short time spans; the linear polarization in U on JD 2446471.27 was around 9.9%, whereas that after a mere 7 days' interval was as high as 14.6%. Larger changes in polarization and position angle are found to occur in ultraviolet (~ 14% and 55° in U) than in red (~ 6% and 30° in R).

The phases, at which the polarimetric observations are obtained, are indicated in Figures 4 and 5 by arrows.

From Figure 4, it is seen that the deeper minimum occurs at $0.^{P}0$, and the polarimetric observations obtained on JD 2446007.44, 053.44 and 114.28 fall, respectively, at $0.^{P}77$, $1.^{P}38$ and $2.^{P}19$.

The AAVSO visual estimates are few in number during the interval JD 2446352-568, resulting in a larger uncertainty in the corresponding mean light curve (Figure 5). The deeper minimum occurs around $0.^{P}92$, and the polarimetric data of JD 2446471-8 falls at $0.^{P}95-1.^{P}05$, during the ascending branch close to the primary minimum, whereas the data of JD 2446503-8 lies in the range $1.^{P}38-1.^{P}45$, on the descending branch of the secondary minimum.
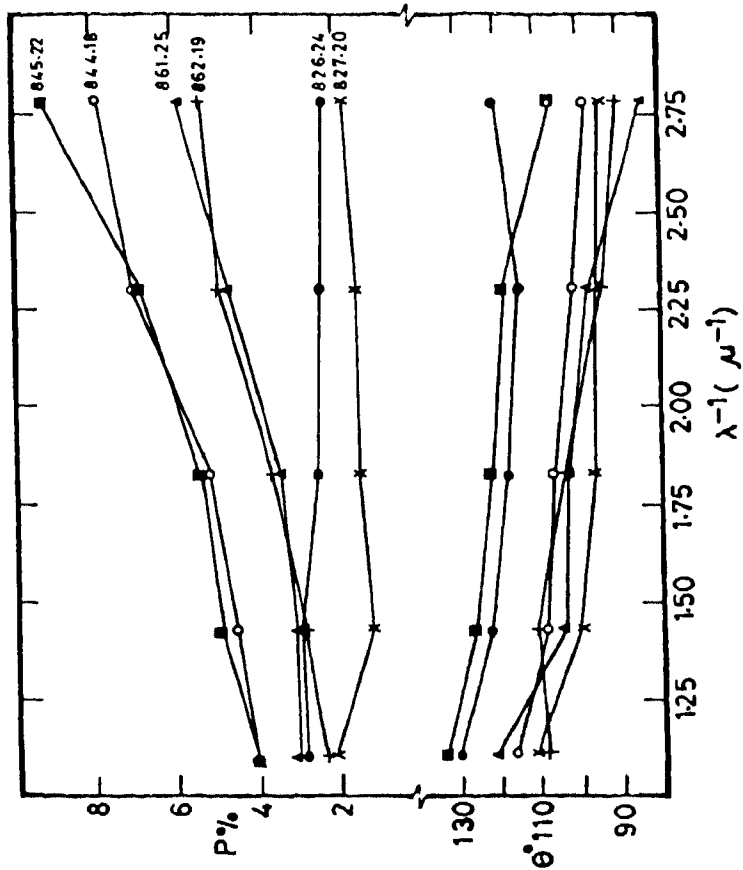
The linear polarization values in the V band obtained during JD 2446826-62 are plotted in Figure 10 along with the V and (B-V) values against the corresponding Julian days of observation.

The polarimetric data when combined with the simultaneous photometry (Figures 7 & 4, 8 & 5, and Figure 10) clearly indicates that the observed large time dependent variations, both in the amount and wavelength dependence of polarization, are not isolated events but are definitely cyclic and related to the light variation. From the changes seen in polarization close to and after light minima, it is fairly obvious that polarization increases largely close to the epochs of light
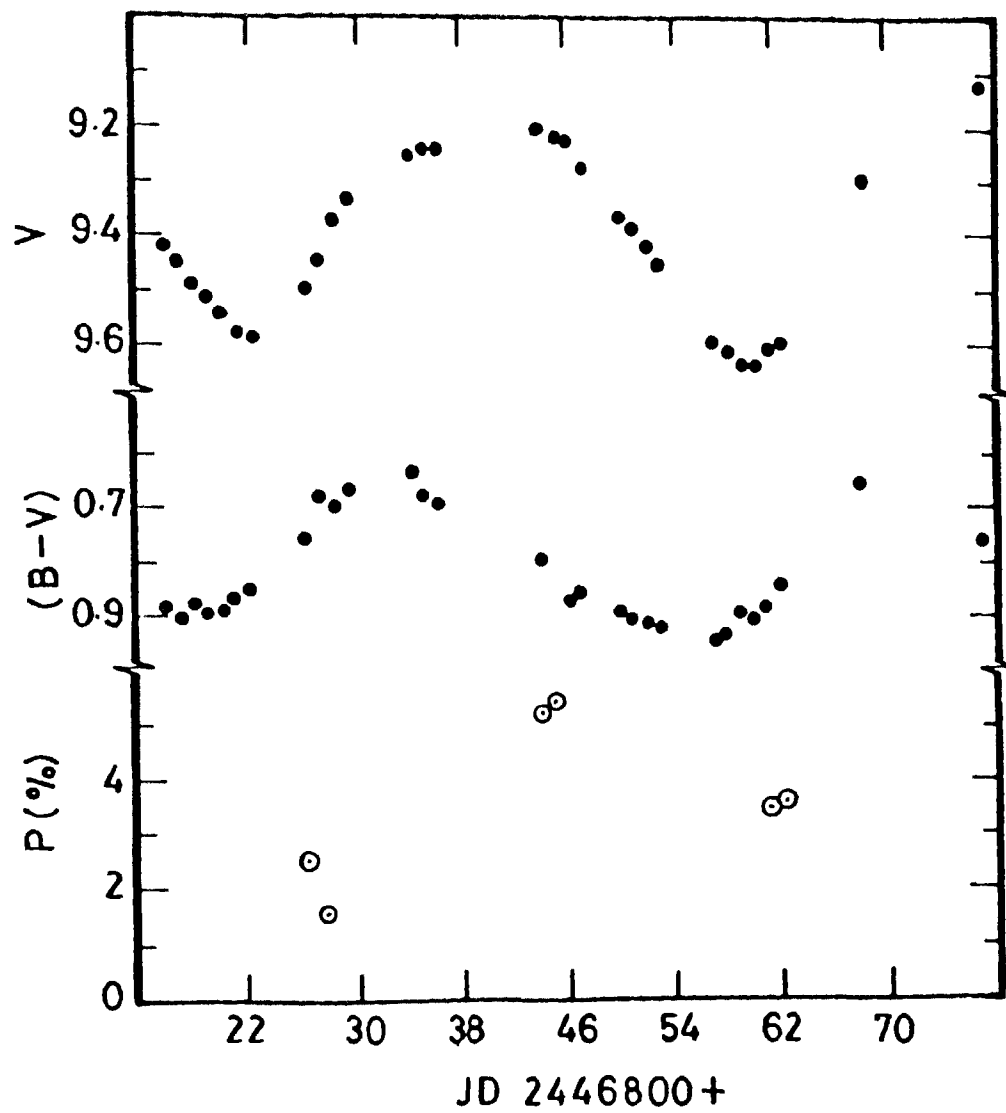
Plots of V, (B-V) and P% in V band of AR Pup against the corresponding Julian days of observation. Note that polarization was low close to the light minimum.

Figure 10

minima, during the ascending branch of the light curve.

1.4.3. WAVELENGTH DEPENDENCE OF POLARIZATION

The most striking characteristic evident from Figures 8 and 9 (and to a certain extent from Figure 7) is the apparent dependence of the shape of $P(\lambda)$ curve on the polarization level itself. It is found that as polarization increased from JD 2446471.27 (Figure 8) onwards the $P(\lambda)$ curve became steeper towards ultraviolet and became nearly flat when the polarization decreased later. A very similar pattern in the behaviour of $P(\lambda)$ curve is seen in Figure 9 also, thus confirming the cyclic variation in both the level and wavelength dependence of polarization. Unfortunately, it was not possible to follow up the polarization variation after JD 2446508 or JD 2446862, in the declining branches of the polarization-time curve; but observations obtained on JD 2446007.44 may be indicative of the fact that $P(\lambda)$ curve might change direction if polarization level decreased significantly. The polarization was low just before the minimum that occurred around JD 2446025 and around JD 2446823. Hence, the qualitative agreement in the nature of wavelength dependence seen on JD 2446053.25 and during JD 2446844-45 suggests that, most probably, just before or close to the minimum of JD 2446469 also the polarization level was low. The observations of JD 2446114.28 are more immediate following a light minimum than that of JD 2446053.35 or JD 2446844.5. Hence, from the behaviour of $P(\lambda)$ curve seen during JD 2446471-508 and JD 2446844-62 one would expect a wavelength dependence on JD 2446114.28 that monotonously increased towards ultraviolet, contrary to what is actually observed. It is possible that the polarization level, and the peculiar nature of dependence of polarization and position angle on wavelength observed on JD 2446114.28 may be the result of modification of existing polarization by the changes that occurred close to the minimum of JD 2446200.

1.4.4. COMPARISON WITH O CET

In the Mira variable o Cet, the polarization is found to

increase rapidly at about the beginning of the steep part of the ascending branch of the light curve (Shawl 1975). Most probably, a similar behaviour is being seen in AR Pup also, but on a much larger scale (14.5% against 3.5% in U band). From the available data on AR Pup it is difficult to fix the exact phase at which the rapid changes begin to occur. The position angles of polarization at all wavelengths observed on JD 2446827.20 differ by more than $20°$ from that observed on the previous night. Hence, it is possible that large changes in polarization begin to occur immediately after a light minimum; the polarization probably attains a maximum value somewhere on the ascending branch of the light curve (close to (B-V) maximum ?) which then decreases slowly later. Unfortunately, no polarimetric measurements could be obtained close to the phase of (B-V) maximum.

It is quite possible that in many other Mira variables also increase in polarization occurs after the 'eruption point', the beginning of the linear and steep increase in brightness (Materne 1976), but systematic observations are lacking. It is only in the case of o Cet that the most complete set of polarization observations exists so far.

1.4.5. PATH OF POLARIZATION IN THE (Q-U) PLANE

An inspection of Figure 8 (observations obtained during JD 2446471-508) reveals that for a particular wavelength a possible correlation between the amount of polarization and position angle exist; the more the position angle departs from $100°$ the less is the percentage polarization, and it becomes very clear when the (P, θ) measurements are transformed to Stokes parameters, $Q = P \cos 2\theta$ and $U = P \sin 2\theta$. Figure 11 gives the results of such a transformation which shows that the observations in each wavelength band fall on separate near straight lines, implying a systematic variation in the physical parameters which produce the polarization. Here it is worth noting that the first set of observations, namely that obtained on JD 2446471.21, falls in the middle of each line. The straight lines drawn in Figure 11 are the least square

86
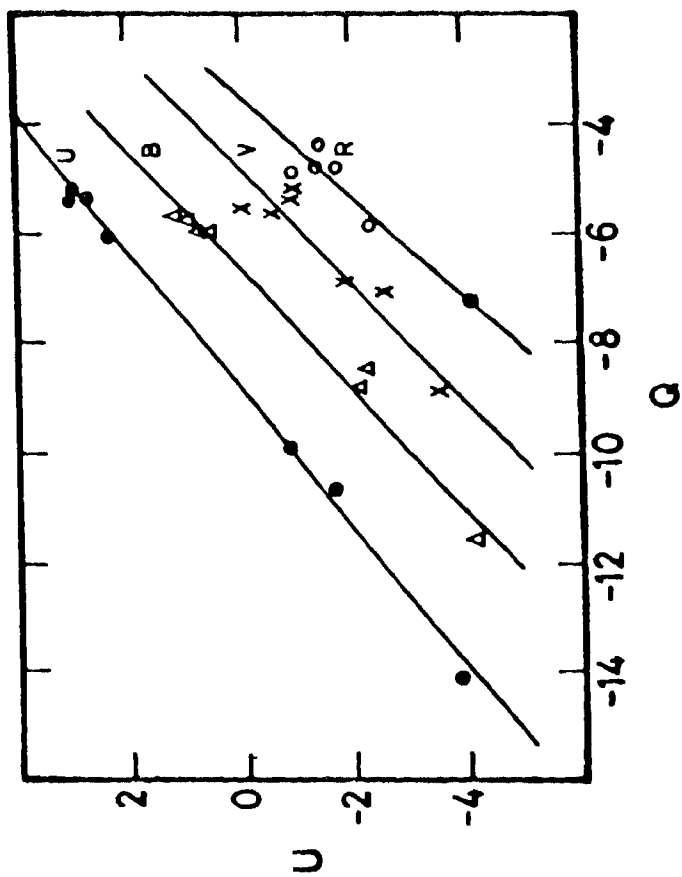
Figure 11

The path of polarization of AR Pup observed during JD 2446471-
508 in the (Q,U) plane. Note that the first set of observa-
tions fall nearly in the middle of each line.

fits for the observed (Q,U) values for each of the filter used. The slopes of the lines for U, B ,V and R are 0.78±0.02, 0.91±0.05, 0.85±0.12 and 1.00±0.11, respectively, and indicate a slow increase in the slope from ultraviolet to red.

1.5. UBVRI photometry

The V magnitudes and the various broadband colours obtained using the the PRL-polarimeter are given in Table 6. As already mentioned, it was not possible to devote much time in improving photometric accuracy because of the very limited telescope time available. The main sources of error in the measurements were the transparency variations during the observations. The uncertainty in V is ~ 0.1 mag and those in the colours are ~ 0.06 mag. The above values were estimated from the internal consistency in the individual measurements of standard stars. A comparison of the V and (B-V) data given in Table 6 with that given in Table 3, wherever observations overlap, shows differences of the order mentioned above.

The V magnitudes given in Table 6, also plotted in Figures 4 and 5 (open circles), are found to lie systematically above the mean curves constructed from the AAVSO visual data.

Preston et al. (1963) have found that RV Tauri stars, typically, execute elongated loops in the (U-B), (B-V) plane. The observations of AR Pup given in Table 6 are plotted in Figure 12 in the (U-B), (B-V) plane. No correction for interstellar reddening, which is expected to be negligible compared to the observational error (section 1.4.1.), is made. Whenever possible, more accurate values of (B-V) given in Table 3 are taken. The solid line is the locus for Ib supergiants, taken from Fernie (1963). Equivalent Ib spectral types are indicated across the top. The limited available observations are not sufficient to construct the path traced during the pulsational cycle; but AR Pup is seen to lie in the region occupied by stars of spectroscopic group B, in the position corresponding to earlier spectral types in relation to group A.

UBVRI photometry of AR Pup.

JD 2446000+	V	U-B	B-V	V-R	R-I
007.44	9.10	-	0.51	0.54	0.42
052.43	9.19	0.32	0.82	0.64	0.50
053.35	9.27	0.46	0.78	0.55	0.56
114.28	9.25	0.20	0.73	0.60	0.61
471.27	10.03	-	-	0.72	-
472.27	-	0.62	-	-	-
478.17	9.87	0.57	0.89	0.62	-
503.20	9.50	0.56	0.76	0.51	-
504.20	9.48	0.58	0.88	0.56	-
505.18	9.54	0.62	0.82	0.55	-
508.16	-	0.72	1.01	0.64	-
826.23	-	0.30	0.74	0.62	0.38
827.20	9.19	0.25	0.71	0.53	0.41
844.18	9.04	0.56	0.74	0.77	0.46
845.22	9.08	0.60	0.78	0.80	0.52
861.25	9.52	0.48	0.90	0.56	0.51
862.19	-	0.56	0.85	0.67	0.38

Table 6
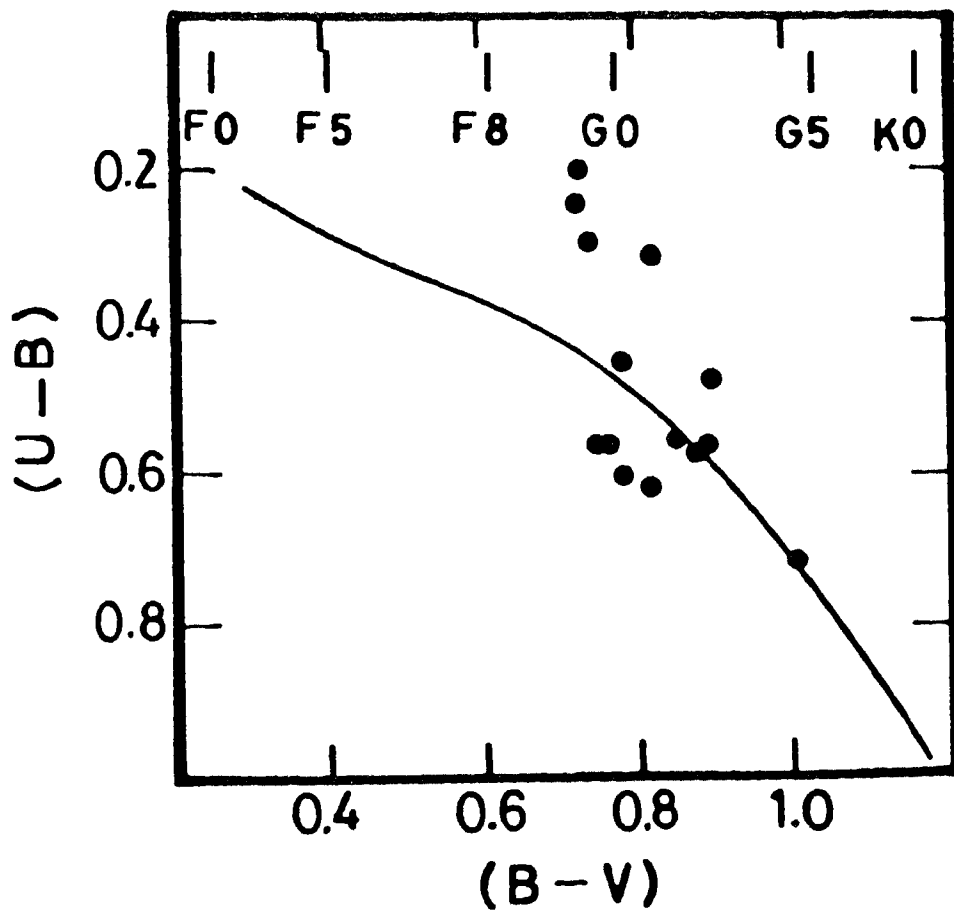
AR Pup in the (U-B), (B-V) plane. The solid
line is the locus for Ib supergaints. Equi-
valent Ib spectral types are indicated across
the top.

Figure 12

2. AC Herculis

The RV Tauri star AC Her has a period of 75.4 day between two consecutive deep minima. The presence of strong bands of CH and CN in the optical region was first reported by Rosino (1951). Preston et al. (1963) subsequently placed it in the spectroscopic group B, defined by them. From an analysis of high dispersion spectrograms obtained at well-distributed light phases, Baird (1981) found AC Her to be a metal-poor, carbon-rich star. He found that the carbon abundances derived from C I and CH lines are mutually inconsistent, and suggested that AC Her is surrounded by a substantial cloud of circumstellar gas where many of the molecular lines and some of the low excitation atomic lines originate.

Henson, Kemp & Kraus (1985) obtained polarimetric observations of AC Her in B band over one complete light cycle, and found that the light and polarization changes are strongly correlated, with the maximum of polarization occurring just after the primary light minimum. Though their study clearly demonstrated how polarization varies over the light cycle, information on the wavelength dependence was lacking.

2.1. Polarimetry

AC Her was observed polarimetrically on 24 April 1985 in BVRI bands. The results are given in Table 7 and are plotted in Figure 13. From the figure it is clear that the dependence of polarization on wavelength is rather weak; there is only a marginal increase towards blue. This is consistent with the results which Henson, Kemp & Kraus (1985) obtained from the very limited simultaneous measurements they had in B and V bands. From Figure 13, it is also clear that the position angle of polarization is essentially independent of wavelength; however, there is an indication of a shallow dip $(2-3^\circ)$ in the V-R region.

UBVRI polarimetry of cepheids and RV Tauri stars.

Star/JD 2446000+	U P%	θ°	B P%	θ°	V P%	θ°	R P%	θ°	I P%	θ°
V 553 Cen										
118.39	1.00±0.45	15±13	0.30±0.17	176±16	0.28±0.09	49±9	0.31±0.12	163±9	0.08±0.09	-
RU Cam										
116.34	0.55±0.62	-	0.40±0.14	162±10	0.25±0.05	154±5	0.27±0.07	168±8	0.31±0.04	172±4
RU Cen										
115.35	1.26±0.65	55±15	1.63±0.20	71±3	1.10±0.11	62±3	0.95±0.12	59±4	0.92±0.10	54±3
471.36	0.67±0.19	55±8	0.88±0.07	53±2	0.89±0.06	51±2	0.89±0.09	52±3	-	-
503.23	1.67±0.22	67±4	1.79±0.12	66±2	1.26±0.08	64±2	1.05±0.13	60±3	-	-
826.49	1.78±0.28	55±4	1.24±0.09	53±2	0.85±0.07	50±2	1.00±0.13	50±4	-	-
861.48	1.19±0.43	0±10	0.83±0.12	30±4	0.76±0.08	31±3	0.81±0.11	35±4	-	-
862.49	-	-	1.30±0.09	41±2	1.02±0.08	43±2	-	-	-	-
SX Cen										
862.46	1.08±0.72	27±19	0.37±0.15	51±11	0.49±0.08	55±5	0.50±0.14	52±8	0.45±0.39	-
AC Her										
180.40	-	-	0.67±0.06	37±3	0.48±0.05	32±3	0.47±0.06	33±4	0.40±0.05	40±4

Table 7

92
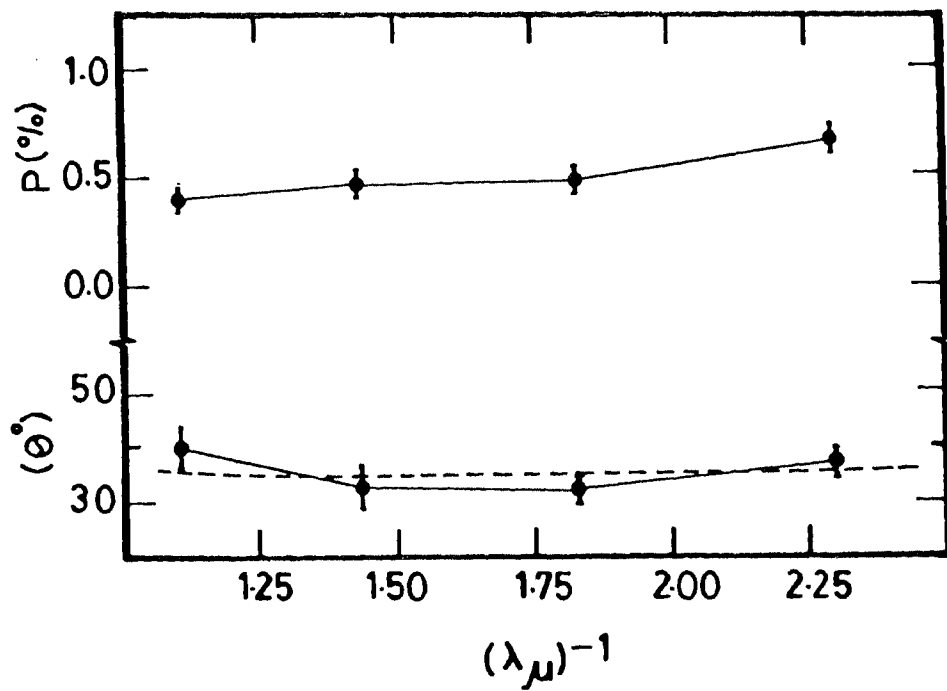
Plot of linear polarization (P%) and position angle ($\theta°$)
of AC Her against the inverse of the effective wavelength
of observation. The dashed line represents the mean position
angle.

Figure 13

93

2.2. Interstellar component of polarization

The normalized Stokes parameters of interstellar and intrinsic polarization add approximately as (Dyck, Forbes & Shawl 1971)

$$(Q/I)_o = (Q/I)_\iota + (Q/I)_I$$

$$(U/I)_o = (U/I)_\iota + (U/I)_I,$$

where o, ι, and I refer to the observed, intrinsic and interstellar quantities, respectively. At low polarization levels

$$Q_o = Q_\iota + Q_I \qquad \qquad \text{.... (4)}$$

$$U_o = U_\iota + U_I. \qquad \qquad \text{.... (5)}$$

The position angle and linear polarization observed are

$$\theta_o = 1/2 \, \tan^{-1}(U_o/Q_o) = 1/2 \, \tan^{-1}\{(U_\iota + U_I)/(Q_\iota + Q_I)\}$$

$$P_o = (Q_o^2 + U_o^2)/I = \{(Q_\iota + Q_I)^2 + (U_\iota + U_I)^2\}^{1/2}/I.$$

Hence, when the intrinsic and interstellar components are comparable, the modulation of the intrinsic component by the interstellar component should be easily seen in the observed polarization.

The interstellar reddening, E(B-V)=0.1 mag, estimated by Cardelli (1985), gives a value of $P_{max} \lesssim 0.9\%$ (using equation (2)), larger than the observed value of polarization. Henson, Kemp & Kraus (1985) have suggested a similar value ($\sim 1.0\%$) for the interstellar component. Most likely, the interstellar component of polarization is much less than this; otherwise by the arguments presented above either a rotation of the plane of polarization with wavelength, or a maximum in the $P(\lambda)$ curve that is typical of the interstellar polarization, or both should have been observed. The only exception to this would be when the intrinsic polarization has the same position angle as the interstellar component and the particular

94

wavelength dependence required to cancel the modulation by the interstellar component; this possibility is very unlikely. An indirect indication of a negligible contribution by the interstellar component to the observed polarization in AC Her is the near identical wavelength dependences of polarization seen in AC Her and a similar carbon-rich RV Tauri star RU Cen (section 3.2.) which is unreddened (Eggen 1986).

With $E(B-V)=0.1$, the empirical relation (3) gives $\lambda_{max} = 0.552\mu m$; i.e., the maximum effect of interstellar component will be felt in the V band. Hence, the shallow dip $(2-3^{\circ})$ in the position angle in the V-R region seen in Figure 13 may be the effect of the interstellar component. The position angles in B and I are essentially the same, indicating that the interstellar contribution at these bands is negligible. Assuming that the effects of interstellar polarization in P and θ in I band are of the order of observational errors, the maximum possible value for the interstellar component at this band turns out to be $P(\text{I band}) \sim 0.07\%$. The empirical relation (Serkowski, Mathewson & Ford 1975)

$$(P/P_{max}) = exp \{-1.15 \ln^2 (\lambda /\lambda_{max}) \} \qquad \ldots \ldots (6)$$

gives $P_{max} \sim 0.1\%$, peaking in V band. Most probably, the observed polarization is not affected by this much amount; otherwise, a hump or dip would have been seen in the $P(\lambda)$ curve at V band; but it could cause a decrease of $\sim 3^{\circ}$ in θ if the position angle of interstellar polarization is $\sim 170^{\circ}$.

Accurate polarimetry over still longer wavelength base line is needed to assess the contribution of the interstellar component to the observed quantities more exactly.

2.3. Regularity in the polarimetric behaviour

One of the classification criteria for the membership of RV Tauri group is the interchange of the primary and secondary minima (section I-2.2.). From an analysis of 587 primary and secondary minima, Erleksova (1984) has reported that no shallow minima were found at the phases of primary minima, and

that the deepest secondary minimum never reached the depths of the primary ones, contrary to the general belief (Payne-Gaposchkin, Brenton & Gaposchkin 1943; Kukarkin et al. 1969; Baird 1981).

The times of primary minima estimated from the American Association of Variable Star Observers' data (Mattei 1986, private communication), obtained around the times of polarimetric observations plotted in Figure 13, are found to satisfy the ephemeris

$$\text{Min I} = \text{JD } 2445231.7 + 75.^{d}46 \text{ E} \qquad \dots \text{ I}$$

given by Henson, Kemp & Kraus (1985). According to this, the polarimetric observations fall on the ascending branch ($\phi = 0.^{P}57$) of the light curve after a secondary minimum. A plot of the AAVSO data, shown in Figure 14, confirms this; the time of polarimetric observations is indicated in the figure by an arrow.

The values of P% and θ° in B bands estimated from the plots of Henson, Kemp & Kraus (1985) are 0.45±0.1 and 25±6. These values are only marginally different from that observed by us when we consider the fact that θ varies from 22° to 55° and P reaches as high as 1.4%. Shawl (1975) has reported a set of observations at inverse effective wavelengths, $2.17\mu m^{-1}$ (B) and $1.87\mu m^{-1}$ (V), obtained on JD 2440699 (22 April 1970). The phase computed using ephemeris I is $\phi = 0.^{P}93$. From·a revision of the photographic observations of AC Her presented by Payne-Gaposchkin, Brenton & Gaposchkin (1943), Erleksova (1984) has given the following ephemeris

$$\text{Min I} = \text{JD } 2435052 + 75.^{d}439 \text{ E} \qquad \dots \text{ II}$$

which gives a phase $\phi = 0.^{P}86$ at JD 2440699.0. From the plots given by Henson, Kemp & Kraus (1985), it is found that in the phase interval $0.^{P}86 - 0.^{P}93$, P% and θ° are 0.55±0.1 and 45±5, very close to the values of 0.40±0.04 and 41±3 given by Shawl (1975).

The agreement in the values of polarization and position

96
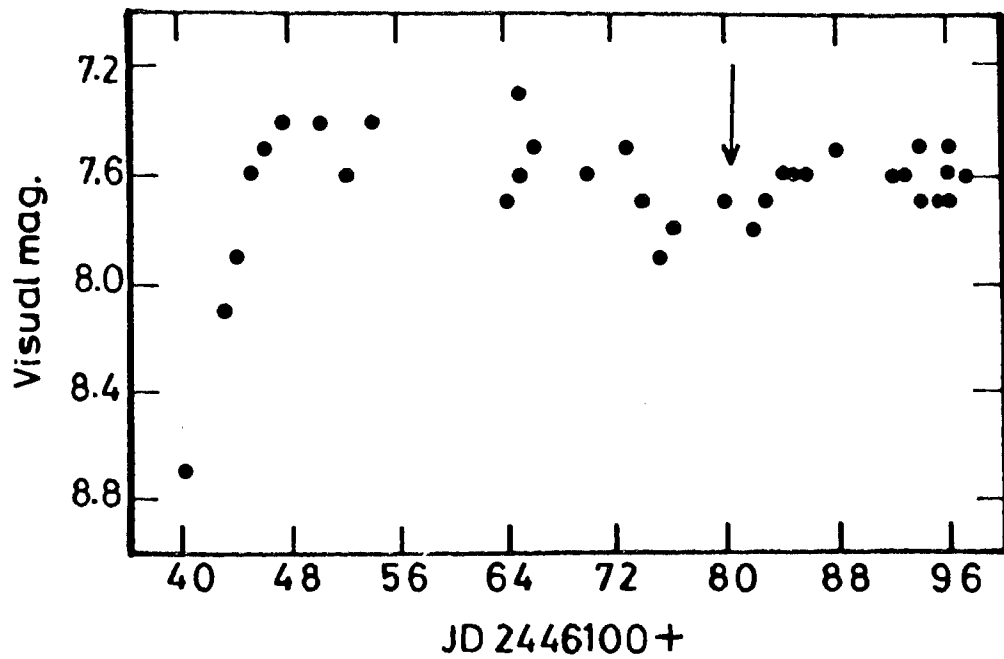
Plot of AAVSO visual data of AC Her against the corresponding
Julian day of observation. The arrow indicates the time of pola-
rimetric observations.

Figure 14

angle obtained at largely separated epochs indicates that the behavior of polarization of AC Her is also probably regular like its (B-V) colour curve (Cardelli 1985). However, small changes in the amount of polarization from cycle-to-cycle are reported by Henson, Kemp & Kraus (1985).

3. RU Centauri

Although discovered in 1896, it was only after more than 60 years RU Cen finally got the definite classification as an RV Tauri star (O'Connell 1961). In the early years of its discovery it was considered to be a cepheid (Shapley & Walton 1927; Shapley & Payne 1930) and later as an eclipsing binary of β Lyrae type (Hertzsprung 1928; Gaposchkin 1953). Previous to the publication of O'Connell's (1961) paper, Rosino (1951) had already included RU Cen in his list of 25 RV Tauri stars then known. RU Cen has a period of 64.7 days and its mean brightness is found to be nearly constant, typical of an RVa type star.

In a survey of RV Tauri and related objects, Gehrz & Ney (1972) found that the infrared spectrum of RU Cen in the 2.2-22μm region is extremely similar to that of AC Her, and hence suggested that like AC Her, RU Cen is also carbon-rich and so would show up strong CH and CN bands in the optical spectrum. The close resemblances in the optical spectra of RU Cen and AC Her had already been reported by Bidelman (O'Connell 1961); but it was not then known whether RU Cen also goes through a stage of strong CH and CN bands during its light cycle. In an investigation of the suggested correlation between the infrared and photographic spectra of RV Tauri stars (Gehrz & Ney 1972), Lloyd Evans (1974) reported the presence of strong bands of CH in the optical region and classified RU Cen as a spectroscopic group B star on the system of Preston et al. (1963).

During the period February 1985-March 1987, RU Cen was observed polarimetrically on 6 nights - one night in UBVRI, four nights in UBVR and one night in BV bands. Reliable

98

magnitudes and colours of RU Cen could not be derived on all nights of observation because of poor sky conditions. Whatever values could be derived, with uncertainties around 0.06 mag, are given in Table 8.

3.1. Photometric phases

Even though there are large differences in the depths of minima, especially of secondary minima, the times of minima observed during the years 1925-51 (over 143 cycles) satisfy a 64.727 day period (O'Connell 1961). Systematic deviations from the calculated times occur in the observed times of minima; however, the deviations are smaller (extreme range for primary minimum is from $6.^{d}1$ to $-3.^{d}9$) than those of all other RV Tauri stars so far studied in detail, except AC Her. The available extensive photographic observations indicate that there are periods when the light curve has little fluctuations for several successive cycles. This, probably, is the reason for mistaking RU Cen as a cepheid and an eclipsing binary.

Recently, Eggen (1986) has reported the photometry of RU Cen which contains a well-observed primary minimum that occurred in early 1981. The estimated time of its occurrence is JD 2444633.8, and the expected time calculated from the ephemeris

$$\text{Min I} = 2428015.51 + 64.727^{d}\ E$$

given by O'Connell (1961) is JD 2444650.35, around 16.5 days after the actually observed time. Definitely, the difference is not due to any accumulated effect of an error in the period, because if the period is decreased to P=64.663 day to satisfy the recently observed time of minimum, the residuals of the old times are found to increase systematically with cycle count from the chosen starting epoch.

Table 8, gives the photometric phases at the times of polarimetric observations, computed using the ephemeris

$$\text{Min I} = 2444633.8 + 64.^{d}727\ E,$$

Photometric phases and colours of RU Cen.

JD 2446000+	Phase	U-B	B-V	V-R	R-I
115.35	22.89	-	1.03	0.59	0.63
471.36	28.39	0.49	0.79	0.52	-
503.23	28.88	-	1.12	0.70	-
826.49	33.88	-	1.04	0.65	-
861.48	34.42	-	-	-	-
862.49	34.43	-	-	-	-

Table 8

where the initial epoch corresponds to the minimum mentioned before. Since the period of light variation of RU Cen is fairly stable, as found by O'Connell (1961), the maximum possible error in the computed phases is expected to be ~ $0.^{P}1$.

At the minimum of the narrow band colour curve, (b-y)=0.60 mag (Eggen 1986) which with the relation (1) corresponds to (B-V)=0.95 mag. Eggen's data indicates that (b-y) leads the V curve by ~ $0.^{P}08$, similar to that observed in other RV Tauri stars. The actual error in the computed phases given in Table 8 may be less than $0.^{P}1$, since the values of (B-V) are in satisfactory agreement with that expected at the minimum of the (B-V) curve that occurs close to $0.^{P}9$.

3.2. Wavelength dependence of polarization

Values of P% and θ° of RU Cen given in Table 7 are plotted in Figure 15. It is clear that both the amount and position angle of polarization show significant changes with time. As in the case of AC Her, the dependence of polarization on wavelength is very weak; there is only a slight increase towards ultraviolet. The position angle is essentially independent of wavelength.

By the same arguments presented in the case of AC Her, from the near flat dependence of P and θ on λ, the possibility of any contribution by the interstellar polarization to the observed quantities is ruled out. The reddening E(B-V)=0.15 for RU Cen, assumed by Goldsmith et al. (1987), is probably too high. Using the results of narrow band photometry of neighbouring stars, Eggen (1986) has suggested that the interstellar reddening for RU Cen is negligible (E(B-V) ~ 0.0); the polarization observations are consistent with this suggestion.

3.3. Dependence of polarization on position angle

It is seen from Table 8 that the polarimetric observations are spread over 12 cycles and the phase coverage is poor; three observations are obtained close to $0.^{P}9$ and the other
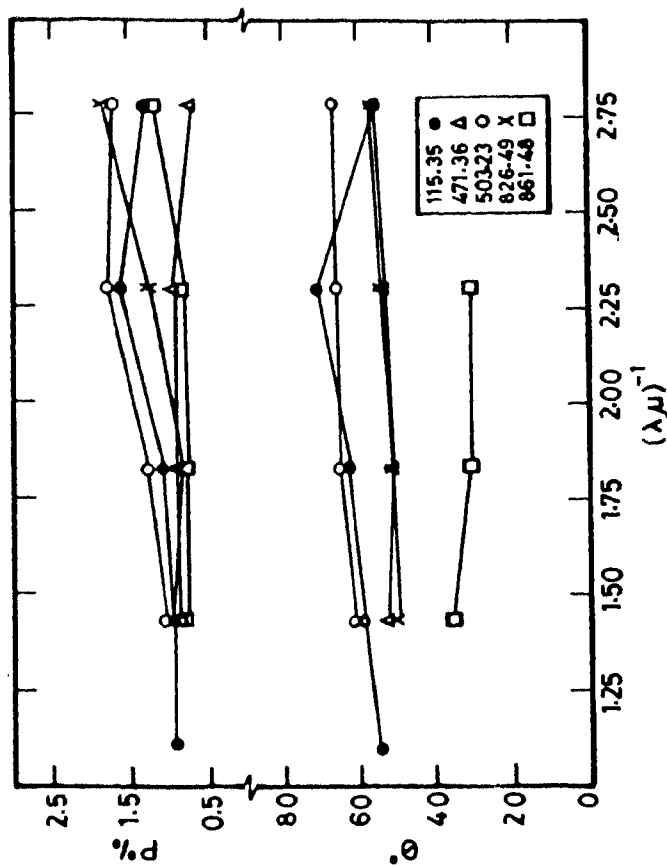
Plot of linear polarization (P%) and position angle (θ°) of RU Cen against the corresponding inverse of the effective wavelength of observation.

Figure 15

three close to 0.^{P}4. From the limited available data, it is difficult to estimate the amplitude of polarization variation, but it is not expected to be significantly larger than 1.0%.

The P% and θ° of RU Cen given in Table 7 reveal a possible correlation between the changes in polarization and position angle, in the sense that an increase in polarization is always accompanied by an increase in position angle. This is evident if the data obtained during a particular light cycle is considered. In Figure 16 the values of P obtained in V band are plotted against θ. Though the available observations are only a few in number, a clear correlation is indicated, which attains more significance when it is realized that data obtained during different light cycles are combined. The path of polarization in the (Q,U) plane (Figure 17) is probably elongated along a particular axis as found in the case of AC Her by Henson, Kemp & Kraus (1985). Similar behaviour is seen in all wavelength bands; the V observations were chosen for illustration because of the relatively smaller observational errors.

4. SX Centauri

Among the one hundred or so objects with the RV Tauri classification (Kukarkin et al. 1969), SX Cen has the shortest period of 32.8 days between two consecutive deep minima. The mean brightness of SX Cen varies with a period of 615 days (O'Connell 1933). Because the near infrared broadband spectrum was similar to that of RV Tauri, Gehrz & Ney (1972) suggested that like its prototype, SX Cen is also oxygen-rich. However, observations by Lloyd Evans (1974) showed that SX Cen belongs to the carbon-rich spectroscopic group B.

SX Cen was observed polarimetrically on 7 March 1987 in UBVRI bands. The data given in Table 7 is plotted in Figure 18. The uncertainties in U and I bands are comparable to the polarization values themselves; however, values in BVR bands, where the observational errors are much less, clearly show that SX Cen exhibits significant polarization.

103
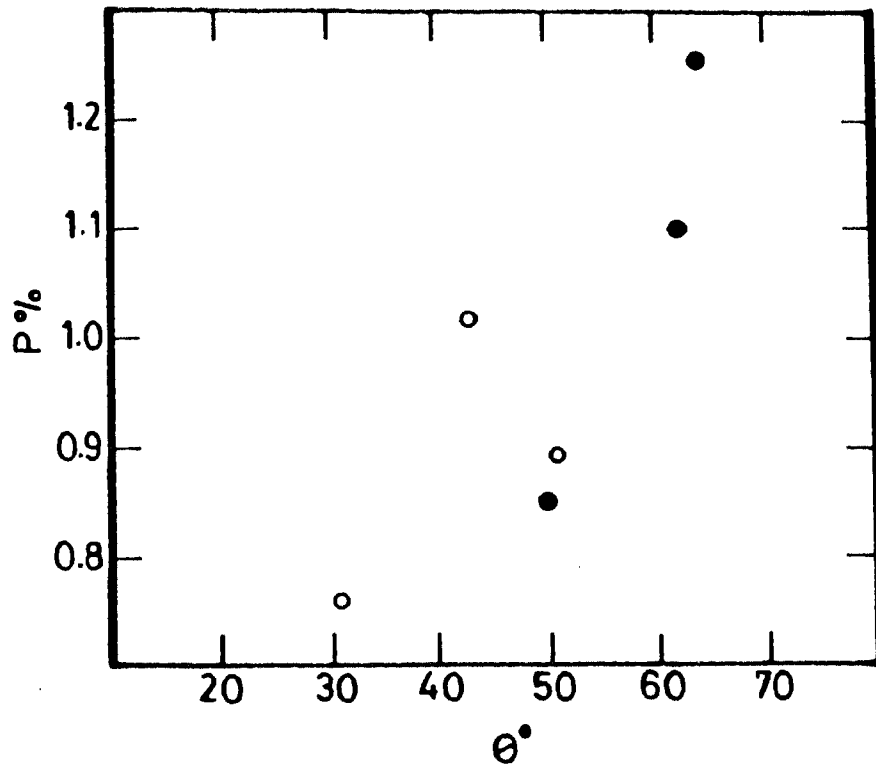
Plot of polarization of RU Cen in V band against the corresponding position angle. Open and filled circles represent the observations obtained close to 0.°4 and 0.°9, respectively.

Figure 16
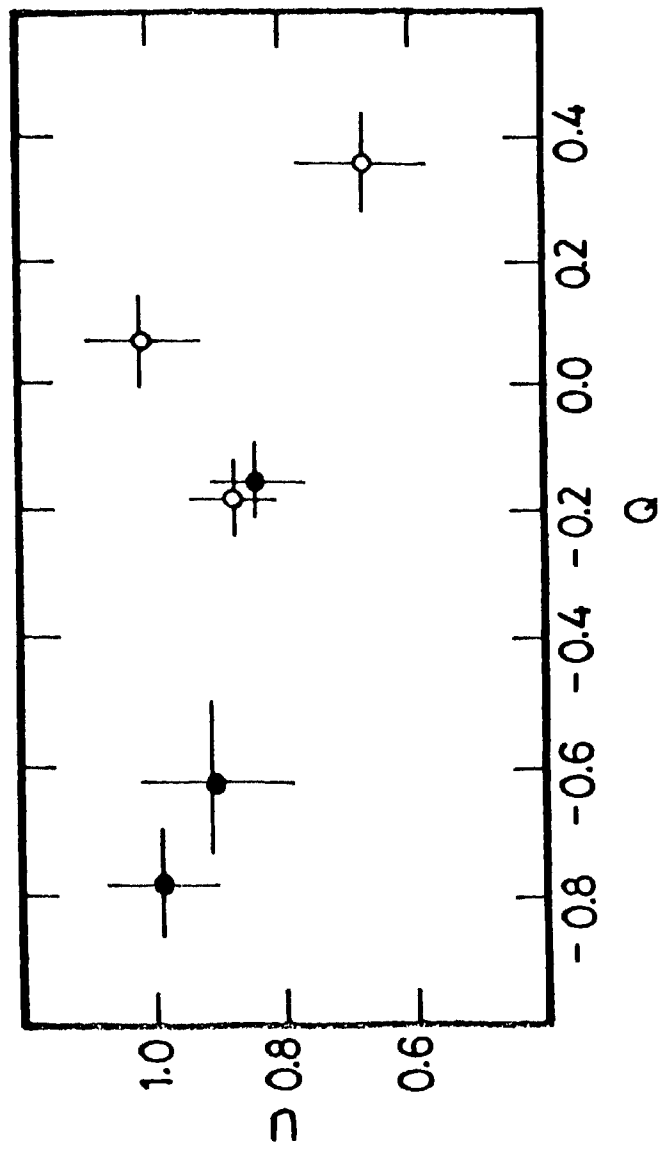
Path of polarization in V band of RU Cen in the (Q,U) plane.
Open and filled circles represent the observations obtained close
to $0^p.4$ and $0^p.9$ respectively.

Figure 17
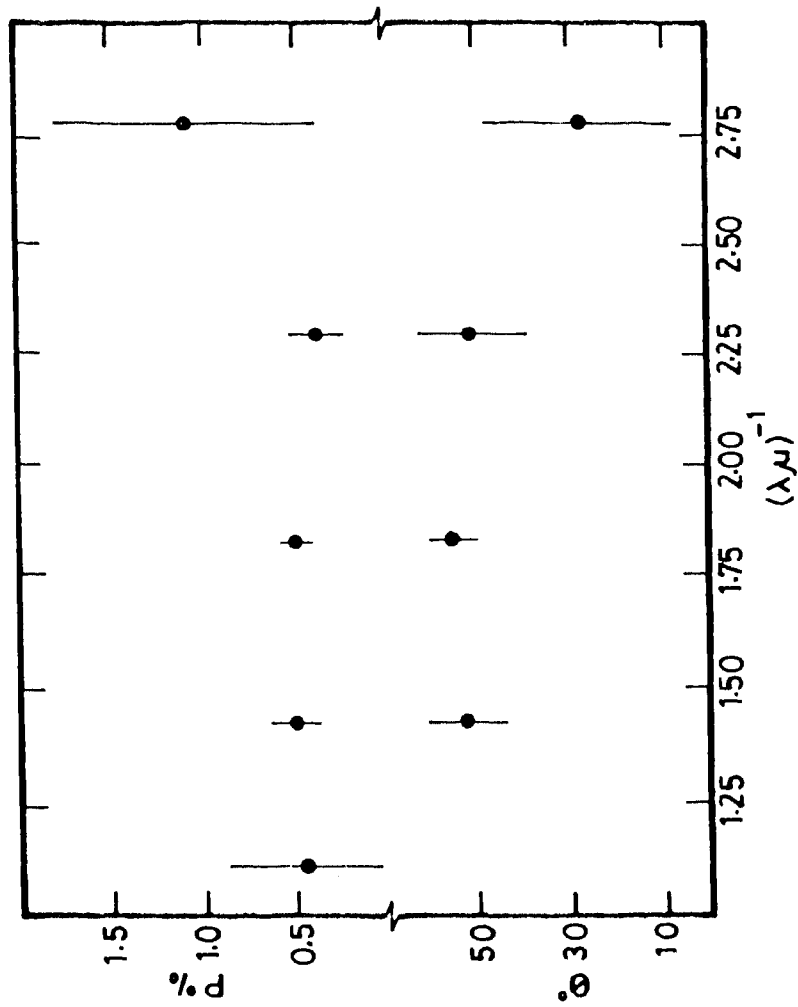
Plot of linear polarization (P%) and position angle
(θ°) of SX Cen against the corresponding inverse of
the effective wavelength of observation.

Figure 18

The interstellar reddening for SX Cen assumed by Dawson (1979) and Goldsmith et al. (1987), E(B-V)=0.25 and 0.15, respectively, are probably high. In the sky, SX Cen is only a few degrees away from RU Cen (see section 3.2.), and hence the interstellar reddening is expected to be small. Recently, Eggen (1986) has derived a value of E(b-y)=0.06 for SX Cen. From the relation given by Crawford (1975)

$$E(b-y) = 0.73 \ E(B-V),$$

we arrive at E(B-V)=0.08, and the maximum possible value for the interstellar component of polarization is $P_{max} \leq 0.7\%$ (from equation (2)) for SX Cen. But the near flat wavelength dependence of both the amount and position angle of polarization, and its close similarity with that of the other carbon-rich and interstellar polarization-free RV Tauri stars AC Her and RU Cen, indicate that the contribution by the interstellar component to the observed polarization is negligibly small. More accurate polarimetry is needed to assess the interstellar contribution exactly.

5. RU Camelopardalis

No other star similar to the 22.1 day period W Virginis type star RU Cam is known; though the changes in period and amplitude of light variation, which are the characteristics of Type II cepheids, were known to occur, it was a surprise when Demers & Fernie (1966) reported the near cessation (amplitude ~ 0.1 mag) of its light variation. Prior to 1964, the amplitude of light variation was around 1.0 mag. The sudden change in amplitude was initially thought to be part of a cyclic variation (Detre 1966), but ever since the star has remained in the low state. Extensive photometry by Broglia, Conconi & Guerrero (1978) during the years 1973-78 shows that RU Cam has essentially maintained the same amplitude and mean brightness, and that the period, which was nearly constant before 1964, shows instability without any systematic fluctuations. The more recent AAVSO observations (Mattei 1986,

private communication) also show that the amplitude of light variation of RU Cam is very small. RU Cam shows strong bands of C_2 and CN in the optical spectrum (Gauzit 1959). The carbon characteristics were discovered by Sanford (1928).

RU Cam was observed on 19 February 1985 in UBVRI bands. The results are given in Table 7 and plotted in Figure 19. It is clear from the figure that the position angle depends on wavelength, with a dip in θ occurring around the V band. In view of the rather high colour excess E(B-V)=0.36, quoted by Michalowska-Smak & Smak (1965), the interstellar contribution to the observed polarization is expected to be significant.

Assuming that the intrinsic polarization in V and I bands are nearly the same, as seen in the case of AC Her, RU Cen and SX Cen, which are nearly unaffected by the interstellar medium, the interstellar and hence the intrinsic component of polarization can be estimated. From equations (3) and (6), it is found that the interstellar polarization probably peaks in V band and that P(I band)=0.76 P(V band). If there is a systematic change in the size and direction of alignment of grains along the line of sight, a rotation of position angle of interstellar polarization results. Most of the stars polarized by interstellar medium do not show such an effect, indicating that the combination of anomalies in the magnetic field which aligns the grains, and in the particle size, is not encountered frequently in the galaxy (Coyne 1974). RU Cam is located at a fairly high latitude (b=+29°), and hence it is reasonable to expect that the position angle of interstellar component of polarization is wavelength independent. Hence, using equations (4) and (5),one can write

$$Q_{i,v} + Q_{I,v} = Q_{o,v} \quad ; \quad U_{i,v} + U_{I,v} = U_{o,v}$$

$$Q_{i,v} + 0.76\ Q_{I,v} = Q_{o,I} \quad ; \quad U_{i,v} + 0.76\ U_{I,v} = U_{o,I},$$

where the second subscripts refer to the wavelength bands of observation. Solving the above equations, interstellar polarization in V band turns out to be 0.76±0.26% and the
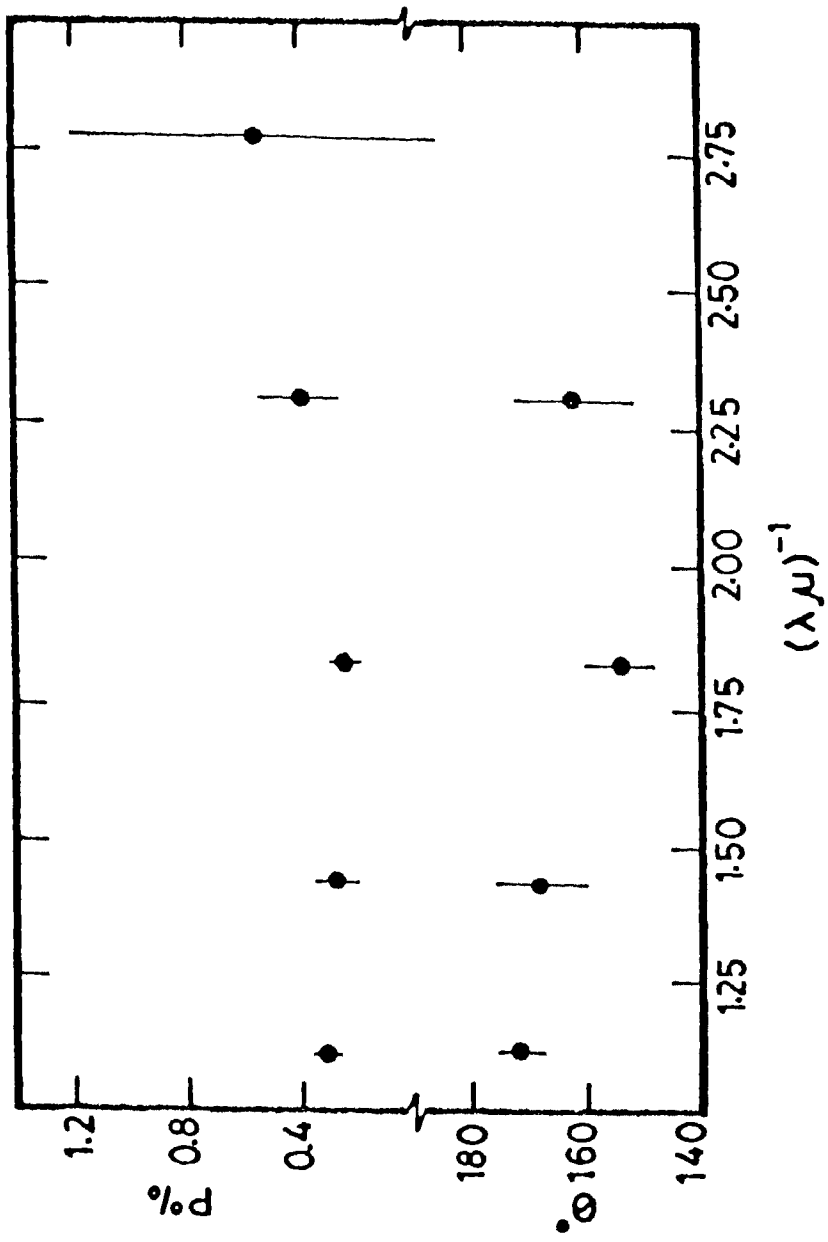
Plot of linear polarization (P%) and position angle (θ') of RU Cam against the corresponding inverse of the effective wavelength of observation.

Figure 19

109

corresponding position angle, 109±10°.

Polyakova (1984) has given a value of 0.23% for the interstellar polarization towards RU Cam; it can be in error because of the following reasons.

(i). He used no filters for the polarimetric observations; since the interstellar polarization is wavelength dependent, the effective wavelength of observation is uncertain.

(ii). The variable polarization shown by cepheids is found to trace a three-lobed figure in the (Q,U) plane. Polyakova's ad hoc assumption that the radius vector of interstellar component points to the base of the three-lobed figure so traced may not be valid, because it implies that at the base of the figure the intrinsic polarization vanishes. His conclusion is based on a very limited sample with indirectly assumed interstellar component of polarization. For example, he assumed that in the case of W Vir the interstellar polarization is zero because of its high galactic latitude (b=+58°). But the interstellar component may be appreciable because of the fairly large colour excess E(B-V)=0.25 derived for this object (Michalowska-Smak & Smak 1965). With P=0.76% and θ=109° for the interstellar component, the observed polarization implies that the corresponding values for the intrinsic component in V band are 0.80 and 9°. A couple of polarimetric observations of RU Cam were obtained by Schmidt (1958) when the amplitude of light variation was ~ 1.0 mag; it is interesting that the position angles given in Table 7 are not very much different from the mean value (θ=161°) obtained by him.

6. V553 Centauri

The 2.06 day period cepheid-like variable V553 Cen was discovered by Hoffmeister, and its spectral peculiarities similar to carbon stars were first noted by Herbig (Hoffmeister 1957). Lloyd Evans, Wisse & Wisse (1972), who made a detailed study of the object, found that the strong C_2, CH and CN bands show pronounced variation with the light

110

phase. They suggested that the carbon-rich star V553 Cen probably belongs to the old disc population. Cottrell (1979) has reported that the overall metal abundance, except for carbon and nitrogen, in this object is nearly solar.

Polarimetric observations of V553 Cen were obtained on 21 February 1985 in UBVRI bands. The results are given in Table 7 and are plotted in Figure 20. Since the instrument did not function properly on that night, the observational errors are quite high, and hence it is difficult to make any definite conclusions. Possibly, there is a change in position angle with wavelength. Lloyd Evans, Wisse & Wisse (1972) find that a comparison of the broad band colours of V553 Cen with those of non-variable supergiants yields E(B-V)=0.14, which they further find in satisfactory agreement with that calculated from the cosec formula (b=+25°; E(B-V)=0.08) of Arp (1962). As a result of appreciable reddening, the interstellar polarization is expected to be not negligible. Definitely, more accurate polarimetry is needed for V553 Cen.
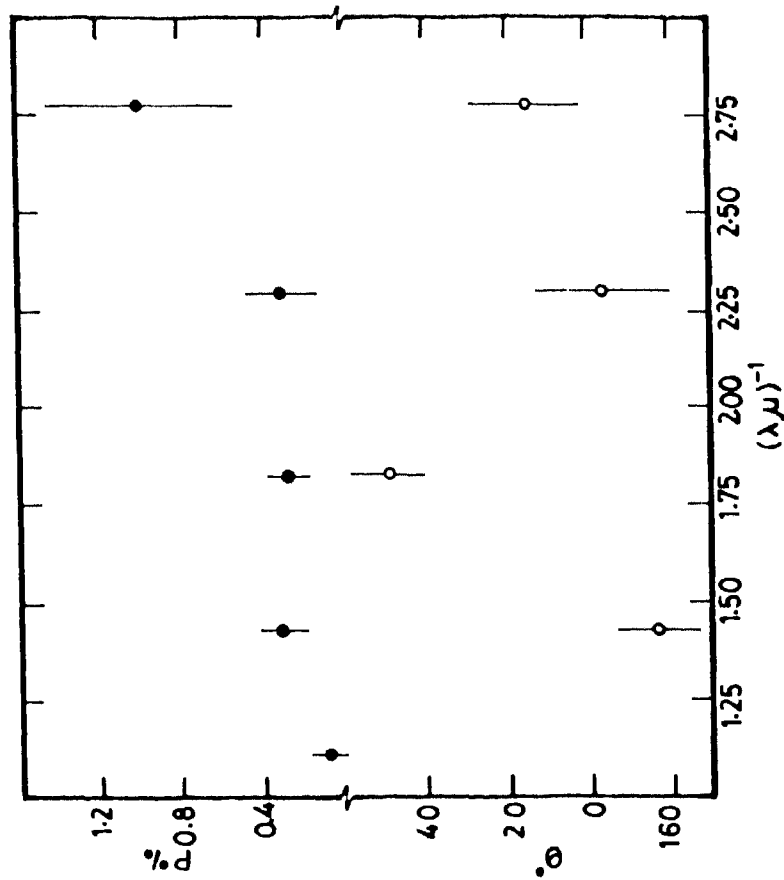
Plot of linear polarization (P%) and position angle (θ°) of V553 Cen against the corresponding inverse of the effective wavelength of observation.

Figure 20

112

B) CARBON STARS

Some of the basic data on the programme stars, taken from Kukarkin et al. (1969), are listed in Table 9. Representative objects belonging to the various variability types were included in the observational programme. A few of the objects for which polarization measurements are reported were included because for these objects, in addition to wavelength dependence, information on time dependence can also be obtained. The main criterion which governed the selection of the objects was that they should be conveniently placed in the sky during the prime observing months - December to April - at Kavalur.

All the objects except Y Hya have been detected in 12, 25 and 60μm passbands in the far infrared by the IRAS and most of them even at 100μm, indicating the presence of extended cool dust envelopes around them. A part of the emission at 12μm may be from the photosphere while at 100μm there may be considerable contamination by the infrared cirrus (Low et al. 1984). The flux density data taken from the IRAS Point Source Catalogue (Beichman et al. 1985) is given in Table 10 along with the corresponding IRAS identification number.

1. Polarimetry

Observations were obtained in BVRI bands during 1984-87 period, and the results are given in Table 11 and plotted in Figures 21 and 24-27. Since the nature of wavelength dependence of polarization observed is different from that expected due to the interstellar medium alone, it is obvious that all the stars are intrinsically polarized.

The salient results of polarization measurements of each object are described in the following sections, and comparisons with the previously published results are made

113

Basic data on the carbon stars.

Star Name	Galactic latitude	Variability type	Period (days)	Spectral type
VX And	-18	SRa	369	N7(C4,3)
UU Aur	+14	SRb	235	N3(C5,4)
T Cae	-40	SR	156	N4(C6,4)
Y CVn	+72	SRb	158	N3(C5,4)
U Hya	+38	SRb	450	N2(C7,3)
Y Hya	+24	SRb	303	N3p(C5,0)
R Lep	-31	M	432	N6e(C7,6e)
RY Mon	0	SRa	466	R(C4,8)
W Ori	-23	SRb	212	N5(C5,3)
Y Per	-10	M	252	C4, 3e
RT Pup	-4	SRb	100	C6, 2
X Vel	+10	SR	140	Nb

Table 9

IRAS data on the carbon stars.

	NAME	Flux in Jansky			
Variable	IRAS	12μ	25μ	60μ	100μ
VX And	00172+4425	52.79	15.42	3.99	1.94
UU Aur	06331+3829	232.06	71.11	18.36	9.74
T Cae	04455-3617	13.47	3.14	0.65	< 1.00
Y CVn	12427+4542	276.26	70.32	16.99	7.51
U Hya	10350-1307	205.50	72.37	16.98	14.06
R Lep	04573-1452	379.48	116.35	25.88	8.82
RY Mon	07045-0728	58.90	17.01	4.88	18.53
W Ori	05028+0106	183.77	51.64	14.03	6.04
Y Per	03242+4400	4.50	1.60	0.70	< 1.42
RT Pup	08035-3837	7.02	2.03	0.59:	< 10.53
X Vel	09533-4120	88.62	24.99	5.92	2.77

Table 10

115

BVRI polarimetry of carbon stars.

Star/JD 2446000+	B		V		R		I	
	P %	θ°	P %	θ°	P %	θ°	P %	θ°
VX And								
056.14	0.57±0.37	37±18	0.58±0.04	70±2	0.44±0.04	62±3	0.34±0.02	71±2
UU Aur								
056.21	0.55±0.07	176±4	0.41±0.02	172±1	0.56±0.08	2±4	0.44±0.03	178±2
118.31	0.52±0.08	138±4	0.70±0.03	166±1	0.54±0.02	160±1	0.15±0.02	177±3
T Cae								
055.21	0.25±0.18	179±20	0.15±0.06	7±11	0.19±0.06	171±8	0.13±0.03	168±6
Y CVn								
117.48	0.05±0.04	-	0.01±0.01	-	0.01±0.02	-	0.00±0.01	-
U Hya								
471.38	0.89±0.12	69±4	0.44±0.01	67±1	0.36±0.02	69±1	-	-
Y Hya								
115.25	0.10±0.11	-	0.10±0.04	26±11	0.19±0.02	10±3	0.07±0.01	9±4
R Lep								
055.19	0.60±0.15	57±7	0.73±0.03	50±1	0.60±0.04	46±2	0.51±0.02	52±1
117.16	0.29±0.24	-	0.54±0.04	41±2	0.52±0.03	49±2	0.44±0.01	52±1
470.11	1.05±0.21	71±6	0.56±0.04	46±2	0.68±0.06	39±2	-	-
826.18	0.48±0.15	179±9	0.59±0.03	39±1	0.93±0.04	51±1	1.37±0.07	48±1
RY Mon								
054.35	0.35±0.28	-	0.24±0.07	165±8	0.22±0.06	156±7	0.12±0.04	160±8
116.30	0.60±0.34	59±16	0.25±0.05	146±6	0.14±0.04	6±7	0.11±0.02	171±5
827.23	0.55±0.14	153±7	0.28±0.03	154±3	0.22±0.04	138±5	0.21±0.05	152±7
W Ori								
054.33	0.03±0.11	-	0.15±0.04	129±7	0.08±0.03	125±11	0.03±0.02	122±12

Table 11

| Star/JD 2446000+	B		V		R		I	
	P%	θ°	P%	θ°	P%	θ°	P%	θ°
Y Per								
055.09	0.64±0.46	10±21	0.97±0.13	120±4	0.94±0.09	108±3	0.81±0.05	126±2
117.13	1.86±0.61	101±9	0.85±0.09	117±3	0.76±0.09	121±2	0.68±0.04	116±2
RT Pup								
505.20	0.68±0.06	62±3	0.86±0.04	51±1	0.95±0.05	57±2	-	-
X Vel								
115.28	0.24±0.21	-	0.29±0.03	1±3	0.51±0.04	178±2	0.36±0.02	4±1

Table 11 (cont'd)

117

wherever possible. Information on the light curve around the times of polarimetric observations is derived from the AAVSO visual data (Mattei 1986, private communication).

1.1. R Leporis

The carbon Mira R Lep has a period of 432 days and a very late spectral type. The first polarization measurement of this object was made by Serkowski (1966), and since the observed value was much in excess of the expected interstellar polarization at its galactic latitude ($b=-31°$), he suggested that it is of either stellar or circumstellar origin. Further polarimetric observations were obtained by Kruszewski, Gehrels & Serkowski (1968) in B and V bands on six nights spread over 300 days. Their data did not show any obvious correlation of polarization with the visual brightness of the star, and so to determine the wavelength dependence, they combined these observations with that obtained earlier in three other wavelength bands centred at 0.65, 0.84 and 0.95μm, and found that the polarization decreases towards red but shows a flat wavelength dependence in the yellow-blue region.

During the period from December 1984 to January 1987, R Lep was observed on three nights in BVRI bands and one night in BVR bands. Values of P% and $\theta°$ given in Table 11 are plotted in Figure 21 against the respective inverse of the effective wavelength of the filter band. The inset in the figure shows the mean light curve determined from the AAVSO observations; the epochs of polarimetric observations are indicated. It is clear from the figure that polarization shows significant changes, but apparently they are not directly linked to the light variation. Within the errors the first three sets of measurements show a weak wavelength dependence, with the polarization decreasing towards red in contrast to the last set of observations, obtained on JD 2446826.18 (and which coincided with a light maximum), where it increases towards red. The observations also indicate that in yellow-blue region the wavelength dependence is nearly flat and that the changes in polarization are the least in V band.

118
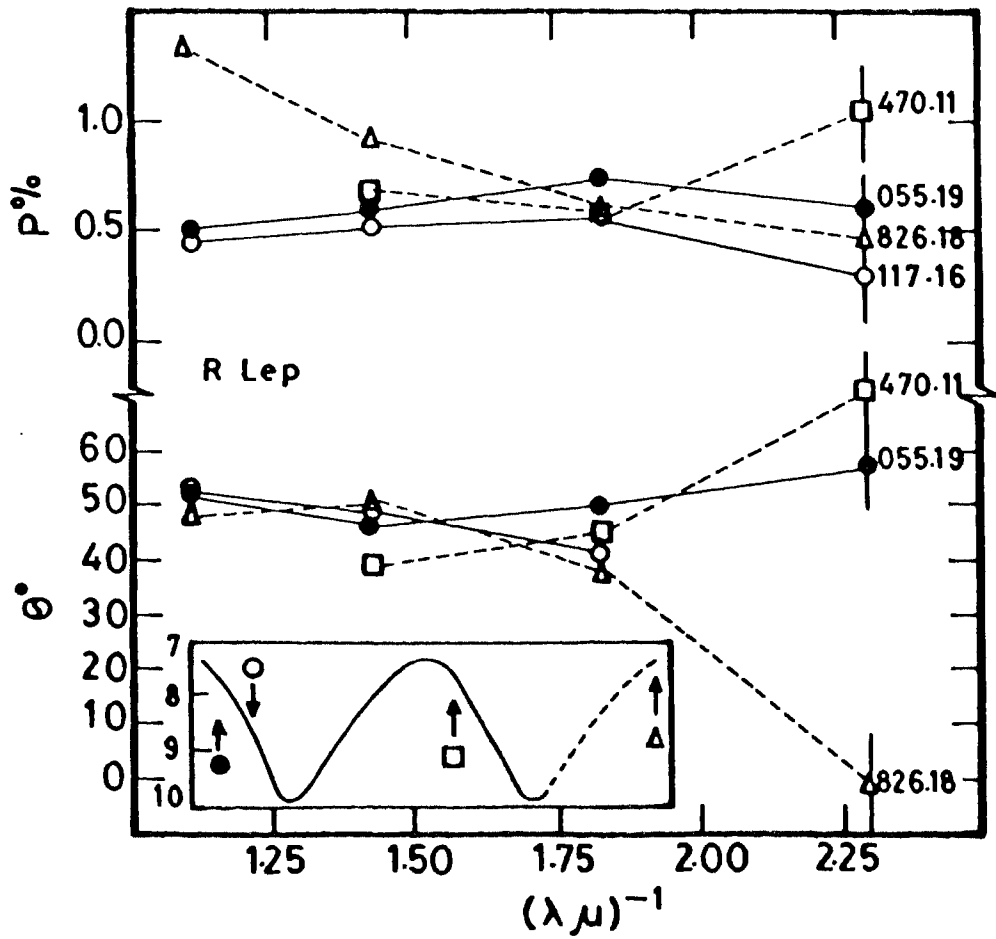
Plot of linear polarization P(%) and position angle (θ°) of
R Lep against the corresponding inverse of the effective
wavelength of the filter band. The Julian day of observation
is indicated against each curve after leaving out the first
4 digits 2446. The inset shows the mean visual light curve
determined from the AAVSO data. The ordinate gives the visual
brightness in magnitude. The epochs of polarimetric observa-
tions are shown. The dashed portion is the expected light
curve.

Figure 21

119

Position angles in VRI bands show significant but only marginal changes; however, the position angles in B show a very large scatter, consistent with the observations of Serkowski (1971). Spectropolarimetry of R Lep shows that the position angle of polarization in the blue region exhibits a large amplitude structure (Landstreet & Angel 1977; Boyle et al. 1986). R Lep has a very late spectral type and the flux blueward of $\lambda 4700A$ is very low. Hence, most probably, the scatter seen in B band is largely due to the slight differences in the effective wavelengths of observation at different epochs.

1.1.1. WAVELENGTH DEPENDENCE OF POLARIZATION

Figure 22 contains the plots of the polarization, normalized to unity at $\lambda^{-1} \approx 2.06\mu m^{-1}$, observed at different epochs. Since the differences in the polarization values are only marginal, the first three sets of observations of R Lep given in Table 11 are averaged and the mean is plotted. Similarly, the polarization in B and V bands given by Kruszewski, Gehrels & Serkowski (1968) are also averaged and combined with their earlier observations at longer wavelength bands to obtain the normalized wavelength dependence. It is evident from the figure that drastic changes have occurred in the normalized wavelength dependence since its first determination in 1967. The polarization spectrum in the region $0.5-1.1\mu m$ of R Lep obtained in the later half of 1974 by Landstreet & Angel (1977) shows that polarization decreases towards red, and probably the corresponding normalized curve would lie in between that of 1967.0 and 1985.5.

From the available data, it is difficult to conclude whether the variation in wavelength dependence is secular or with a time-scale several times the pulsational period as in the case of the semiregular variable L_2 Pup (Magalhaes et al. 1986). Because the changes in polarization are not directly linked appreciably to the light variation, the changes in the normalized wavelength dependence are not definitely cyclic with the pulsational period, as seen in the case of the oxygen
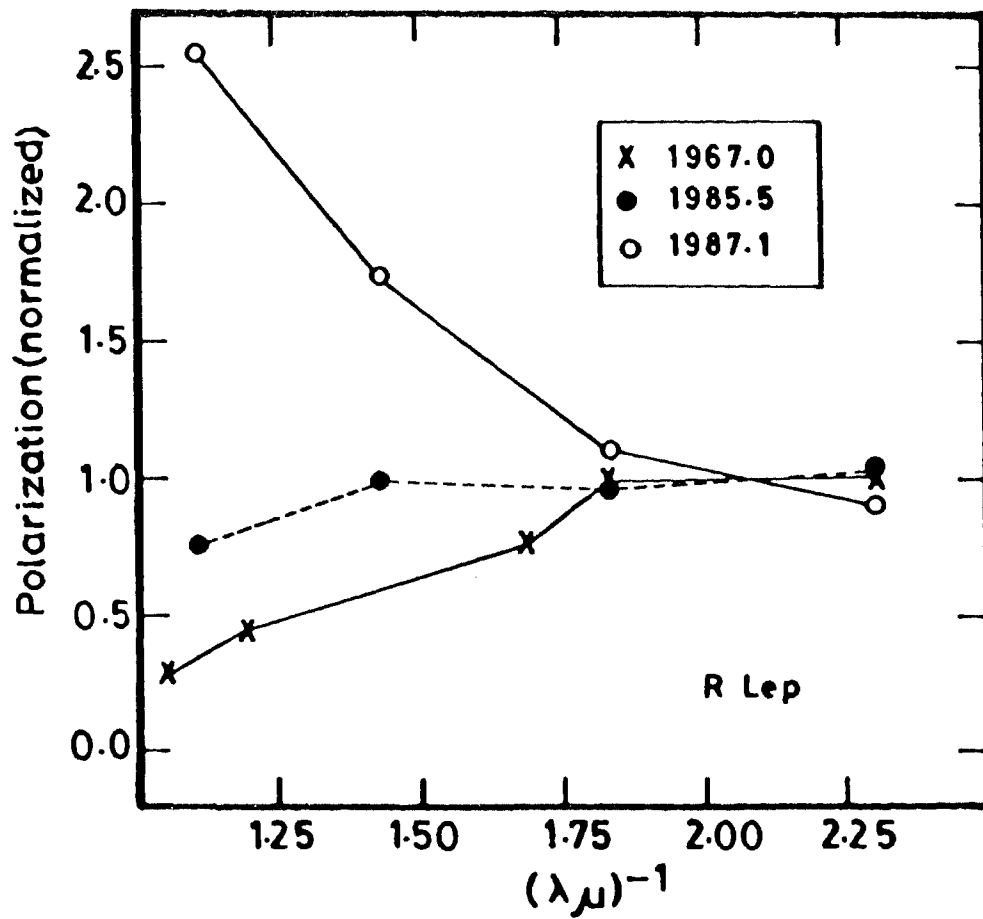
Plot of normalized wavelength-dependence of polarization of R Lep observed at different epochs. The mean epochs of observation are identified by different symbols.

Figure 22

Mira o Cet (Shawl 1975) or the RV Tauri star AR Pup (section IVA-1.4.3.)

1.1.2. POLARIZATION AND POSITION ANGLE

P% and $\theta°$ measurements of R Lep in V band obtained by Serkowski (1971) and Dyck & Sanford (1971) are plotted in Figure 23 along with those given in Table 11. The values of polarization in the region $\lambda\lambda5200-5800A$, estimated from the spectra given by Landstreet & Angel (1977) and Boyle et al. (1986), are also indicated in the figure. The data obtained during the 1966-71 period strongly suggests that the narrow dip in the polarization and the corresponding peak in position angle curves seen during 1968.5-1970.0 are transients that are superposed on more slowly varying components of the respective quantities. However, it is not clear from the data at hand whether the polarization obtained during 1984-87 is a continuation of the slowly varying component, and the comparatively low value observed in the second half of 1974 is part of a transient component, or alternatively, the polarization continued its initial near-linear trend and became low (<1.0%) sometime in 1973 and remained so since then.

1.1.3. BRIGHTNESS AT LIGHT MAXIMUM

The average visual brightness of R Lep at the light curve maximum is ~ 6.7 mag; but it was fainter than 9.3 mag during 1959-60 (Mayall 1963). The recovery from the minimum was very rapid, and by the middle of 1962 the maximum increased to ~ 7.5 mag (Mayall 1970). Most probably, the large value of polarization observed in 1966 is directly related to the faintest light maximum of R Lep ever observed. The trend of the polarization curve suggests that it had a still higher value before 1966. Unfortunately, no polarimetric data exists for R Lep prior to 1966.

Mayall (1963) has pointed out that the variation of brightness at maximum of light curve probably has a period around 40 years. There are only a few red long period variables which appear to have such large amplitude long

Figure 23
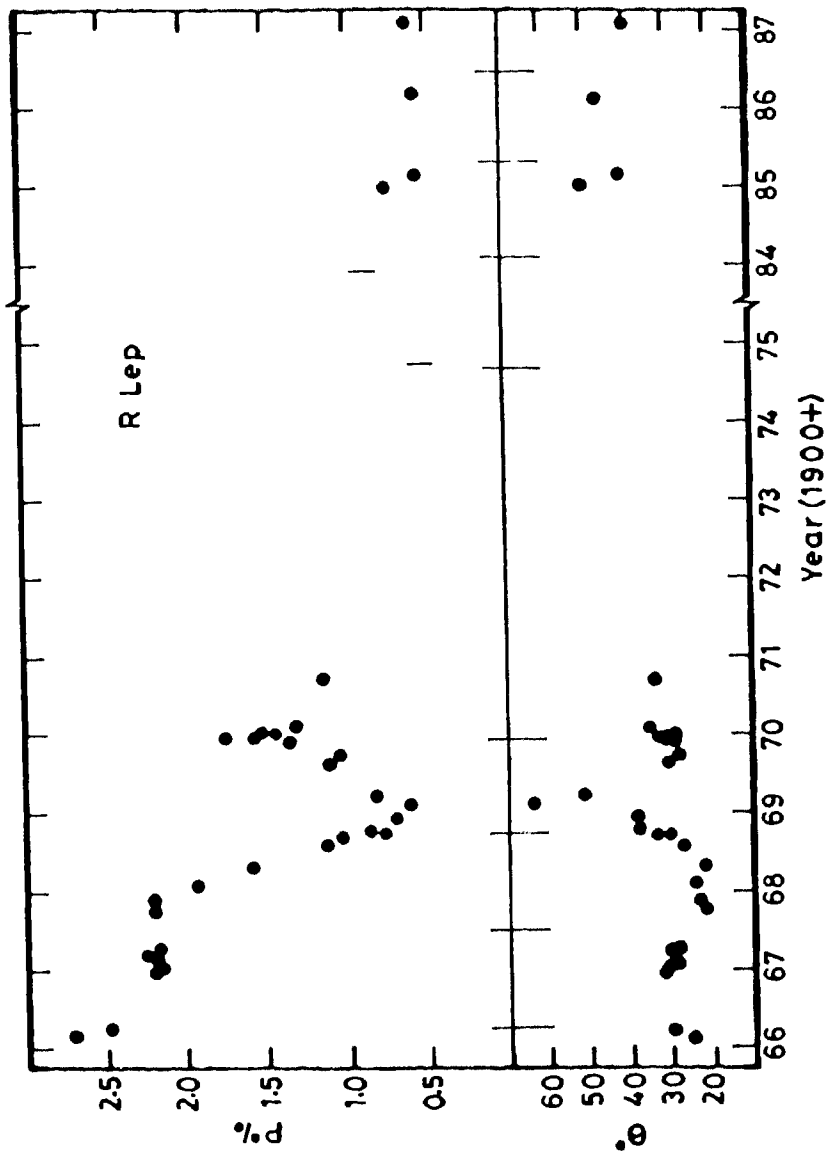
Plot of polarization (P%) and position angle (θ°) in V band against the time of observation. The short vertical lines represent spectropolarimetric observations and the big vertical lines the times of light minima. Note the break in the time axis.

123

period modulation (Mayall 1963). In the case of the carbon variable V Hya, the existence of an 18-year period is well-established (Mayall 1965). Wood (1979) has suggested that if the 18-year period corresponds to the fundamental mode pulsation, then V Hya may be on the verge of ejecting a planetary nebula and if it is not, then the long secondary period may be an indication of shell helium flashes occurring in the star.

1.2. Y Persei

The Mira variable Y Per was observed on two occasions, and the results are plotted in Figure 24 which also contains the mean light curve drawn through the AAVSO data obtained during the corresponding period. The times of polarimetric observations are indicated in the figure. The uncertainties in measurements are higher in B band because of the low photon flux. The results obtained in each band on both the occasions agree within the observational errors; but the values in VRI bands obtained close to the light minimum lie systematically below that obtained on the descending branch of the light curve. The star was fainter by ~ 0.2 mag on the former occasion. The measurements in V and B obtained by Dyck & Sanford (1971) during 1 December 1969 - 2 January 1970 are also plotted in Figure 24. The agreement in both the amount and position angle of polarization , especially in V band, is remarkable. The polarization is nearly constant in BVR spectral region, but decreases towards I band.

1.3. W Orionis

Dyck (1968) has reported polarization measurements of W Ori in V and B obtained on five nights spread over 100 days. The data, although shows a little scatter, is well within the errors of measurement, and hence there is probably no short-term variation associated with its 212 day light variation. The average values obtained by him are: $P_B=0.24\pm0.11\%$ and $P_v=0.34\pm0.09\%$ against $P_B=0.03\pm0.11$ and $P_V=0.15\pm0.04$, presently obtained. The differences in the two sets are significant, indicating a long-term variation in the
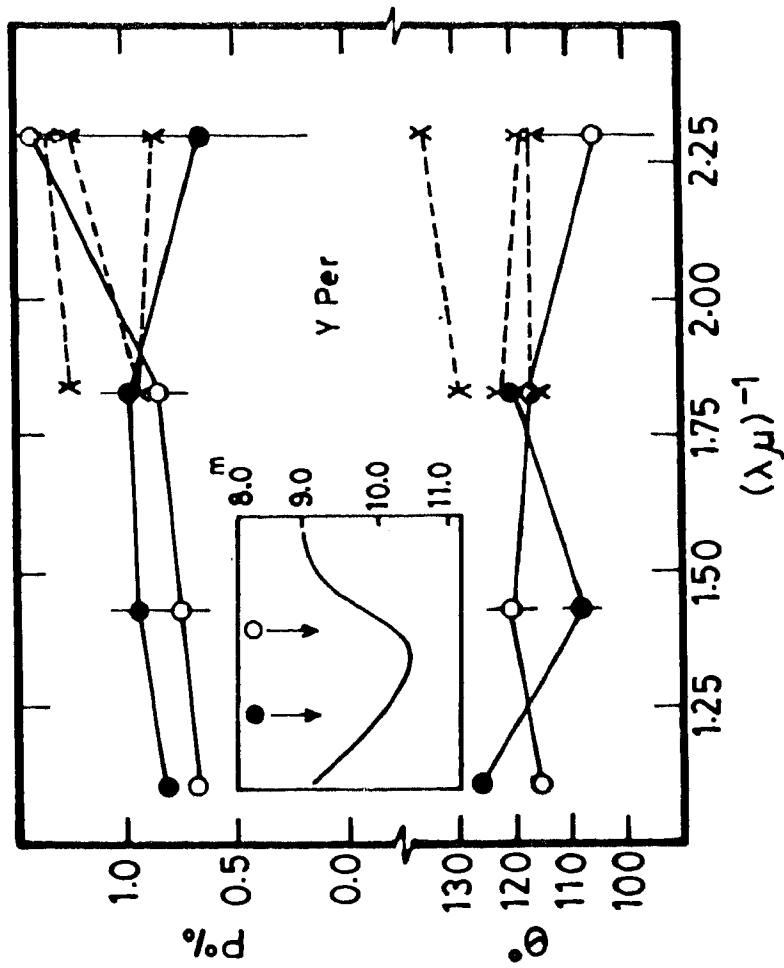
Polarimetirc observations of Y Per. The open and filled
circles represent the observations obtained on JD 2446055.09
and 117.13 and crosses that obtained by Dyck & Sanford (1971).
The inset shows the mean light curve obtained from the AAVSO
data. The arrows indicate the epochs of polarimetric obser-
vations.

Figure 24

polarization. The present very low values in all wavelength bands (Figure 26) suggest the interstellar polarization to be negligible in the direction of W Ori (b=-23°).

1.4. Y Canum Venaticorum

The polarimetric observations of Y CVn are obtained close to a light maximum, and the values are found to be close to zero at all wavelength bands. The plot of polarization in the blue spectral region of late type stars against their spectral types given by Serkowski (1971) indicates a value ~ 0.25% for Y CVn. Dyck, Forbes & Shawl (1971) have reported a polarization of 2.2% at 1.05μm, and 0.0 at 1.6μm (date of observation, 6 March 1971). If the value at 1.05μm reported by them is correct, it shows that Y CVn exhibits a large variation in polarization. The galactic latitude of the object is b=+72°. The very low polarization values listed in Table 11 indicate that the interstellar component of polarization is almost zero. More polarimetric observations are needed.

1.5. Y Hydrae

Again, Figure 1 of Serkowski (1971) indicates a value ~ 0.07% in the blue spectral region for Y Hya, and the present observations (Figure 25) agree with this. Probably, polarization peaks in the V-R region. As already mentioned, Y Hya is not detected at long infrared wavelengths by IRAS. Even though the galactic latitude is +24°, it is possible that the interstellar component of polarization in the direction of Y Hya substantially contributes to the observed polarization, and if the object is intrinsically polarized it may not be variable.

1.6. Other objects

The remaining seven objects given in Table 11 - RY Mon, UU Aur, T Cae, U Hya, VX And, RT Pup and X Vel - do not have previously reported polarization measurements in any spectral region. Only the first two were observed more than once. The observations of RY Mon (Figure 27) span over more than 750 days and do not show any appreciable change in the amount of

126
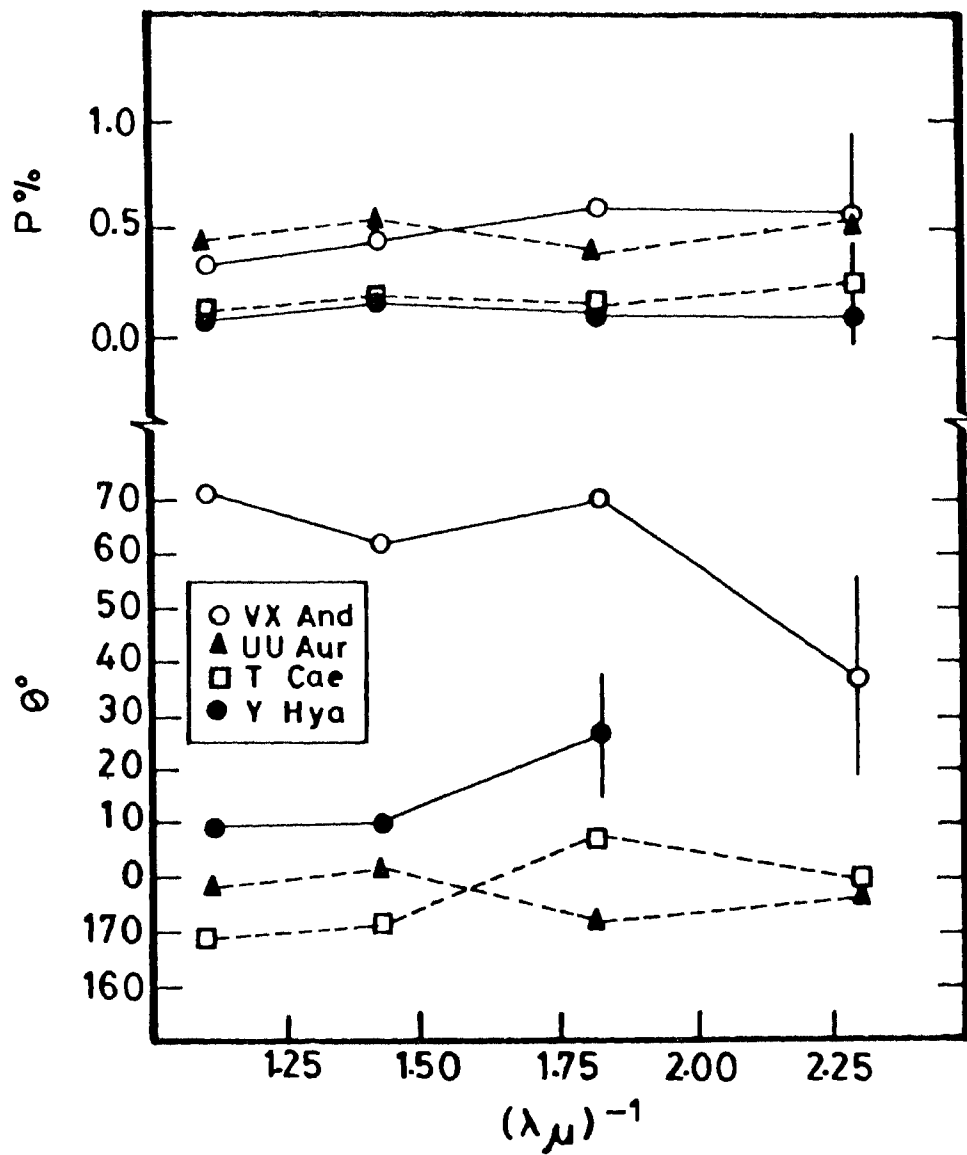
Polarimetric observations of VX And, UU Aur, T Cae and
Y Hya. To avoid confusion, error bars are given only for
the observations which show large deviations.

Figure 25
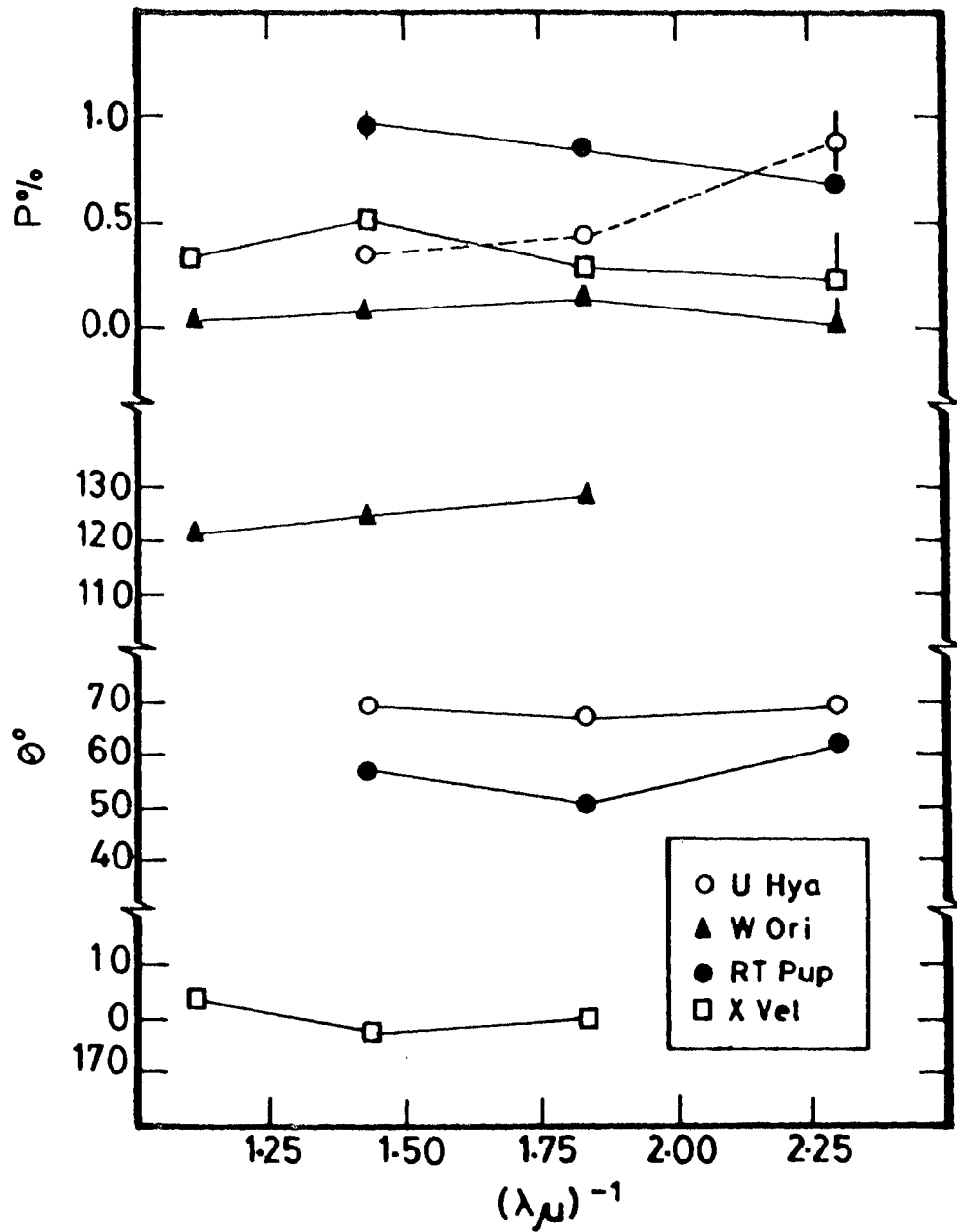
Polarimetric observations of U Hya, W Ori, RT Pup and X Vel.
To avoid confusion, error bars are given only for the obser-
vations which show large deviations.

Figure 26

polarization; however, position angles in R band show a large scatter, significantly in excess of the errors of measurement.

On the second night of observation of UU Aur, unfortunately, the instrument did not function satisfactorily. But from the results obtained, it is fairly certain that considerable short-term variations in polarization do not occur in UU Aur either.

2. Wavelength dependence of polarization

Leaving out R Lep, of the ten objects with significant polarization, it is found that the polarization increases towards red only in RT Pup. UU Aur shows a dip in the polarization curve around the V band. In X Vel, the polarization is larger in R band than in V, and probably it again increases towards blue. Apart from R Lep, only two other carbon stars - V CrB and SS Vir, both Miras - have published multi-wavelength observations. The polarization in V CrB is found to decrease towards red, whereas in SS Vir it shows a dip in the yellow region. At low levels, the distortion of the wavelength dependence of intrinsic polarization by the interstellar component would be significant. Extensive multi-band polarimetric observations by Serkowski, Mathewson & Ford (1975) show that the interstellar polarization has a peak occurring at a median wavelength $\lambda=0.545\mu m$. Hence, the maximum effect of interstellar polarization will be felt in the yellow spectral region. The wavelength dependence of polarization in SS Vir was determined when the polarization was very low (~ 0.10% in V band) and the interstellar polarization was presumed to be negligible because of its high galactic latitude (b=+63°) (Dyck 1968). Using the cosec law

$$E(B-V) = 0.058 \text{ cosec } b$$

given by Arp (1962) and the equation (2) of section IVA-1.4.1., it is found that the interstellar component towards SS Vir can have a value of P ≤0.58%. Since the dips in the polarization curves of UU Aur and X Vel, which are at
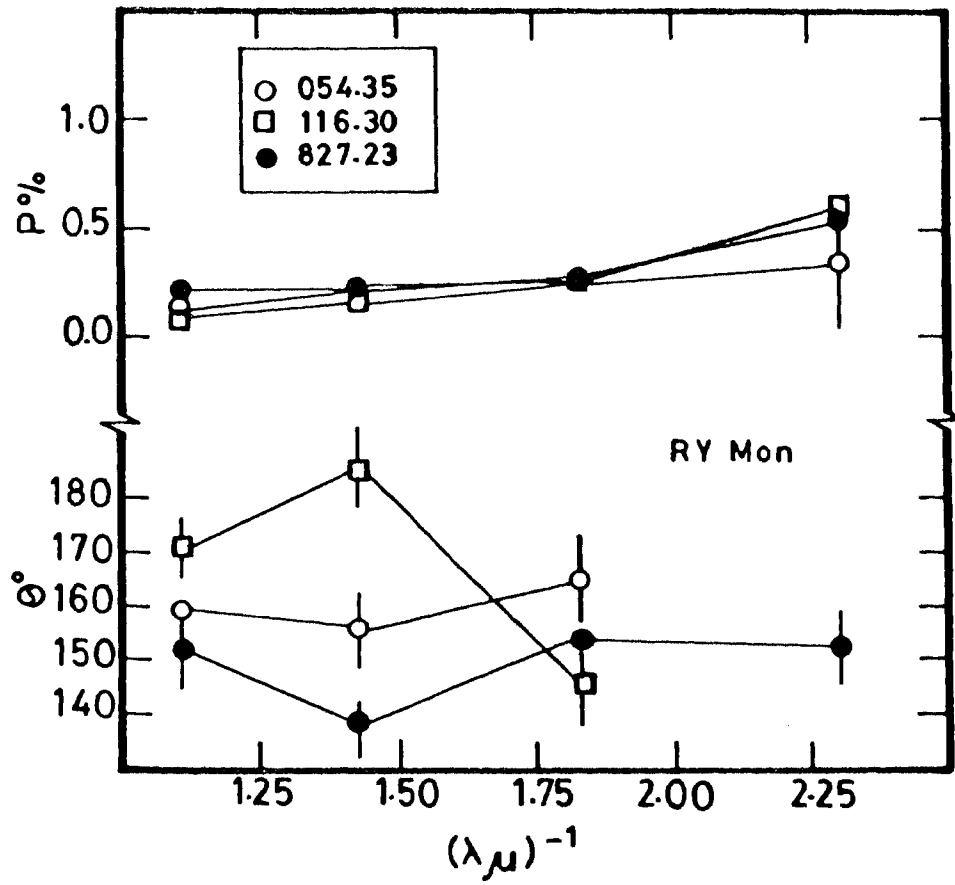
Polarimetric observations of RY Mon. Note the large scatter in position angles in the R Band.
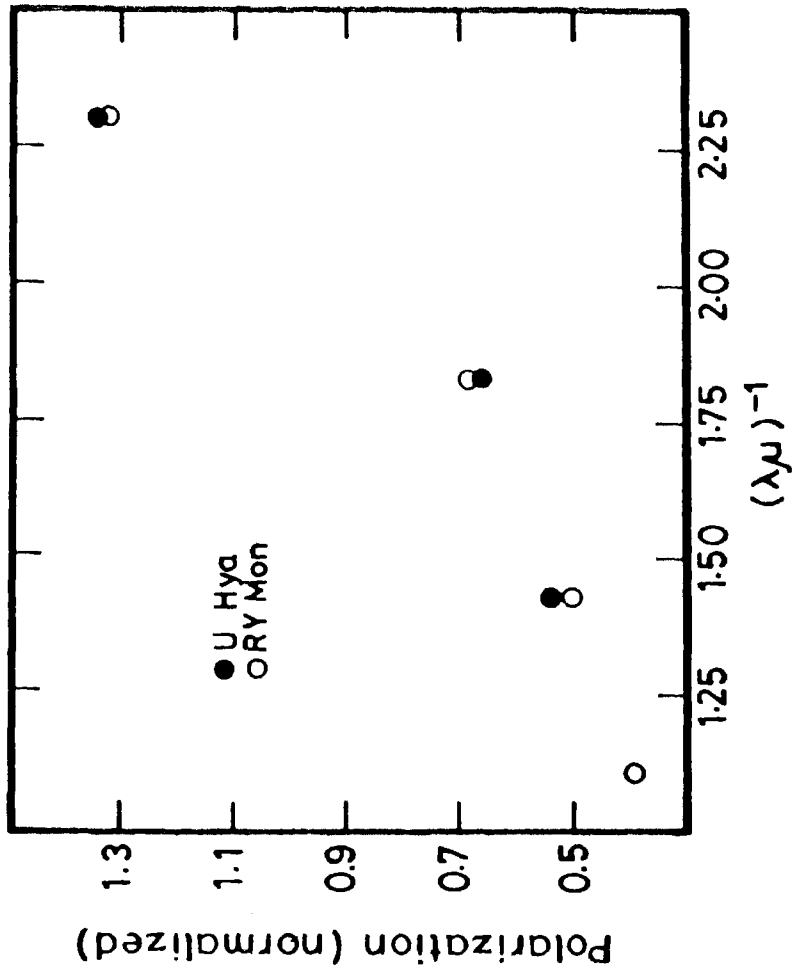
Figure 27

lower galactic latitudes, +14° and +10°, also occur around the V band, it is likely that the modulations by the respective interstellar components are appreciable and the observed wavelength dependence in these objects does not represent the intrinsic polarizations.

The normalized wavelength dependences of RY Mon and U Hya, which are at galactic latitudes, 0° and +38°, are plotted in Figure 28. The remarkable mutual agreement shows that the interstellar component in the direction of RY Mon is negligible even though it lies almost on the galactic equator.

The similarity in the wavelength dependence observed in the majority of objects indicates that in carbon stars, in general, polarization decreases towards red. A major source of scatter in the wavelength dependences observed is probably the uncertainty in the effective wavelength of observation due to the large differences in the spectra of carbon stars.

3. Comparison with oxygen-rich stars

Figure 29 shows a plot of the average of the normalized wavelength dependence (unity at $\lambda^{-1} \approx 2.06 \mu m^{-1}$) of six objects - Y Per, RY Mon, VX And, T Cae, U Hya and R Lep (excluding the last set of observations) - which show qualitatively similar wavelength dependences. Shawl (1975) has published extensive multi-band polarimetry of several oxygen-rich stars. Some of the objects like V CVn and VY CMa show very large amounts of polarization. The observed polarizations in B band in all the above mentioned carbon-rich objects do not exceed 1.0%. It would be more appropriate to compare these objects with the oxygen-rich stars which show similar amounts of polarization. The paper of Shawl (1975) contains good data on five such oxygen-rich objects - R Hya, R Boo, X Her, Z UMa and g Her - in which the observed polarizations in B band are always less than 1.5%. The first two are Miras and the rest variables of semiregular type. The averages of the normalized wavelength dependence of these objects are also plotted in Figure 29. There is a considerable scatter in the behaviour of each

131

Plots of normalized polarization of U Hya and RY Mon.
Note the close mutual agreement.

Figure 28
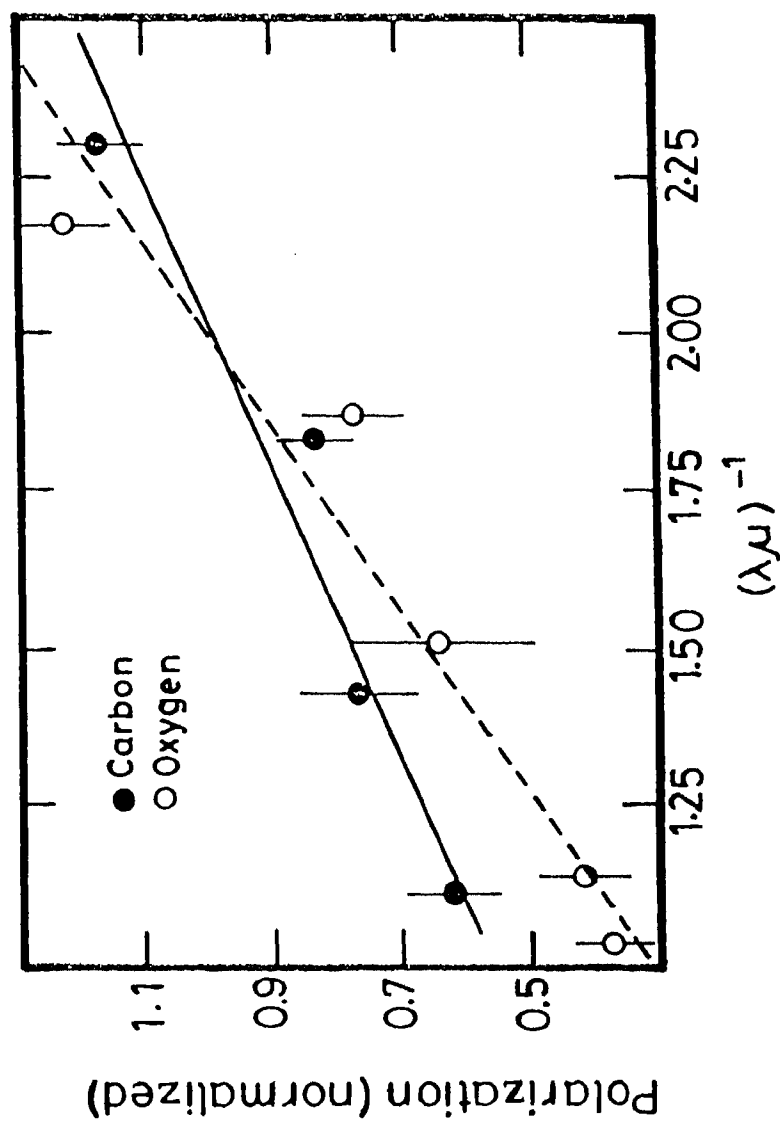
Plots of average normalized polarizations of six carbon stars and that of five oxygen-rich stars which show similar low levels of polarisation (see text). The vertical bars represent standard deviations of the mean values. The straight lines are the respective least square solutions.

Figure 29

133

object at different times. The largest scatter in the normalized polarization of oxygen-rich objects occurs in ultraviolet (Dyck & Sanford 1971; Dyck & Jennings 1971; Shawl 1975). It is interesting to see from Figure 29 that, on average, the carbon stars show a flatter wavelength dependence than the oxygen-rich objects. If only oxygen Miras are considered, then the average normalized wavelength dependence of polarization is found to be still steeper towards blue (Dyck & Sanford 1971).

V. DISCUSSION

1. Dust envelopes around RV Tauri stars

From an analysis of the IRAS data (Beichman et al. 1985) of RV Tauri stars, Jura (1986) found that the flux measurements are consistent with the dust density in the envelope varying as r^{-1}, where r is the radial distance, and suggested that the mass loss rates from RV Tauri stars have substantially decreased during the past ~ 500 years. In what follows an analysis of the IRAS data of RV Tauri stars with the help of the far infrared two-colour diagram and a grid computed using a simple model of dust envelope is presented. Such two-colour plots have already been employed extensively by several investigators to study the circumstellar envelopes around oxygen-rich and carbon-rich objects which are in the late stages of stellar evolution (Hacking et al. 1985; Zuckerman & Dyck 1986; van der Veen & Habing 1988; Willems & de Jong 1988).

Table 1 summarizes the basic data on the 17 objects detected at 60μm. Apart from the IRAS identification and the flux densities in 12, 25, 60 and 100μm wavelength bands, it gives the spectroscopic groups of Preston et al. (1963), the light curve classes of Kukarkin et al. (1969) and the periods of light variation. The list which contains about 20 per cent of all the known RV Tauri stars is essentially the same as that given by Jura (1986). The spectroscopic subgroups are either from Preston et al. (1963) or Lloyd Evans (1985).

1.1. Description of the envelope model

Assuming that the dust grains in the envelopes are largely of the same kind and are in thermal equilibrium, the luminosity at frequency ν in the infrared is given by

135

Data on the RV Tauri stars detected by IRAS.

Name		IRAS flux density (Jy)				Sp. group	period (days)	Lt. curve type	T₀K
Variable	I R A S	12μ	25μ	60μ	100μ				
TW Cam	04166+5719	8.27	5.62	1.82	<1.73	A	85.6	a	555
RV Tau	04440+2605	22.53	18.08	6.40	2.52	A	78.9	b	460
DY Ori	06034+1354	12.44	14.93	4.12	<11.22	B	60.3		295
CT Ori	06072+0953	6.16	5.57	1.22	<1.54	B	135.6		330
SU Gem	06108+2734	7.90	5.69	2.16	<11.66	A	50.1	b	575
UY CMa	06160-1701	3.51	2.48	.57	<1.00	B	113.9	a	420
U Mon	07284-0940	124.30	88.43	26.28	9.24	A	92.3	b	480
AR Pup	08011-3627	131.33	94.32	25.81	11.65:	B	75.0	b	450
IW Car	09256-6324	101.06	96.24	34.19	13.07	B	67.5	b	395
GK Car	11118-5726	2.87	2.48	.78	<12.13	B	55.6		405
RU Cen	12067-4508	5.36	11.02	5.57	2.01	B	64.7		255
SX Cen	12185-4856	5.95	3.62	1.09	<1.50	B	32.9	b	590
AI Sco	17530-3348	17.68	11.46	2.88	<45.62	A	71.0	b	480
AC Her	18281+2149	41.47	65.33	21.12	7.79	B	75.5	a	260
R Sct	18448-0545	20.88	9.30	8.10	<138.78	A	140.2	a	
R Sge	20117+1634	10.63	7.57	2.10	<1.66	A	70.6	b	455
V Vul	20343+2625	12.39	5.72	1.29	<6.96	A	75.7	a	690

Table 1

136

$$L(\nu) = \int_{envelope} \rho(r) \; Q_{abs}(\nu) \; B\{\nu, T_g(r)\} \; e^{-\tau(\nu,r)} \, dV, \ldots (1)$$

where $Q_{abs}(\nu)$ is the absorption efficiency at frequency ν, $\rho(r)$, the dust grain density, $T_g(r)$, the grain temperature, $B\{\nu, T_g(r)\}$, the Planck function and $\tau(\nu, r)$, the optical depth at distance r from the centre of the star.

The temperature $T_g(r)$ is determined by the condition of energy balance which states that the amount of energy radiated is equal to the amount of energy absorbed. The amount of energy absorbed at any point is proportional to the total available energy at that point and consists of: (i) the attenuated and diluted stellar radiation, (ii) the scattered radiation, and (iii) the re-radiation from other grains.

Detailed solutions of radiative transfer in circumstellar dust shells by Rowan-Robinson & Harris (1983,1983a) indicate that the effect of heating by other grains becomes significant only at large optical depths at the absorbing frequencies ($\tau(uv) \gg 10$), and at optical depths $\tau(uv) < 1$ do the grains have approximately the same temperature that they would have if they were seeing the starlight unattenuated and no other radiation.

The Planck mean optical depths of circumstellar envelopes around several RV Tauri stars, derived from the ratios of the luminosities of the dust shell (at infrared wavelengths) and the star, range from 0.07 to 0.63 (Goldsmith et al. 1987). There is much uncertainty in the nature and the optical properties of dust grains in circumstellar envelopes. The carbon-rich RV Tauri stars also show the 10μm emission feature typical of oxygen-rich objects (Gehrz & Ney 1972; Olnon & Raimond 1986). The pure terrestrial or lunar silicates are found to be completely unsuitable to account for the infrared emission from circumstellar dust shells around M-type stars (Rowan-Robinson & Harris 1983). In the present analysis it is assumed that the absorption efficiency $Q_{abs}(\nu)$ in the infrared varies as ν^{γ}; $\gamma=1$ appears to provide a reasonable fit in a

137

variety of sources (Harvey, Thronson & Gatley 1979; Jura 1986). Under these circumstances the condition of energy balance implies that the dust temperature T_g will vary as r^{β}.

In view of the low values of the observed Planck mean optical depth for the stellar radiation and the nature of the assumed frequency dependence of the absorption efficiency, the extinction of the infrared radiation by the dust envelope can be neglected. If the envelope is considered to be spherically symmetric, equation (1) reduces to

$$L(\nu) = \int_{r1}^{r2} 4\pi \ r^2 \rho(r) Q_{abs}(\nu) \ B\{\nu, T_g(r)\} \ dr, \qquad \dots (2)$$

where r_1 and r_2 are the inner and outer radii of the shell. For a dust density distribution $\rho(r) \propto r^{\alpha}$ and $r_2 \gg r_1$, equation (2) reduces to

$$L(\nu) \propto \nu^{2+\gamma-Q} \int_{X_0}^{\infty} \left\{ x^Q / (e^x - 1) \right\} dx, \qquad \dots (3)$$

where $Q = -(\alpha+\beta+3)/\beta$ and $X_0 = (h\nu/KT_0)$. T_0 represents the temperature at the inner boundary of the dust shell where the grains start condensing. In a steady radiation pressure-driven mass outflow in optically thin case, values of α lie near -2 (Gilman 1972). γ and β are related by $\beta = -2/(\gamma+4)$.

1.2. IRAS system of flux density

In the IRAS Point Source Catalogue (Beichman et al. 1985), the flux densities have been quoted at the effective wavelengths 12, 25, 60 and 100μm, assuming a flat energy spectrum ($\nu F(\nu)=1$) for the observed sources. If the energy distribution of the source is different from this a correction, called the colour-correction, has to be applied to the quoted flux densities to derive the true fluxes at the effective wavelengths. For this a knowledge of the intrinsic energy distribution of the astronomical source is needed.

The flux measured by a detector system is given by

$$F = f(\nu_0)[\text{actual}]\int \{ f(\nu)/f(\nu_0) \}[\text{actual}]\ R(\nu)\ d\nu$$

$$= f(\nu_0)[\text{quoted}]\int \{ f(\nu)/f(\nu_0) \}[\text{quoted}]\ R(\nu)\ d\nu.$$

Hence

$$f(\nu)[\text{actual}] = f(\nu)[\text{quoted}]\ /\ K,$$

where

$$K = (\int \{ f(\nu)/f(\nu_0) \}[\text{actual}]\ R(\nu)\ d\nu\ /$$

$$\int \{ f(\nu)/f(\nu_0) \}[\text{quoted}]\ R(\nu)\ d\nu\ ).$$

In the above equations, ν_0 is the effective frequency of a passband and $R(\nu)$ is the relative system response at frequency ν. The effective frequencies of the four IRAS passbands are 25, 12, 5 and 3×10^{12} Hz, and the relative system response at these bands are given in Beichman et al. (1985a). For each model given by equation (3), the values of K in various IRAS passbands were calculated and the fluxes were converted into flux densities expected for a flat energy distribution, as assumed in the IRAS PSC, so that the computed colours could be directly compared with the colours determined from the catalogue quantities. Such a procedure would be more appropriate than correcting the IRAS colours for the energy distribution given by a particular model and then comparing them with that computed from the model.

1.3. IRAS colour-colour diagram

The IR colour is defined as

$$[\nu_1] - [\nu_2] = -2.5 \log \{ f(\nu_1)/f(\nu_2) \},$$

where ν_1 and ν_2 are any two wavelength bands, and $f(\nu_1)$ and $f(\nu_2)$ are the corresponding flux densities assuming a flat energy spectrum for the source.

In Figure 1, the [25]-[60] colours of RV Tauri stars are plotted against their corresponding [12]-[25] colours, derived
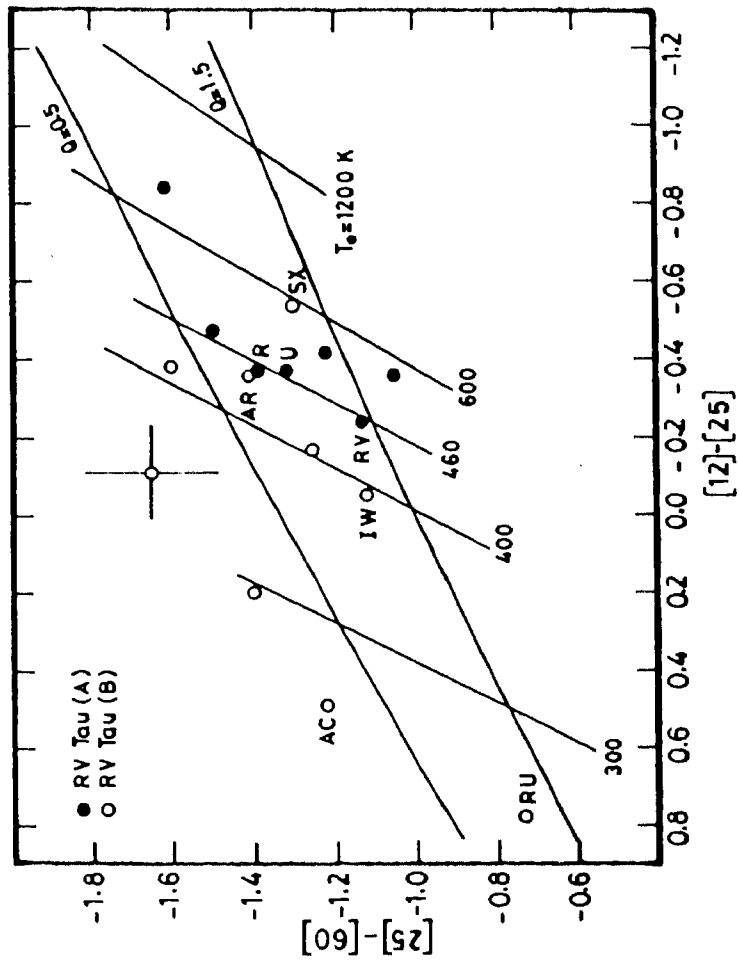
Plot of [25]-[60] colours of RV Tauri stars against their [12]-[25] colours. Some of the objects are identified by their variable star names. Typical error bars are indicated. The lines represent the loci for constant inner shell temperature and the quantity Q. Note the separation of group A and B stars at $T_0 \sim 460$ K.

Figure 1

from the IRAS data. Filled circles represent stars of group **A** and open circles stars of group **B**. The two sets of near-parallel lines represent the loci of constant 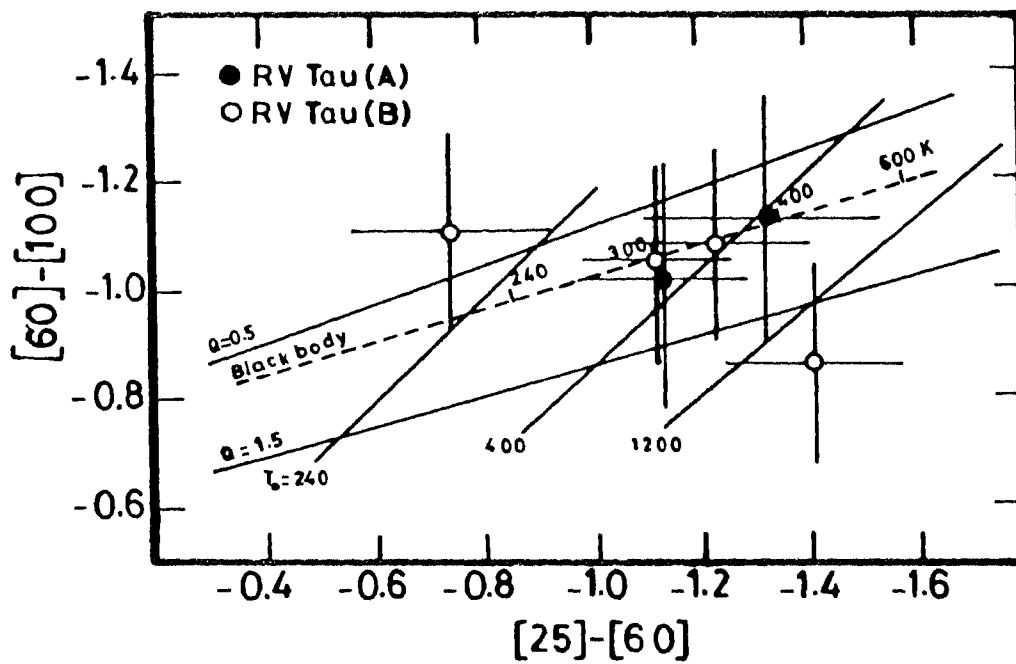inner shell temperature T_0 and the quantity Q defined above. The models correspond to the case of absorption efficiency $Q_{abs}(\nu)$ varying as ν (with $\gamma = 1$ and hence $\beta = -0.4$). R Sct has been omitted in Figure 1 because it shows a large deviation from the average relation shown by all the other objects. R Sct has a comparatively large excess at $60\mu m$; but the extent of a possible contamination by the infrared cirrus (Low et al. 1984) is unknown. Goldsmith et al. (1987) found no evidence of the presence of a dust envelope at near IR wavelengths and the spectrum was consistent with a stellar continuum. This explains why R Sct lies well below the mean relation shown by stars of group A and C between the [3.6]-[11.3] colour excess and the photometrically determined (Fe/H) (Dawson 1979). R Sct has the longest period of 140 day among the RV Tauri stars detected at the far infrared wavelengths and does not have the $10\mu m$ emission feature seen in other objects (Gehrz 1972; Olnon & Raimond 1986). Probably, R Sct is the most irregular RV Tauri star so far known (McLaughlin 1932).

The inner shell temperature (T_0) derived for the various objects are also given in Table 1, and the majority of them is found to have temperatures in the narrow range 400-600 K. If the dependences of $Q_{abs}(\nu)$ on ν, and $\rho(r)$ on r are similar in all the objects considered, then in the colour-colour diagram they all should lie along a line corresponding to different values of T_0, and in Figure 1 this is found to be essentially the case. In view of the quoted uncertainties in the flux measurements, not much significance can be attached to the scatter seen in the figure.

At $100\mu m$ the infrared sky is characterized by emission, called infrared cirrus, from interstellar dust on all spatial scales (Low et al. 1984), thereby impairing the measurements at far infrared wavelength. In Figure 2, the [60]-[100] colours of the six RV Tauri stars detected at $100\mu m$ are plotted against their [25]-[60] colours, along with the grid

Plot of the [60] − [100] colours of RV Tauri stars against their [25] − [60] colours. The solid lines represent the loci for constant inner shell temperature and the quantity Q. The dashed line shows the locus for a black-body distribution.

Figure 2

showing the regions of different values for inner shell temperature T_0 and the quantity Q, as in Figure 1. The results indicated by Figure 2 are consistent with that derived from Figure 1. AR Pup shows a large excess at 100μm, but in view of the large values for the cirrus flags given in the catalogue, the intrinsic flux at 100μm is uncertain.

1.4. Radial distribution of dust

It is evident from Figure 1 that all RV Tauri stars lie between the lines corresponding to Q = 1.5 and Q = 0.5. With

$$\alpha = - (1 + Q) \beta - 3$$

these values suggest limits of $r^{-2.0}$ and $r^{-2.4}$ for the dust density variation, indicating a near constant mass loss rate. Jura (1986) has suggested that the dust density in the circumstellar envelope around RV Tauri stars varies as r^{-1}, implying a mass loss rate that was greater in the past than it is currently. By fitting a power law to the observed fluxes, such that $f(\nu)$ varies as ν^q, values of q determined by him for the various objects given in Table 1 lie in the range 0.6-1.2, with a mean value of 0.98. The assumption of a power law corresponds to the case of $X_0 = 0$ in equation (3), and hence we get

$$q = 2 + \gamma - Q.$$

Since $Q_{abs}(\nu)$ is assumed to vary as ν, the resulting value for Q = 2.0. None of the objects is found to lie in the corresponding region in the colour-colour diagram. Even this extreme value for Q implies a density which varies as $r^{-1.8}$.

Goldsmith et al. (1987) have reported that the simultaneous optical and near IR data of AC Her can be fitted by a combination of two black-bodies at 5680 K and 1800 K, representing, respectively, the stellar and dust shell temperatures, and suggested that in RV Tauri stars the grain formation is a sporadic phenomenon and not a continuous process. Apparently, they have been influenced by the remark by Gehrz & Woolf (1970) that their data in the 3.5-11μm region

of AC Her indicated a dust temperature of ~ 300 K. It is found that the K-L colours given by Gehrz (1972), Lloyd Evans (1985) and Goldsmith et al. (1987) are all consistent with each other. Surely, hot dust (~ 1800 K), if present at the time of observations by Goldsmith et al. (1987), would have affected the K-L colour significantly. AC Her, like other members of its class, is found to execute elongated loops in the (U-B), (B-V) plane (Preston et al. 1963), indicating that significant departure of the stellar continuum from the black-body is to be expected. Further, their data show only a marginal excess at the near IR wavelengths. It is clear that the case for the existence of hot dust around AC Her and hence for the sporadic grain formation around RV Tauri stars is not strong. In Figure 5, (section 1.7.) AC Her and RU Cen are found to lie very close to R Sct which, according to Goldsmith et al. (1987), shows no evidence for the presence of a hot dust envelope.

1.5. Comparison with black-body distribution

In a study of IR excesses in G-type stars, Odenwald (1986) has reported that the far infrared emissions in U Mon and RU Cen can be well-represented by single temperature black-body materials rather than materials with an emissivity which varies as ν, whereas in R Sge the IR continuum peak is broader than expected for a single temperature component requiring a temperature gradient in the emitting material. A strictly black-body distribution implies that either the dust envelope is optically thick at infrared wavelengths, or the size of the dust grains dominating the emission between 12 and 100μm are much larger than 10μm. The first case can be almost ruled out in view of the small values of Planck mean optical depths at absorbing wavelengths derived for RV Tauri stars (section 1.1.) and the second case involves the problem of dust grain growth to such large sizes.

In Figure 3, the IR colours of RV Tauri stars are replotted, and the corresponding error bars determined from the flux uncertainties given in the catalogue are indicated. The black-body line transformed to the flux density system

144
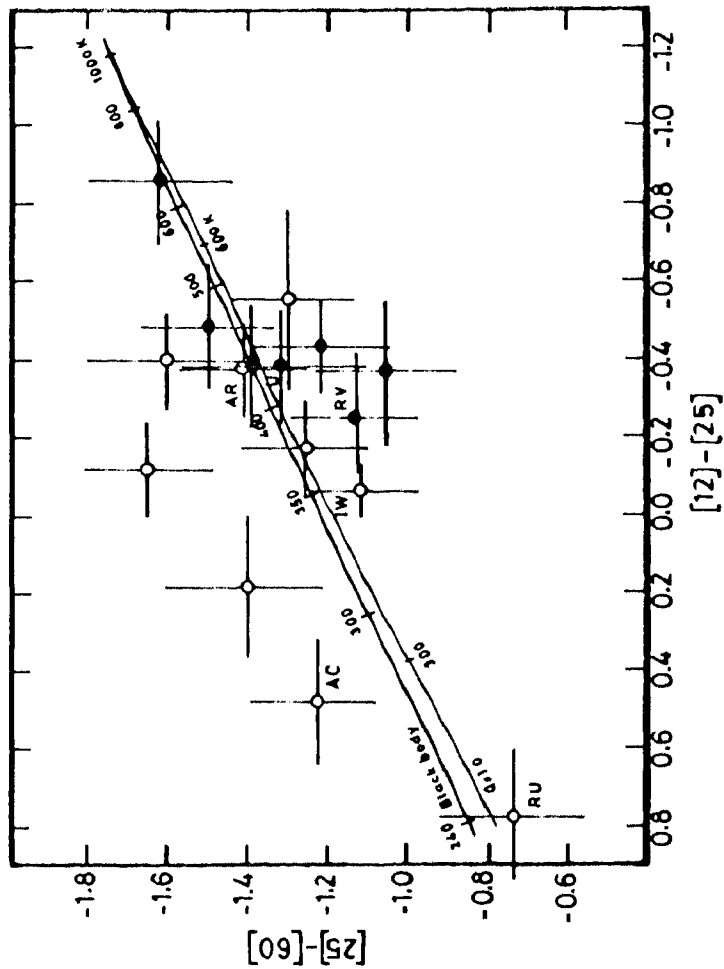
Figure 3

Plot of the [25] – [60] colours of RV Tauri stars against their
[12] – [25] colours with the corresponding error bars. Some of
the objects are identified by their variable star names. The
black-body line and the locus for Q = 1.0 are also shown.

145

quoted in the IRAS PSC (Beichman et al. 1985) and the line corresponding to the case $Q = 1$ (equation (3)) are also shown in the figure. It is clear that the present data is insufficient to resolve between the two cases. However, the latter case is physically more reasonable; the evidences in favour of single temperature black-body materials in the circumstellar envelopes are not strong.

1.6. Comparison with oxygen and carbon Miras

The positions of a sample of oxygen-rich and carbon-rich Miras in the two-colour diagram are shown in Figure 4., along with those of RV Tauri stars. At the low temperatures characteristic of the Miras a part of the emission at $12\mu m$ comes from the photosphere. For a black-body at 2000 K, the ratio of fluxes at wavelengths $12\mu m$ and $2\mu m$, $(f_{12}/f_2) \sim 0.18$. The Miras shown in the figure have the (f_{12}/f_2) ratios larger than twice the above value. It is clear that the three groups of objects populate three different regions of the diagram. Hacking et al. (1985) have already noticed that there are distinct differences between the IRAS colours of oxygen-rich and carbon-rich objects. On the basis of an analysis, using a bigger sample of bright giant stars in the IRAS catalogue, this has been interpreted by Zuckerman & Dyck (1986) as being due to a systematic difference in the dust grain emissivity index. Willems & de Jong (1988) have found that while a general sample of carbon stars show a large spread in the [12]-[25], [25]-[60] colour diagram, the carbon Miras are concentrated near the 800-1000 K region on the black-body line and that the few carbon stars with silicate feature in the IR region, indicating an oxygen-rich circumstellar envelope, lie in the upper part of the diagram, above the black-body line; from Figure 4 it is seen that this is exactly the region occupied by the oxygen Miras.

U Mon shows the $10\mu m$ silicate emission convincingly and in most of the other objects for which low resolution spectra in the near infrared have been reported (Gehrz 1972; Olnon & Raimond 1986), the $10\mu m$ emission may be partly attributed to

146
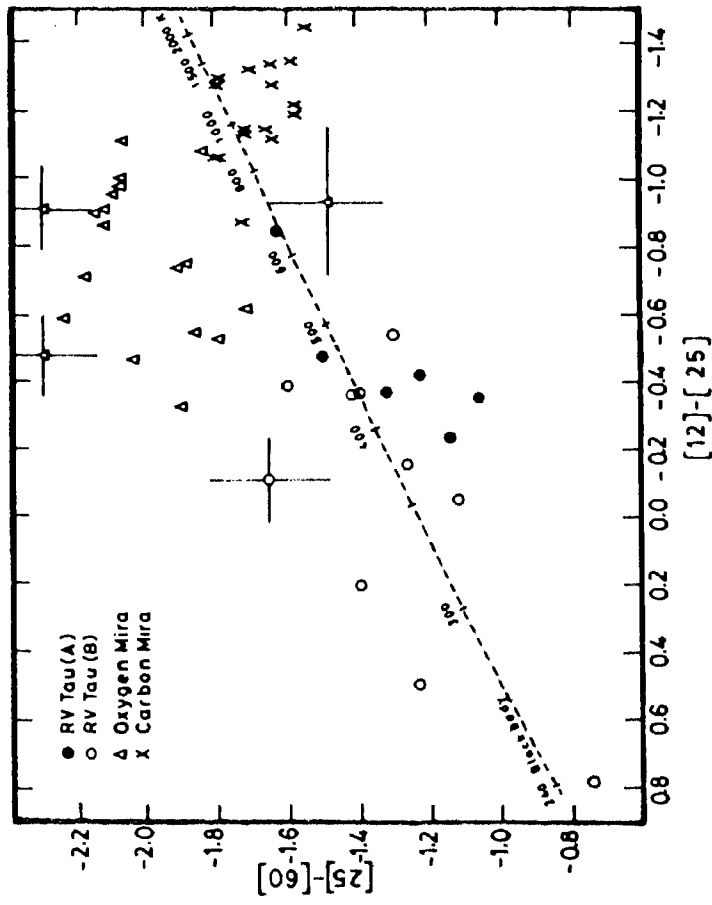
Plot of the [25] - [60] colours of RV Tauri stars, oxygen Miras and carbon Miras against their [12] - [25] colours. Typical error bars are shown. The dashed line gives the locus for a black-body distribution.
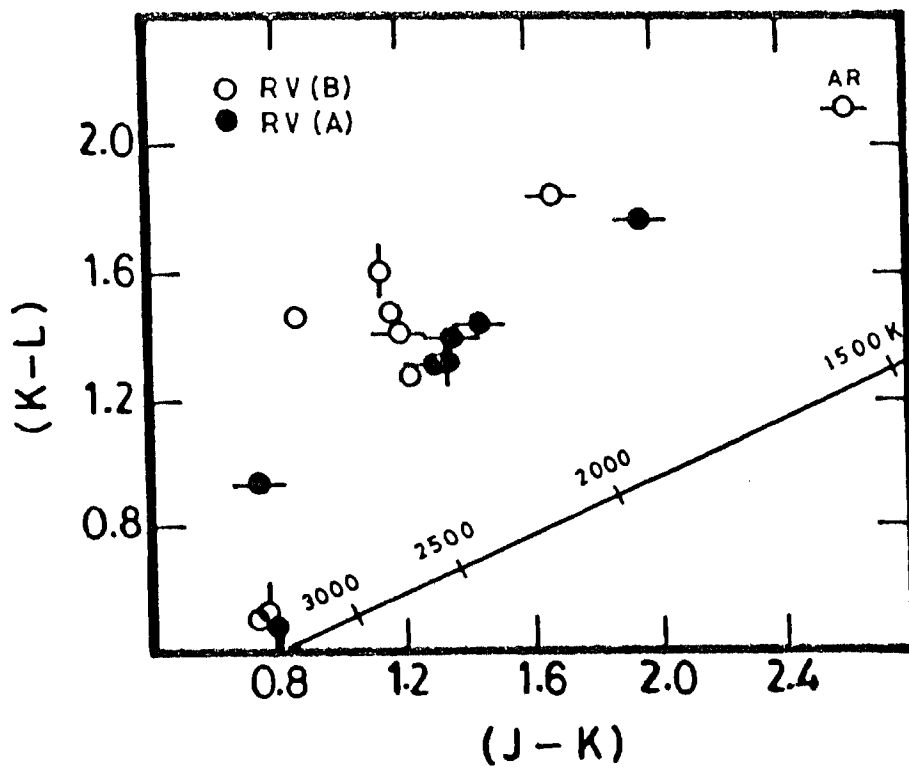
Figure 4

147

silicates. Hence, it is reasonable to expect that in the envelopes around at least some of the RV Tauri stars the dust grains are predominantly of silicates, as in the case of oxygen Miras (Rowan-Robinson & Harris 1983). The fact that none of the RV Tauri stars is found in the region of the two-colour diagram occupied by the oxygen Miras indicates that the emissivity indices of the silicate grains in the two cases are different. This is to be expected because the environment of grain formation will be different in RV Tauri stars due to their higher temperatures and luminosities.

1.7. Correlation with subgroups

It is interesting to see that Table 1 contains no group C objects and that in Figure 1 there is a clear separation of the two spectroscopic subgroups A and B, with the demarcation occurring at an inner shell temperature of about 450 K, group B objects having lower temperatures than group A. SX Cen is the only exception. Lloyd Evans (1974) has reported that metal lines are stronger in SX Cen than in other group B objects. It may be worth noting that SX Cen has the shortest period among the one hundred or so odd objects with the RV Tauri classification. RU Cen has the coolest inner shell temperature, as already suggested by the near infrared spectrum (Gehrz & Ney 1972).

Group B objects follow a different mean relationship to those of group A, having systematically larger 11μm excess for a given excess at 3μm (Lloyd Evans 1985). For a general sample of RV Tauri stars the distinction between the oxygen-rich and carbon-rich objects is not that apparent in the JHKL bands. In Figure 5, the near IR magnitudes of the objects given in Table 1 (except V Vul which has no available measurements) are plotted in the (J-K), (K-L) plane. The colours, taken from Lloyd Evans (1985) and Goldsmith et al. (1987), are averaged if more than one observation exists, because the internal agreements are found to be often of the order of observational uncertainties, in accordance with the earlier finding by Gehrz (1972) that variability has relatively little effect on

Plot of (K-L) colours of RV Tauri stars detected by
IRAS against their corresponding (J-K) colours. The
position of AR Pup is indicated.   The   three   objects
lying close to the black-body line are AC Her, RU Cen
and R Sct.

Figure 5

colours. Barring RU Cen and AC Her, it is evident that stars belonging to group B show systematically larger excesses at L band for a given excess at K. The low excesses at near IR wavelengths for AC Her and RU Cen are consistent with the very low dust temperatures indicated by the far infrared colours.

It is already well-established that from UBV photometry one can distinguish between group A and B, members of group A being significantly redder than those of group B (Preston et al. 1963). Similarly, Dawson (1979) has found that the spectroscopic groups are well-separated in the DDO colour-colour diagram when mean colours are used for the individual objects.

The clear separation of the spectroscopic subgroups A and B in the IR two-colour diagram suggests that the nature of dust grains in the envelopes in the two cases are not identical. This is to be expected because of the differences in the physical properties of the stars themselves. The average colours of group B stars are bluer than group A, but the envelope dust temperatures of B are cooler than those of A. The near IR spectra of AC Her and RU Cen are extremely similar (Gehrz & Ney 1972). The striking similarities in the optical spectra of AC Her and RU Cen have been pointed out by Bidelman (O'Connell 1961). It appears that the physical properties, including the chemical composition, of the grains formed in the circumstellar envelope strongly depend on those of the embedded star. This, probably, explains the diversity in the energy distributions of RV Tauri stars in the near infrared found by Gehrz & Ney (1972). On the basis of the observed differences in chemical abundances and space distribution of RV Tauri stars, Lloyd Evans (1985) has already pointed out that there is no direct evolutionary connection between group A and group B objects, thus ruling out the possibility that group B objects are the evolutionary successors of group A, in which grain formation has stopped and the cooler temperatures for the former are caused by an envelope expansion.

Extensive observations in the near infrared show that, on

average, RVb stars are redder than RVa stars, and Lloyd Evans (1985) has suggested that in RVb stars dust shells are denser in the inner regions, and hence radiate strongly in the 1-3μm region. Figure 5 confirms this; RVb objects (denoted by horizontal bars) show systematically larger (J-K) and (K-L) than RVa objects (denoted by vertical bars). Apparently, there is no distinction between objects of the two light curve types at far infrared wavelengths (Figure 1).

1.8. Mass loss rates and envelope masses

The amount of data on circumstellar envelopes around RV Tauri stars available at present is quite small. Also, it is seen in the previous section that the physical properties of the dust grains in the envelopes strongly depend on those of the embedded star. Hence for an estimation of the mass loss rates from these objects, the various physical quantities will have to be assumed, thus resulting in large uncertainties in the estimated values.

From the IRAS fluxes, Jura (1986) has estimated the dust loss rates around RV Tauri stars assuming that the mass extinction coefficient of the grains at 60μm $\chi_{60}=$ 150 cm^{2}gm^{-1} and that the outflow velocity v=10 km sec^{-1}. The values thus estimated show relatively small scatter and are typically near 5×10^{-9} M$\odot$ yr^{-1}. Further, assuming the metallicity of these objects to be low ($\sim$ 0.1 of solar value) and hence a dust to gas ratio of 4.5×10^{-4}, he has suggested that the total mass loss rates from these stars is about 10^{-5}M$\odot$ yr^{-1}.

To estimate the total envelope mass, the epoch of the onset of the mass losing phase or the extent of the radiating envelope must be known, and both the quantities are very uncertain. A characteristic value for the radius in which 50% of all the 60μm radiation is emitted is 1.5×10^{11} km (Jura 1986). With an outflow velocity v=2.5 km sec^{-1} (Bujarrabal et al. 1988), it implies that the RV Tauri stars have existed in the active mass losing phase for at least 2000 years, giving a lower limit of 0.02M$\odot$ for the envelope mass.

The mass loss from RV Tauri stars estimated by Jura (1986)

are probably high. The outflow velocities derived for R Sct and AC Her from CO microwave emissions are found to be only 2.5-5 km sec^{-1}. Similarly, the dust to gas ratios derived for objects, which are considered to be pre-planetary nebula objects, are typically around 10^{-2} (Likkel et al. 1987). If these quantities are used the mass loss from RV Tauri stars turns out to be less than 10^{-7}M$\odot$ yr^{-1}.

The present status of mass loss from these objects is not clear. According to Jura (1986; 1989, private communication), the current mass loss rates from RV Tauri stars are much less than the value in the past (around 500 years ago) and the cooler temperatures at the inner boundaries of the envelopes are caused by the envelope expansion following the cessation of mass loss and hence the grain formation processes in these objects. From the low outflow velocities observed by them, Bujarrabal et al. (1988) have concluded that the mass loss process that produced the observed material around RV Tauri objects ceased about 2000-3000 years ago. Since RV Tauri stars still present evolved spectral types, the above authors have supported the view raised by Jura (1986) that probably for a good fraction of RV Tauri stars their envelopes will dissipate before the central cores become hot enough to ionize them; hence such objects would never become planetary nebulae.

It is not definite that RV Tauri stars are post asymptotic giant branch objects in which mass loss has stopped. Most likely, RV Tauri stars are currently in active mass losing phase, and the low temperatures at the inner shell boundaries are as a consequence of low absorption efficiencies of the dust grains. The molecular outflow velocities observed in RV Tauri stars are much smaller than the values usually found for red asymptotic giant branch objects (~ 10 km sec^{-1}, Bujarrabal et al. 1988) and those considered to be pre-planetary nebula objects (~ 15 km sec^{-1}, Likkel et al. 1987), and hence the envelope dissipation time also would be correspondingly higher. So there is a possibility of a substantial fraction of the objects producing detectable planetary nebulae. But the major uncertainty is the length of time it takes for these

stars to evolve to the hotter temperature regions of the H-R diagram to ionize the surrounding gas.

It would be interesting to see if there is any substantial spread in the envelope masses of the individual objects and also if there is any systematic variation in the envelope masses with the spectral types of the embedded stars; these will provide important information on the evolution of the objects. For this better estimates of the envelope masses of the individual objects are needed.

2. Polarization mechanisms

There are two main mechanisms usually invoked to explain the intrinsic polarization of late-type stars in general. Harrington (1969) has shown that the light emerging from the limb of a star would be highly polarized due to Raleigh scattering by molecules or atoms if the Planck function has a steep gradient in the atmosphere. However, for a net observable polarization, photospheric asymmetry should be present and the proposed sources of asymmetry are non-radial pulsation of the star, variation of temperature over the surface and the presence of giant convection cells (Harrington 1969; Schwarzschild 1975). The other suggested mechanism is the scattering by molecules or dust grains in an extended asymmetric circumstellar envelope (Kruszewski, Gehrels & Serkowski 1968; Shawl 1975a; Daniel 1978).

The discovery of polarization changes across spectral features in several cool objects is consistent with the photospheric mechanism (Landstreet & Angel 1977; Coyne & McLean 1979; Boyle et al. 1986). However, there are a few problems; objects of similar spectral types show diverse polarization spectra. Detailed calculations by Doherty (1986) indicate that photospheric scattering produces only a very low polarization (<0.3%) even under the best conditions. Recently, Marcondes-Machado (1987) has presented a model of circumstellar scattering by dust grains aligned by a magnetic

field, which reproduces the observed polarization changes across molecular bands and atomic lines. Both photospheric and circumstellar processes may be involved in the production of the observed polarization, the relative contribution being different in different objects.

2.1. RV Tauri stars

2.1.1. IN GENERAL

Detailed polarimetry has been reported only for three objects, U Mon, R Sct and AC Her (Serkowski 1970; Henson, Kemp & Kraus 1985), and there is no general agreement in the models suggested to explain the observed polarization. The origin of polarization in U Mon and R Sct has been ascribed to their non-radially pulsating photospheres by Serkowski (1970). U Mon exhibits a systematic pattern in the variation of the direction of polarization, whereas R Sct does not show any such behaviour. Spectropolarimetry of R Sct, obtained by Landstreet & Angel (1975), does not exhibit any change in either polarization or direction across the spectral features, and hence rules out a photospheric origin for polarization. Henson, Kemp & Kraus (1985) have found that in AC Her the phases of the most rapid and extreme polarization change coincide with the phases where Baird (1981) has observed blue-shifted radial velocities that suggest an outward passage of atmospheric shock waves. Hence they concluded that polarization most likely arises in the region upon which the shock waves are acting.

At low polarization levels, the fractional contribution by the interstellar component may be substantial, thereby masking the real variation in the intrinsic polarization. Since the normalized Stokes parameters Q and U add linearly (section IVA-2.2.), the variations in the polarization can be analysed in the (Q,U) plane advantageously. It is remarkable that U Mon, R Sct and AC Her (and possibly RU Cen also) show similar three lobed structures in the (Q,U) plane. Polyakova (1984) has presented polarimetry of several cepheids in integrated light; they also show similar behaviour in the (Q,U) plane,

indicating a direct connection between pulsation and polarization changes. Such regular variations in the (Q,U) plane imply regular variations in the geometry involved during the pulsation. The position angles (which are related to geometry) are found to vary cyclically in AC Her and U Mon. The possibility of a regular variation in the geometry of the extended infrared emitting envelope coupled with the pulsation of the star is very remote. From extensive infrared observations of a number of objects which show large polarization variations, Forrest, Gillett & Stein (1975) have already concluded that the relationship between the infrared excess and polarization is not very direct. Ultraviolet observations of the 0.22μm absorption feature of circumstellar dust obtained at two different phases of light cycle in AC Her do not show any major changes, indicating that polarization variations are not produced by changes in the dust shells (Baird & Cardelli 1985).

AR Pup follows the mean relationship between the average intrinsic polarization and [11]-[3.5]μm colour, found by Dyck et al. (1971), while the polarization seen in U Mon, AC Her, RU Cen and SX Cen are too small for their observed infrared excesses.

Henson, Kemp & Kraus (1985) have suggested that the apparent path of polarization in the (Q,U) plane observed in AC Her is either due to non-radial pulsations in the star, or radial or non-radial pulsations propagating into an asymmetric circumstellar medium. It is very likely that the variations in polarization observed in RV Tauri stars during the light cycle are rather caused by changes in asymmetries associated with the pulsation of the star than due to changes in an asymmetric envelope. The wavelength independent position angles shown by AC Her, RU Cen and SX Cen, which are least affected by the interstellar medium, are consistent with the polarization arising from photospheric asymmetries. The near-flat wavelength dependence of polarization seen in the above objects indicates that circumstellar grain scattering is the main polarization mechanism. (Electron scattering also

155

produces flat wavelength dependence; but, to account for the observed amount of polarization it requires the column densities of electrons to be very large). Hence the observations suggest that the polarization in RV Tauri stars, in general, results from a combination of pulsation related asymmetry (non-radial pulsation ?) and grain scattering in the circumstellar envelope.

2.1.2. AR PUP

The amplitudes of polarization seen in U Mon, R Sct, AC Her and RU Cen are similar (1.0-1.5%) and are much smaller than that seen in AR Pup. The mechanism suggested for the other RV Tauri stars may be operative in AR Pup, but the corresponding contribution to the observed polarization is probably negligible.

Computational models of extended circumstellar scattering envelopes using Mie theory (Shawl 1975a; Daniel 1978, 1982) do not predict a high intrinsic polarization as observed in AR Pup (14.6% in U band). Kruszewski, Gehrels & Serkowski (1968) and Daniel (1980) have suggested that preferential attenuation of direct star light by thick material present in the line of sight might be invoked in order to increase the polarization produced by axisymmetric envelopes. But the rapid changes observed in the polarization in AR Pup during JD 2446471-78 (Figure IV-8) may not be caused by variations in the obscuration of direct star light by thick condensations in the line of sight, because in such a case one would expect a very large change in the brightness and no change in the direction of polarization.

Forrest, Gillett & Stein (1975) find no definite changes in infrared flux in stars which show large polarization variations, and hence they attribute the infrared emission to the total abundance of dust in the envelope, which does not change substantially with time, and intrinsic polarization to scattering and absorption effects from more localized transient regions. The amount of polarization depends on the number of scatterers, and the specific density distribution

156

defines the direction of polarization alone and not its wavelength dependence (Simmons 1982). The variation of position angle with wavelength observed in AR Pup implies that the scatterers have a size distribution and the optical symmetry plane varies systematically with grain size. The change in the wavelength dependence implies a change in the particle size distribution. The regular behaviour of P and θ observed during JD 2446471-508 (Figure IV-11) appears to be a result of some systematic variation in the several parameters which determine the level, direction and wavelength dependence of polarization produced. It is difficult to conceive that the whole extended infrared emitting circumstellar envelope is involved to produce such a regular variation. But it is much more probable that transient localized regions such as those suggested by Forrest, Gillett & Stein (1975) for red variables were largely responsible for the observed polarimetric behaviour. Here it may be mentioned that Bastein & Landstreet (1979) have attributed the changes in position angles observed in RY Tau, a T Tau star, to scattering from blobs of material moving about. Localized condensations, if situated preferentially and closer to the photosphere, might scatter a larger portion of light in the line of sight giving rise to a higher percentage of polarization. A variation in the projected geometry would lead to a variation in the direction of polarization and the change in the observed brightness would be only marginal. In Figure IV-11, it is found that at low polarization levels the scatter in V and R bands is more. The extended circumstellar envelope might be contributing to the observed polarization at longer wavelengths, which becomes significant at low polarization levels.

Baird (1981) has observed blue-shifted radial velocities in AC Her during the rising light after a primary minimum, suggestive of an outward passage of a shock. Such detailed radial velocity studies are lacking for AR Pup. But it is reasonable to expect a similar behaviour in this object also. The rapid and regular changes in polarization observed in AR Pup after light minima (Figures IV-8 & 9) are, most likely,

157

related to the outward passage of shocks. The pressure increase due to shock might help to form small solid particles (Shawl 1975). The conditions existing during the ascending branch, close to the light minimum, may be favouring the formation of more localized condensations which are responsible for the observed polarization. It is possible that the life-times of such condensations are longer than the period of light variation. Hence, the contribution from different regions might produce the peculiar wavelength dependence of P and θ of the type observed on JD 2446114.28 (Figure IV-7).

2.2. Carbon stars

2.2.1. IN GENERAL

The rather weak wavelength dependence of polarization indicates that grain scattering is the main mechanism responsible for the continuum polarization in carbon stars also. The close resemblances in the normalized wavelength dependences indicate that the dust particles involved are of similar nature. Because of the paucity of observational material on individual objects, nothing definite can be said about the time-scales involved in the polarization variation. Nevertheless, in many cases it is fairly safe to conclude that in contrast to the cases of RV Tauri stars, there are no significant changes associated with the light cycles. The slow changes seen in polarization and position angle are probably indicative of long-term variations occurring in the circumstellar envelope.

2.2.2. R LEP

The changes in the normalized wavelength dependence of polarization in R Lep clearly indicate that, at least at wavelengths longward of blue, circumstellar grain scattering is the main contributing factor to the observed polarization. For a net polarization to appear in integrated light, there should be an overall departure from spherical symmetry. The secularly varying component of polarization, seen after 1966 (Figure IV-23) is possibly a result of an episodic asymmetric

158

mass ejection sometime before 1962 (section IVB-1.1.3.) and its subsequent dissipation in the circumstellar envelope.

The periodic changes in the wavelength dependence and level of polarization observed in o Cet have been attributed to the cyclic increase in particle size and their subsequent dissipation (Shawl 1975). Magalhaes et al. (1986) have suggested a similar mechanism of growth in grain size, but with a much larger time-scale than the pulsational period, to account for the secular changes seen in the wavelength dependence of polarization in the semiregular variable L_2 Pup. It is most likely that similar mechanisms of grain growth are operative in R Lep and AR Pup which produce the changes in the wavelength dependence of polarization; the time-scale involved is probably comparable to its pulsation period in AR Pup and much larger in R Lep.

3. Polarization models

The available computational models (Shawl 1975a; Daniel 1978, 1980; Simmons 1982) deal with the scattering of isotropically emitted light from a stellar point source by particles distributed in an envelope around it, and most of the polarization results presented in the literature are for axisymmetric envelopes with uniform particle densities.

Calculations of radiative transfer in dust envelopes by Rowan-Robinson & Harris (1983, 1983a) indicate high inner shell temperatures (~ 1000 K), especially for carbon stars (see also Figure 4), suggesting the presence of dust grains in the close vicinity of the stars. The amount of polarization produced will depend on the angle subtended by the source at the scatterer. For the case of steady mass outflow (section 1.4.), the density falls as the inverse square of the radial distance and hence the contribution by the dust grains close to the star to the net observed polarization will be substantial. Hence, it is expected that the varying size of the star as it pulsates might modify the observed polarization. When the object is most compact, the

159

polarization produced by an envelope would be the largest (Coyne & Magalhaes 1979). A quantitative analysis of the changes in polarization as a result of the changes in the physical size of the star is lacking.

The identification of grains in the envelope presents a major difficulty (section 1.7.) because of the inverse nature of the problem involved. However, polarization models of Shawl (1975a) show that a rough qualitative agreement with observations of several objects can be obtained by using the standard candidates of dust grains (silicates, graphites, etc.) with a suitable choice of their sizes.

The processes leading to the asymmetry of the envelopes around most of the late-type objects, that is needed for a net polarization to be observed, are still open questions. Asymmetric mass ejection, similar to that proposed for the case of R Lep (section 2.2.2.), may be one such mechanism. Another mechanism may be a mass ejection associated with non-radial pulsations. Rotation might play a role in the production of an axisymmetric envelope. A net polarization can also result from the illumination of a spherical cloud by a star with nonuniform surface brightness (Doherty 1986), and may be one of the mechanisms operating in some of the objects.

In what follows the above aspects of polarization produced by grain scattering in a circumstellar envelope are discussed from a theoretical point of view, using numerical modeling.

3.1. Mathematical formulation

The following assumptions are made: (i) the light emitted by the star is unpolarized, (ii) the grains are spherically symmetric (hence the scattering phase function also will be spherically symmetric) and (iii) the single scattering approximation holds good, i.e., the intensity of light scattered by N particles is N times that produced by a single particle. The last assumption implies that each particle sees only the direct light from the star, and it is not in serious conflict with the observations of the objects under consideration in view of the low optical depths derived for

them (Rowan-Robinson & Harris 1983a; also section 1.1.)

Consider an element of area dS on the stellar surface and a volume element dV in the envelope at a distance r. If $\eta(a)$ is the corresponding particle size distribution, the Stokes parameters in terms of the intensity of light scattered by the particles in dV will be given by

$$dI_{sca} = (1/2kD^2) \int_a (i_1(a) + i_2(a)) \frac{I\cos\theta}{r^2} e^{-(\tau_1 - \tau_2)} \eta(a)da\ dS\ dV$$

$$dQ = (1/2kD^2) \int_a (i_1(a) - i_2(a)) \frac{I\cos\theta}{r^2} e^{-(\tau_1 - \tau_2)} \eta(a)da\ dS\ dV\ \cos2\phi$$

$$dU = (1/2kD^2) \int_a (i_1(a) - i_2(a)) \frac{I\cos\theta}{r^2} e^{-(\tau_1 - \tau_2)} \eta(a)da\ dS\ dV\ \sin2\phi$$

$$V = 0.0,$$

where $K = (2\pi/\lambda)$, is the wave number, I, the intensity normal to dS, θ, the angle between the normal and the line joining centres of dS and dV, τ_1, the optical depth between dS and dV, τ_2, the optical depth between the scatterer and the observer, D, the distance between the observer and the scatterer, and i_1 and i_2 are the intensity functions defined by van de Hulst (1957). ϕ is the azimuth of the scattering plane projected over the sky, and the factors $\cos2\phi$ and $\sin2\phi$ appear because it is necessary to refer the contribution arising from each part of the envelope to the same coordinate system. Integrations over the star and the envelope provide the net required quantities. The optical depth is obtained from

$$d\tau = \int_a \pi a^2 \eta(a)\ Q_{ext}(a)\ da\ dl,$$

where dl is the element of path length and $Q_{ext}(a)$, the extinction efficiency. Usually, one is interested in the normalized Stokes parameters defined as $(I_{sca}, Q, U, V)/I_{total}$. If the intensity of direct light received from the star is

161

denoted by I_{dir}, then

$$I_{total} = I_{dir} + I_{sca},$$

with

$$I_{dir} = (1/D^2) \int I \cos\theta \ e^{-\tau} \ dS,$$

where θ is the angle between the normal to dS and the line of sight and τ , the optical depth along the line of sight. The integration is done over the visible hemisphere.

3.2. Computer program

A computer program in Fortran has been developed to calculate the polarization produced by grain scattering in a circumstellar envelope surrounding a star of finite size. A cartesian coordinate system is adopted with the positive x-axis along the line of sight, y- and z- axes in the plane of the sky, and the origin coinciding with the centre of the star. The star is assumed to consist of a specified number of source points distributed uniformly across its surface, and the envelope is divided into a specified number of equal volume elements. The basic program to calculate i_1, i_2 and Q_{ext} are adopted from Shah (1977). The radiation from each of the source points scattered by each of the possible volume elements is calculated and then summed over both the source points on the star and the volume elements in the envelope to give the normalized Stokes parameters Q and U. The program reproduces the results of Zellner (1971), Shawl (1975a) and Simmons (1982) when the corresponding parameters are introduced. Since both Q and U are calculated, the specified envelope need not be axisymmetric as assumed in the earlier investigations (Zellner 1971; Shawl 1975a; Daniel 1978, 1980).
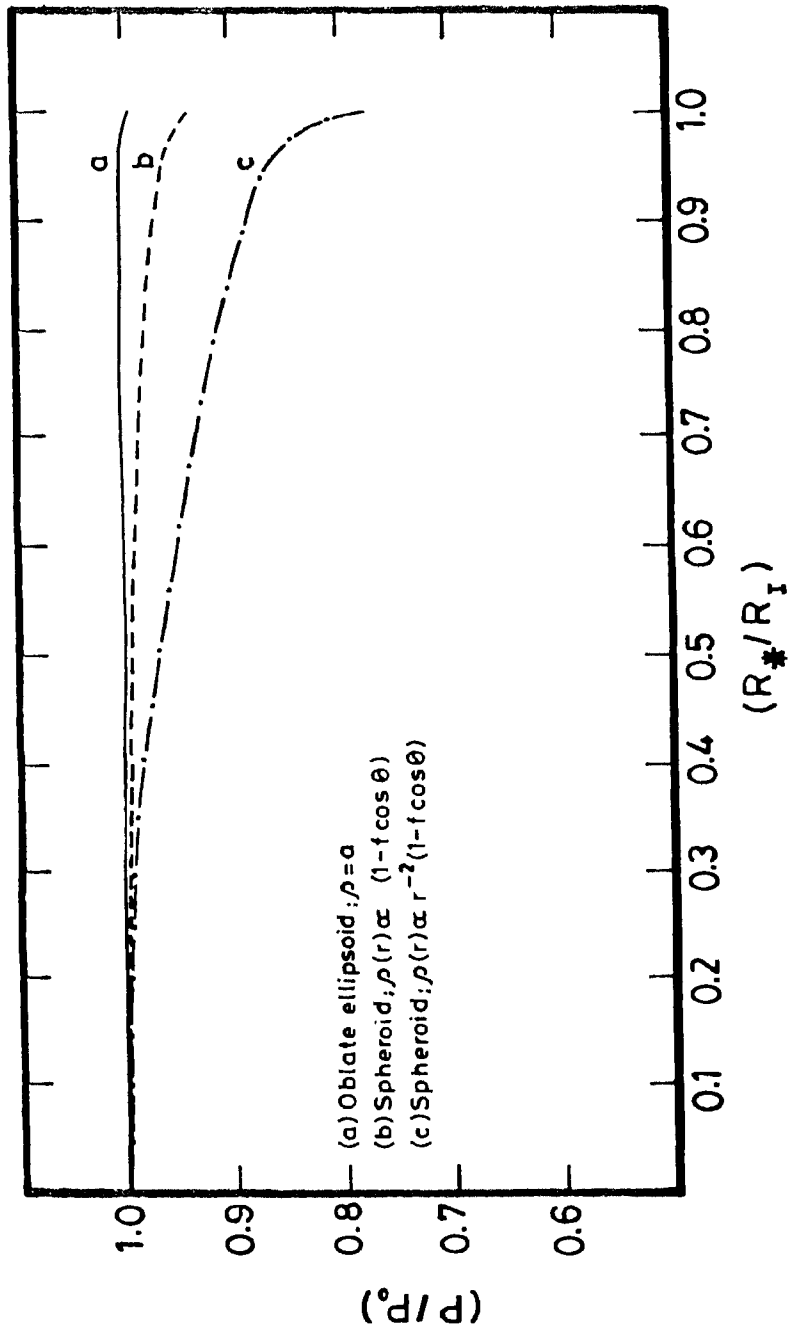
3.3. Computational results

3.3.1. EFFECT OF VARYING SIZE OF STAR

A star of radius R_*, surrounded by a circumstellar dust envelope of inner boundary radius R_I where the dust grains start condensing, was considered and the polarization produced

162

by the envelope for various values of R_* was computed. Three different envelope geometries were considered : (a) an ellipsoid of axial ratio E=3 with a particle density ρ = a constant, and spheroids with particle density distributions, (b) $\rho(\theta) \propto (1-f\cos\theta)$, and (c) $\rho(\theta) \propto r^{-2}(1-f\cos\theta)$, where f is a constant less than unity, and θ is the angle between the radius vector and the positive/negative z-axis (for points above/below the x-y plane). About 8000 volume elements in the envelope and 130 surface elements on the star were taken for the purpose of computing the polarization produced; on doubling these numbers the net polarization changes by 2.3% and 0.3%, respectively.

The grains were assumed to be of size $a=0.1\mu m$ and refractive index m=1.65 (which corresponds to pure silicates, Simmons 1982). Calculations were made for $\lambda=0.5\mu m$, and the optical depth along the equatorial direction in all cases was assumed to be $\tau_N=0.4$. The attenuation of direct and scattered light inside the envelope, and the contribution of scattered light to the total light were neglected while calculating the normalized polarization.

The computations show that the behaviour of normalized polarization is independent of the value of f appearing in the above dust density distributions (b) and (c). In Figure 6, the normalized polarization ($P_0=1$, for a point source) is plotted against the corresponding ratio (R_*/R_I) of the stellar radius to the inner shell radius of the envelope for the three geometries assumed, and it is clear from the figure that the relative change in polarization depends on the radial distribution of particle density; but the actual change in polarization with variation in the relative size of the star is very small. If the temperatures are sufficiently low for grain formation to start at 3-4 stellar radii (especially, in the case of the red variables), the net change in polarization as a result of changes in the physical size of the star during the pulsation (assuming it to be radial) is only a few percent. It is safe to conclude that there is little direct effect of radial pulsation of the star on the polarization

163

(a) Oblate ellipsoid: $\rho = a$

(b) Spheroid; $\rho(r) \propto (1 - f\cos\theta)$

(c) Spheroid; $\rho(r) \propto r^{-2}(1 - f\cos\theta)$

Plots of the normalized polarization against the corresponding ratio of the stellar to the inner shell envelope radius. The assumed envelope geometries are indicated.

Figure 6

164

produced by an envelope as a result of its varying size, and that changes in polarization observed in many red variables may be mainly resulting from changes in the number and sizes of the scattering grains.

3.3.2. THE NATURE OF GRAINS

In the light of the above results, the star was assumed to be a point source, and the polarization produced by a circumstellar envelope surrounding it was computed for a wide range of grain sizes (single size particles in each case) assuming them to be pure silicates, dirty silicates and graphites, in order to assess their suitability in explaining the mean polarimetric behaviours of red variables. The refractive index for pure silicates was taken to be m=1.65 (Simmons 1982) and that for dirty silicates to be m=1.55-0.1i (Jones & Merrill 1976). The optical constants for graphite were taken from Wickramasinghe & Guillaume (1965) after correcting for the misprints (some of the values under k are listed as 1.452 instead of 1.425). The density in the envelope was assumed to vary as $\rho(\theta) \propto r^{-2}(1-0.5cos\theta)$ and about 8000 volume elements were considered in the envelope for computing the polarization produced. The optical depth at $\lambda^{-1}=2.06\mu m^{-1}$ was assumed to be $\tau_N=0.4$ along the x-y plane in all cases. As before, the attenuation of scattered light in the envelope and its contribution to the total light were neglected.

The computed normalized polarization (unity at $\lambda^{-1}=2.06\mu m^{-1}$) for a few grain sizes, which lie close to the observational results, are plotted in Figures 7-9. The dashed lines in Figures 7 and 8 represent the mean polarimetric behaviour of the oxygen-rich stars, and the dashed line in Figure 9 represents that of the carbon stars (Figure IV-29). A comparison of the results of polarization calculations assuming single scattering with that taking into account multiple scatterings (Daniel 1978) shows that significant disagreement between them occurs only for optical depths $\tau >$ 0.6. In all the cases plotted in Figures 7-9, the optical depths in the wavelength regions considered never exceeded
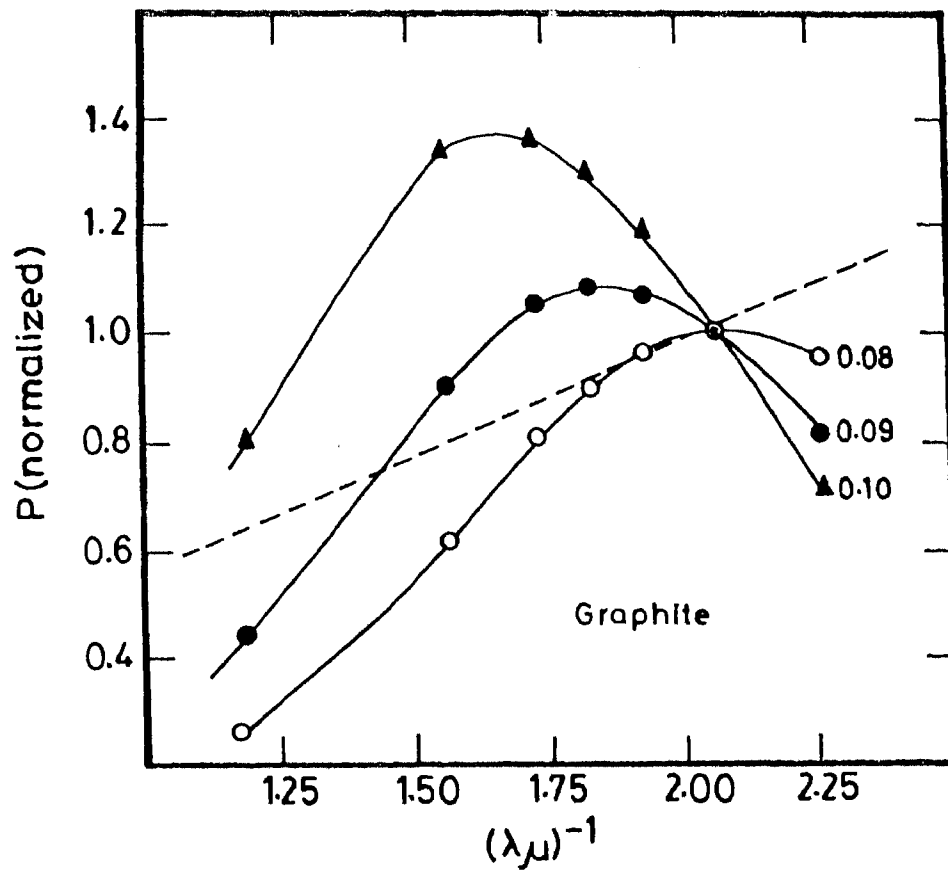
165
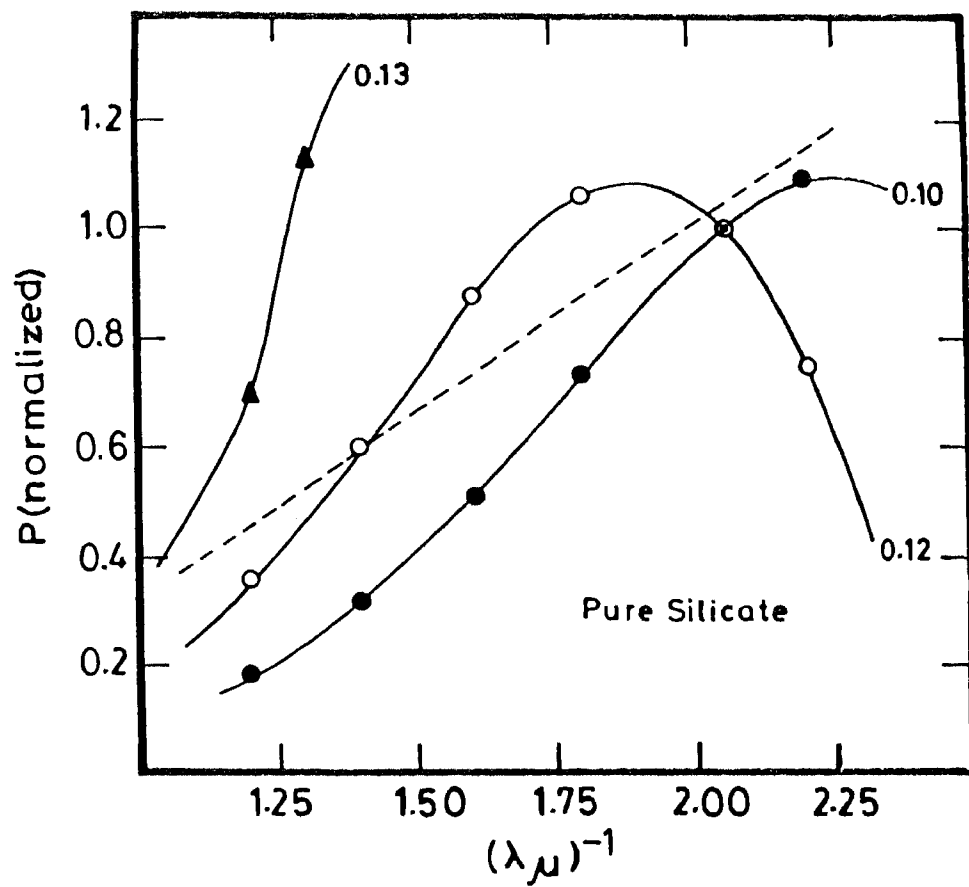
Plots of the normalized polarization (continuous curves) for pure sili-
cates. The values given against the curves are the respective grain
sizes in microns. The dashed line represents the mean normalized pola-
rimetric behaviour of oxygen-rich stars (see text).

Figure 7

166
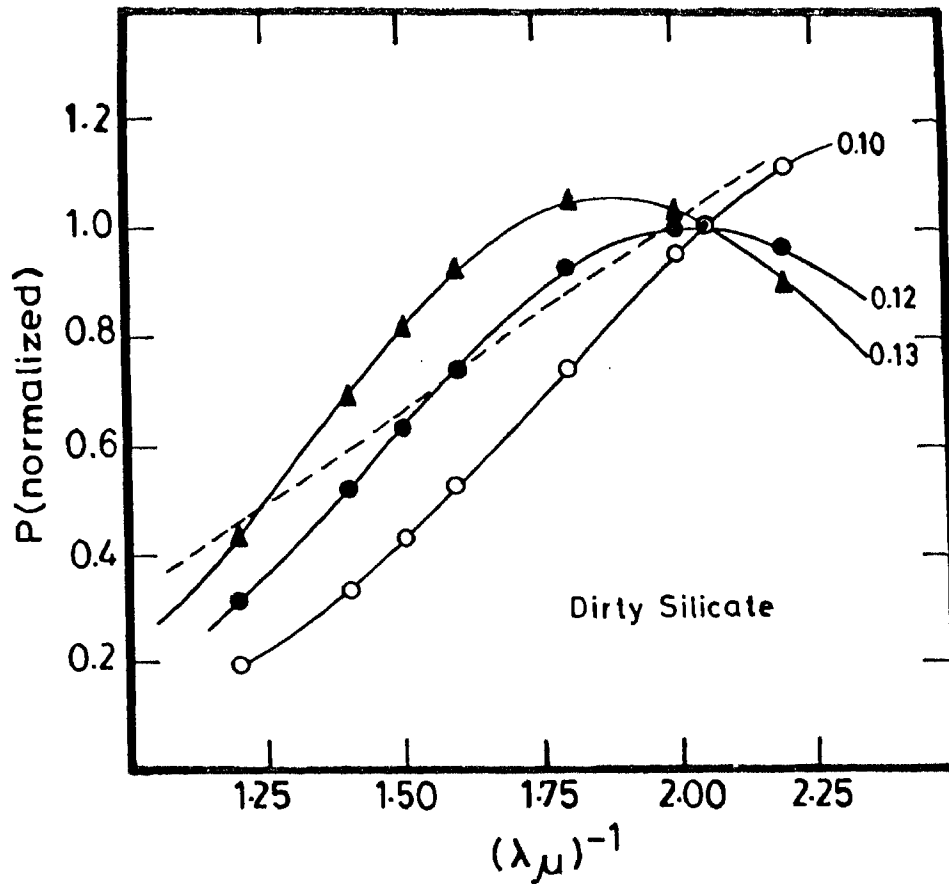
Plots of the normalized polarization (continuous curves) for dirty silicates. The values given against the curves are the respective grain sizes in microns. The dashed line represents the mean normalized polarimetric behaviour of oxygen-rich stars (see text).

Figure 8

Plots of the normalized polarization (continuous curves) for graphites. The values given against the curves are the respective grain sizes in microns. The dashed line represents the mean normalized polarimetric behaviour of carbon-rich stars (see text).
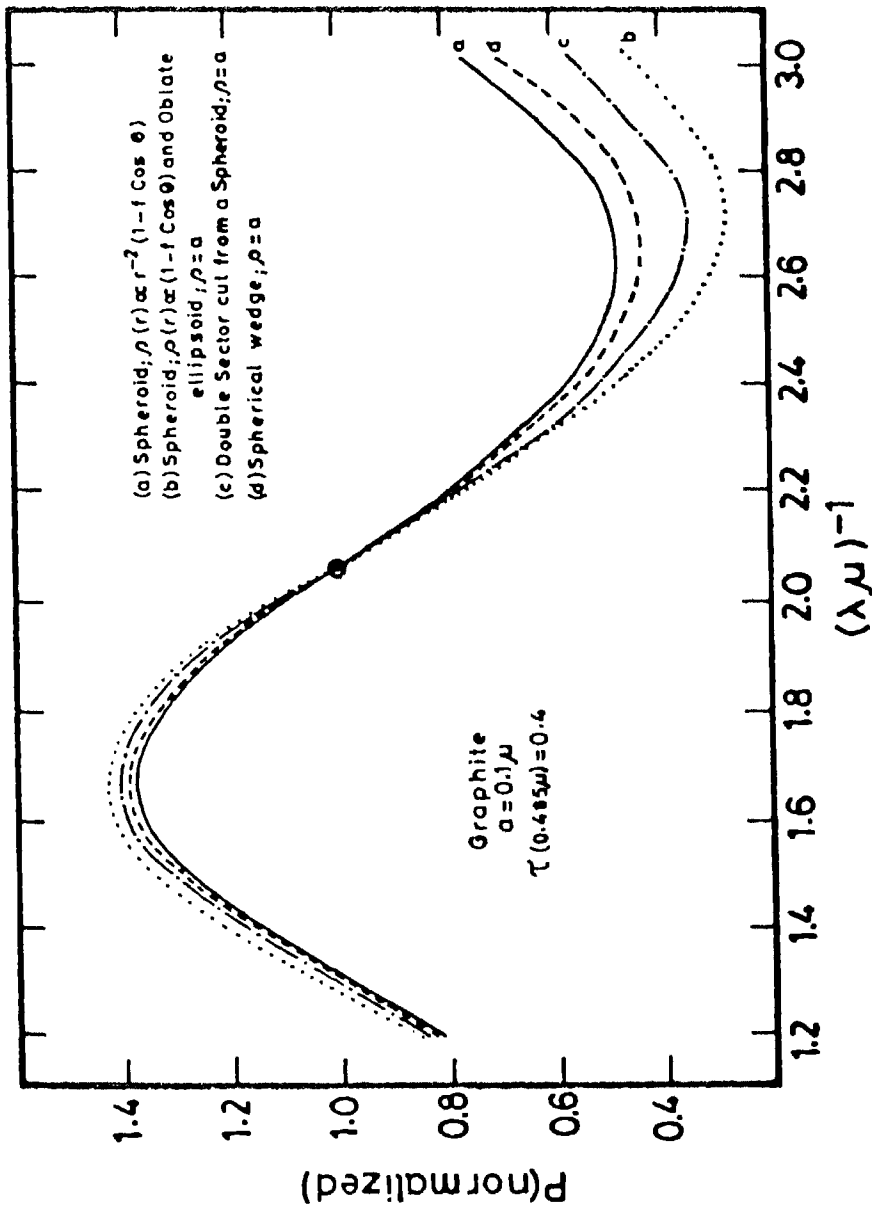
Figure 9

0.6, thereby making the contribution of multiple scattering insignificant.

Rowan-Robinson & Harris (1983) have reported that dirty silicates give an excellent fit to the overall infrared emission from circumstellar dust shells around oxygen-rich stars, and from Figures 7 and 8 it is clear that they provide better approximation to the scattering dust grains than pure silicates in accounting for the polarimetric behaviour also. It is clear from Figure 9 that graphites do not adequately explain the polarimetric behaviour of carbon stars; here it may be mentioned that neither do they adequately explain the infrared spectra of circumstellar dust envelopes around carbon-rich objects (Rowan-Robinson & Harris 1983a). It has been pointed out by Czyzak, Hirth & Tabak (1982) that graphite formation in circumstellar envelopes is a less likely process and carbon grains exist, most likely, in some other form, such as amorphous carbon.

In Figure 10, the polarization, normalized to unity at λ^{-1}=2.06μm, is plotted against the corresponding inverse of the wavelength for graphite grains of size a=0.1μm and for the envelope geometries considered in section 3.3.1; the figure also contains the results for two other envelope geometries: (i) a double sector and (ii) a spherical wedge, both of constant density throughout. In all cases the optical depth along the x-y plane is normalized to τ=0.4 at λ=0.485μm. The results for the last two cases are presented by Shawl (1975a) also. It is found that the normalized wavelength dependence of polarization is independent of the value of f appearing in (b) and (c) of the assumed geometries of section 3.3.1. The close resemblances in the shapes of the various curves plotted in Figure 10 clearly indicate that the envelope geometries have very little effect on the normalized wavelength dependence of polarization, as already pointed out by Shawl (1975a).

3.3.3. EFFECT OF NON-UNIFORM SURFACE BRIGHTNESS

For simplicity, as shown in the inset of Figure 11, the illuminating star was considered to have three brightness

169

Plots of normalized wavelength dependence of polarization for different envelope geometries.

Figure 10

zones – an equatorial zone characterized by a temperature T_E and two polar zones (about y -axis), both characterized by a temperature T_P. The boundaries of polar zones are obtained by rotating a radius vector at an angle θ with the +ve/-ve y-axis. The dust envelope was assumed to be spherical with the density $\rho(r) \propto r^{-2}$, and the scattering grains to be pure silicates (m=1.65) of size a=0.1μm. The optical depth at λ=0.5μm along the radial direction was normalized to τ_0=0.4, and the ratio of the inner dust shell radius to the stellar radius was taken as (R_*/R_I)=0.2. The contribution of scattered light to the total light was taken into account while calculating the net polarization produced; but the attenuation of both direct and scattered light inside the envelope was neglected. Computations of polarization at λ=0.5μm were made for different areas of polar zones (A_p), first by keeping T_E=5000 K and varying T_P, and then keeping T_P=5000 K and varying T_E. In Figures 11 and 12, the net polarization produced by the envelope is plotted against the fractional area $(A_p/4\pi R_*^2)$ of the polar zones. About 500 surface elements both in the polar and equatorial regions and about 7000 volume elements in the envelope were considered; the net polarization computed by this combination for T_P=T_E is found to be $\leq$ 0.04% in each case.

From Figures 11 and 12, it is clear that the polarization produced by a hotter zone at the limb is larger than that produced by a zone of the same temperature and equivalent area about a plane passing through the centre; for example, a 5000K temperature zone covering an area of ~ 10% of the stellar surface produces a polarization ~ 5% when distributed at the poles, whereas the net polarization produced by an equatorial zone of an equivalent area is <1%, the ambient surface temperature being 2000K.

To see the effect of non-uniform surface brightness on the wavelength dependence, the net polarization, produced at wavelengths 0.35, 0.45, 0.50, 0.70 and 0.90μm, was computed for the geometry described above and shown in the inset of Figure 11. The fractional area of the polar zones was taken as
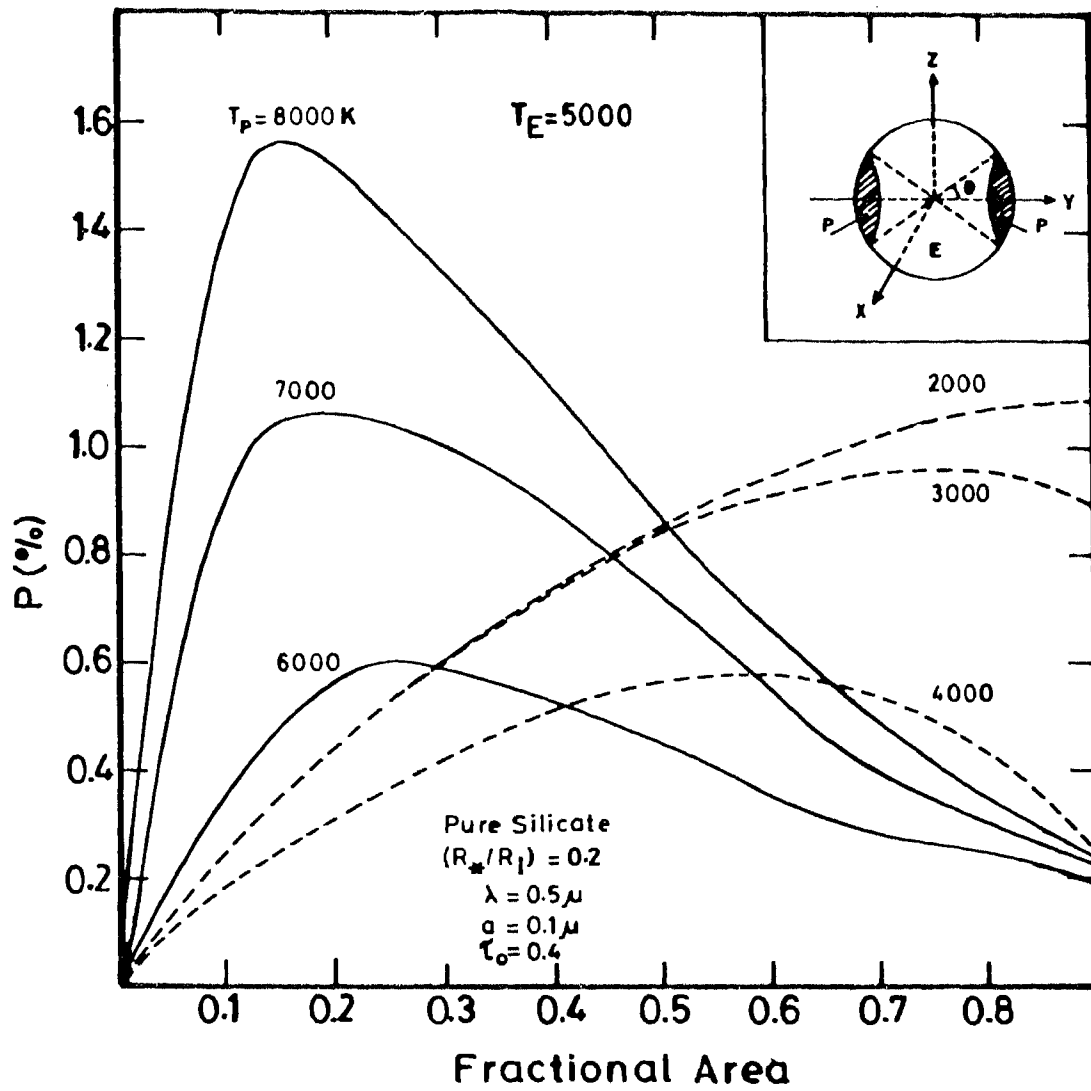
171

Plots of linear polarization produced against the corresponding fractional area of the polar zones (shown in the inset of the figure) for different polar zone temperatures (T_P). The temperature of the equatorial zone is taken as T_E = 5000 K.
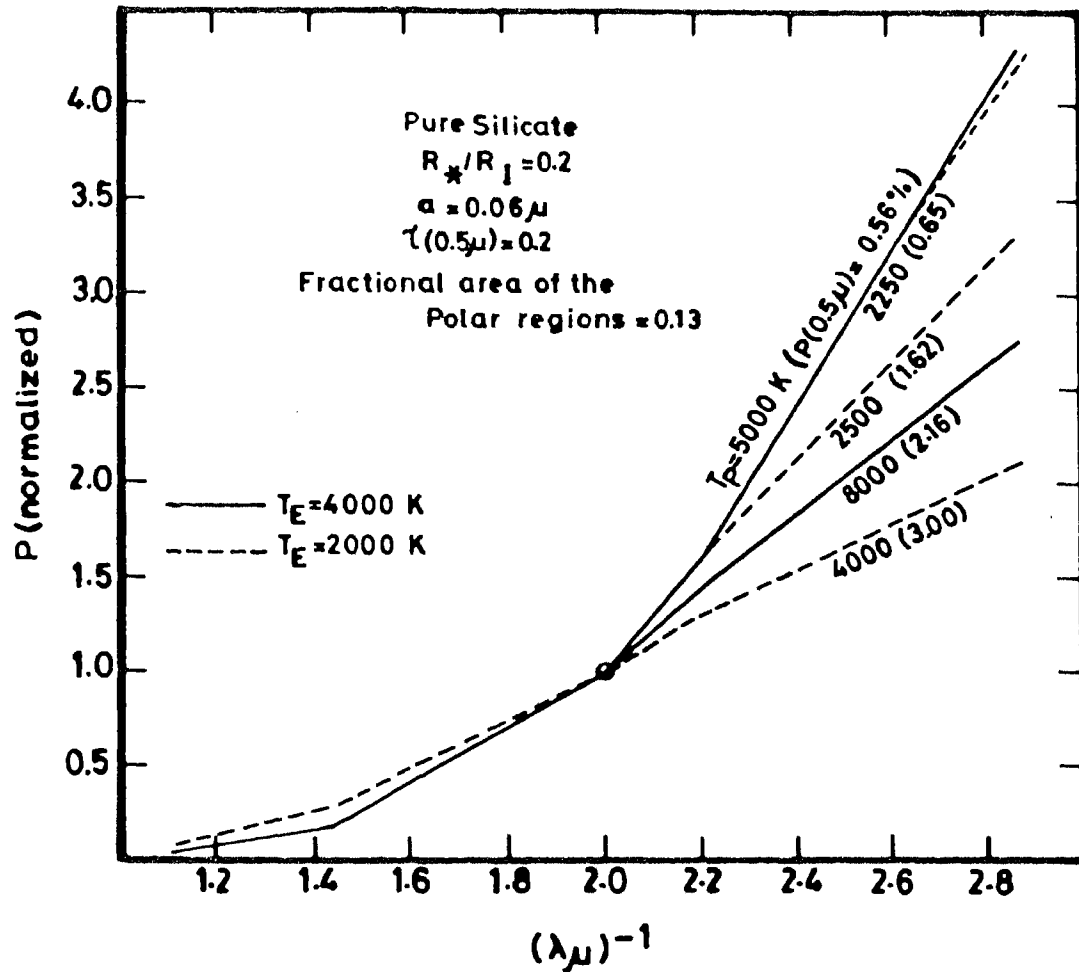
Figure 11
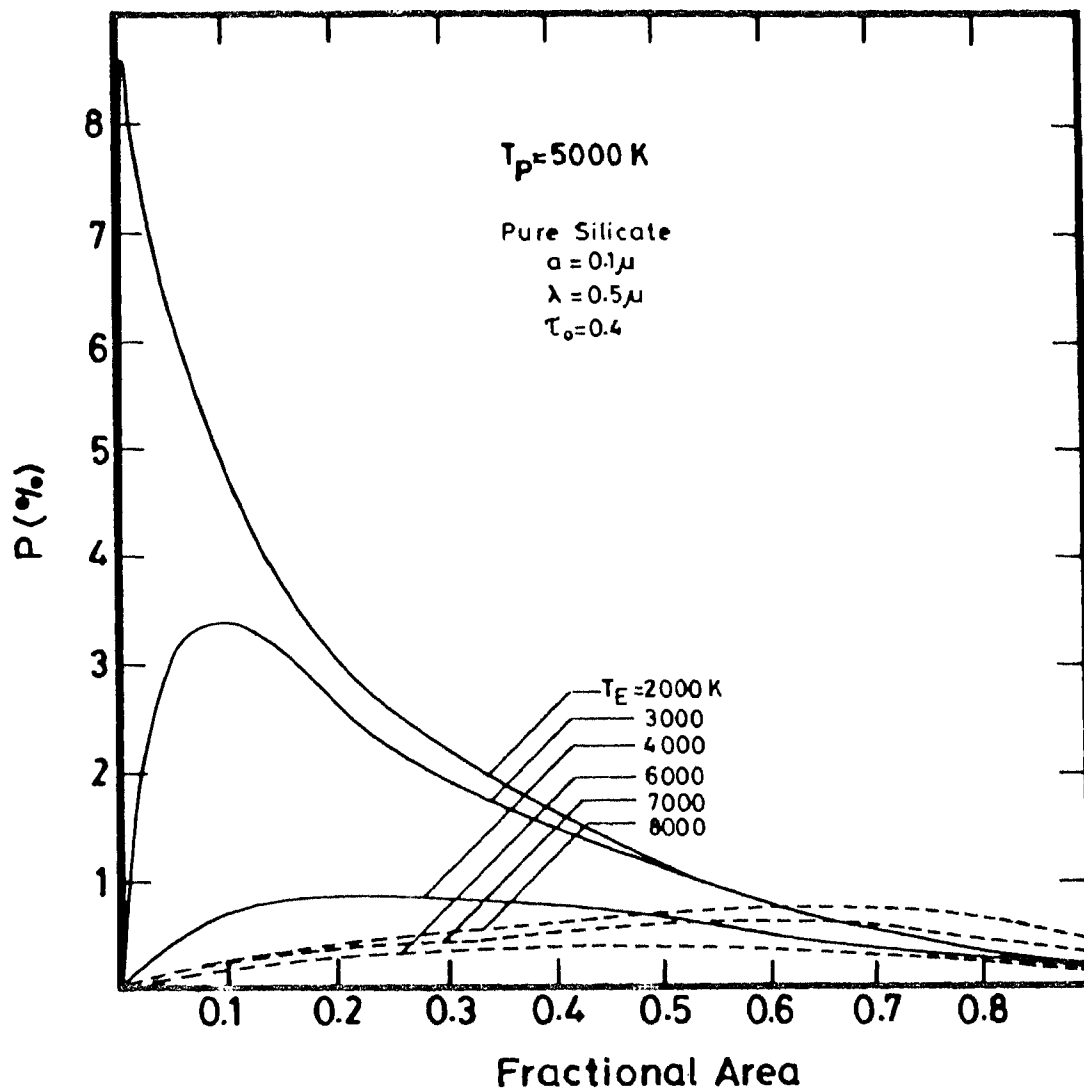
Plots of linear polarization produced against the corresponding fractional area of the polar zones (see the Inset of Figure 11) for different equatorial zone temperatures (T_E). The temperature of the polar zone is taken as T_P = 5000 K.

Figure 12

173

Plots of normalized wavelength dependence of polarization for different combinations of polar and equatorial zone temperatures (see the inset of Figure 11). The solid lines represent the cases for T_E = 4000 K and the dashed lines for the case T_E = 2000 K. The values inside the brackets indicate the percentage of linear polarization at the normalizing wavelength $\lambda = 0.5\,\mu m$ and the numbers outside the brackets, the polar zone temperatures T_P.

Figure 13

0.13. The grains were assumed to be of size $a=0.06\mu m$ and the optical depth at $\lambda=0.5\mu m$ was normalized to $\tau_0=0.2$. Calculations were made for two cases of equatorial zone temperatures, $T_E=2000K$ and $4000K$, and the results are presented in Figure 13 where the polarization, normalized to unity at $\lambda^{-1}=2.0\mu m^{-1}$, is plotted against the inverse of the wavelength. From the figure it is found that the shape of the normalized $P(\lambda)$ curve depends on the relative values of T_P and T_E, the less the difference the steeper the curve towards ultraviolet; for large differences between them all the curves converge to the same. Larger changes occur in the blue-ultraviolet region than in the red-infrared region. The shape of the curve also depends on the relative position of the hotter zone with respect to the centre of the projected stellar disc. The normalized $P(\lambda)$ curves, corresponding to two different positions of the hotter zones, are shown in Figure 14. The curve is less steeper towards ultraviolet when the hotter zone is close to the limb (case a) than when it is about the centre of the projected stellar disc (case b). The fractional areas in the two cases are 0.13 and 0.09, respectively.

In the cases considered above, a net polarization at each wavelength results because of the differences in the emergent fluxes from the polar and equatorial zones at that wavelength. With changes in temperature, the flux in the blue-ultraviolet region changes more rapidly than that in the red-infrared region, thereby producing larger changes in polarization in the blue-ultraviolet region.

Figure 15 is a plot of the polarization at $\lambda=0.5\mu m$ against the corresponding polar zone temperature T_P for the case of an equatorial temperature $T_E=2000K$. The ratios of the blackbody fluxes $[F(T_P)/F(T_E)]$ are also indicated along the x-axis. It is seen from the figure that for a given polar zone area the polarization does not increase monotonously with the ratio of emergent fluxes from the polar and equatorial zones, but rather stays at a nearly constant value after $[F(T_P)/F(T_E)] \sim 50$.

175
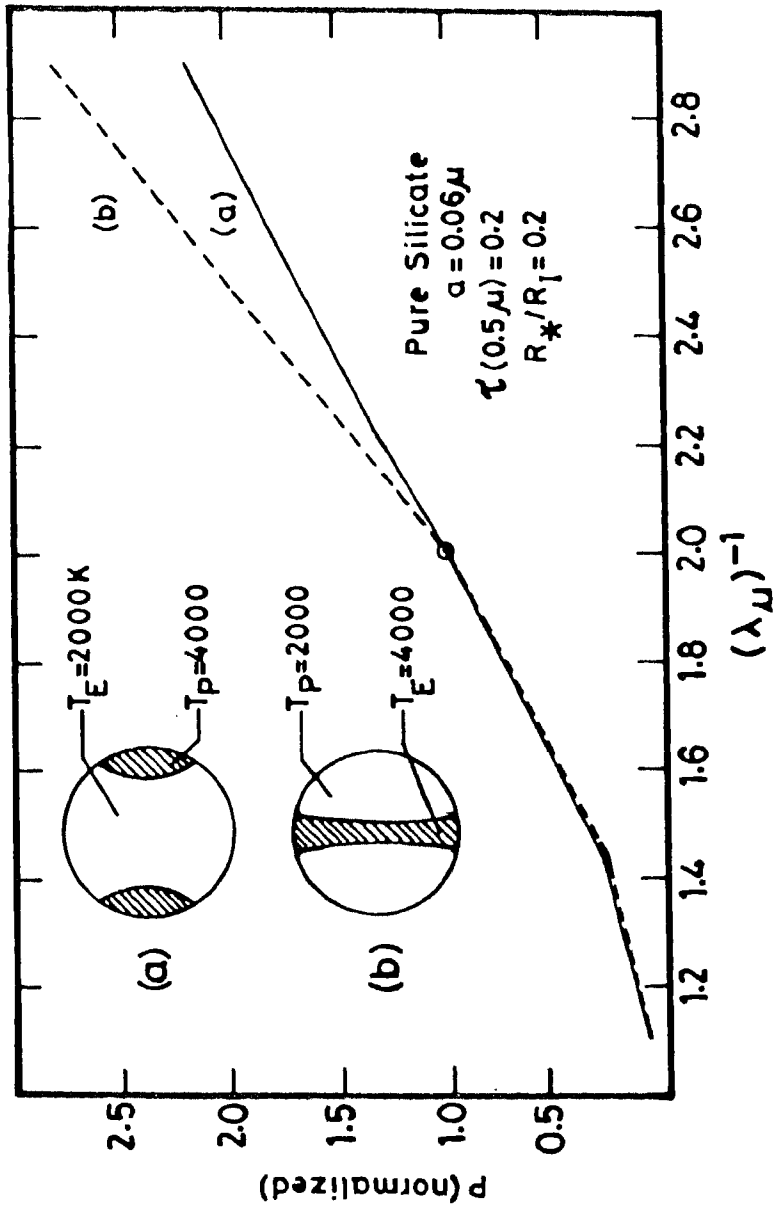
Plots of normalized wavelength dependence for two positions of the hotter zone which are also shown in the figure. The fractional areas in the two cases (a) and (b) are 0.13 and 0.09, respectively.

Figure 14

Pure Silicate

$T_E = 2000$ K

Fractional area of the
Polar regions $= 0.13$
$a = 0.06\,\mu$
$\lambda = 0.5\,\mu$
$\tau_o(0.5\,\mu) = 0.2$
$R_* / R_I = 0.2$

P(%)

$\left[\text{Flux}\,(T_P)/\text{Flux}\,(T_E)\right]$

| 1.00 | 4.95 | 50.61 | 253.18 | 824.69 |

Temperature of Polar zones (T_P)
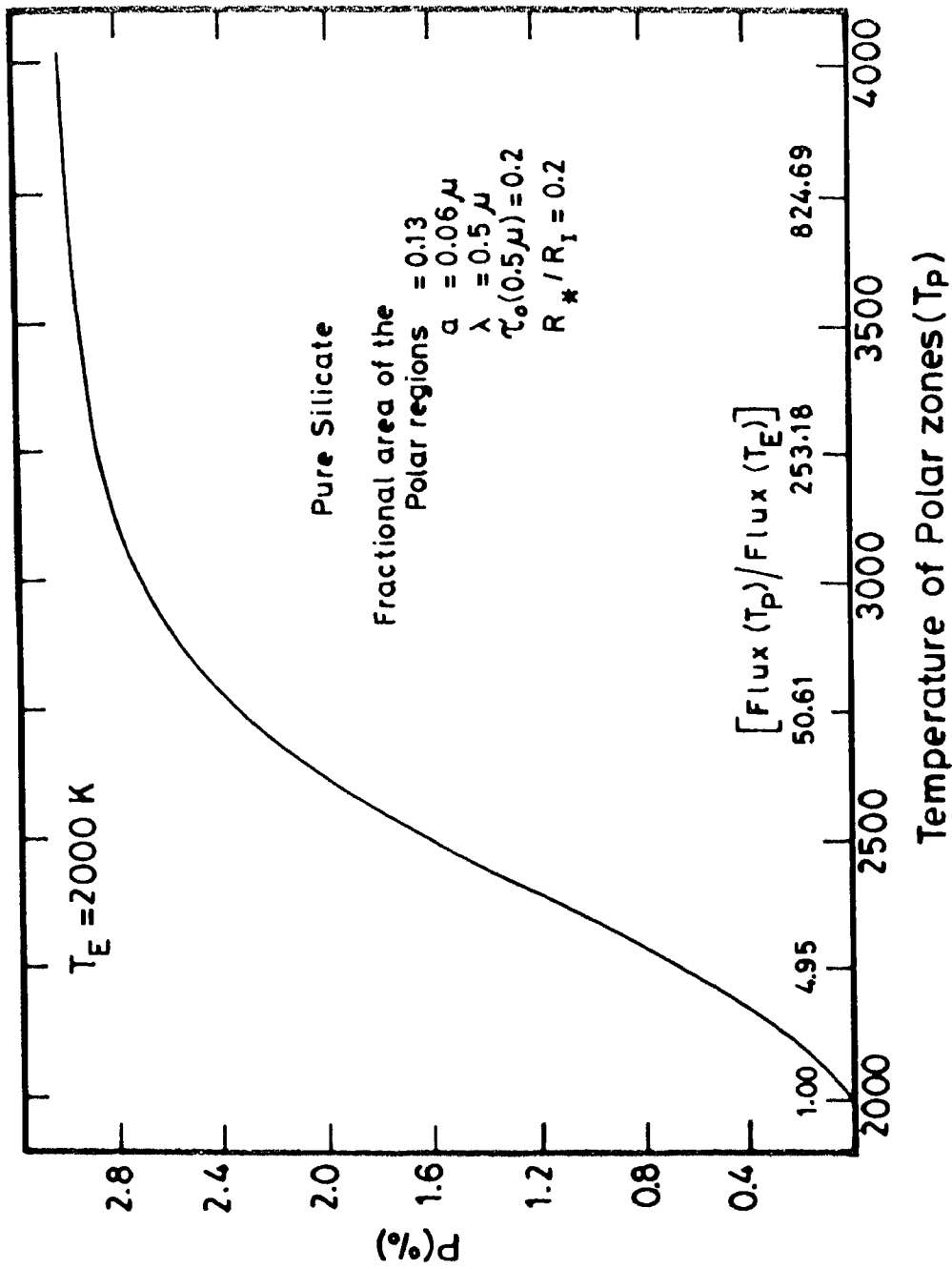
Plot of percentage linear polarization against the corresponding polar zone temperature T_P. The equatorial zone temperature is fixed at $T_E = 2000$ K. The ratios of the blackbody fluxes corresponding to the temperatures T_P and T_E are also indicated along the x-axis inside the figure. Note that the change in polarization is only marginal with increase in T_P above $T_P \approx 3000$ K.

Figure 15

The results presented above have some important implications on the polarization produced, especially by red variables. Polarization changes across spectral features, observed in several cool objects, have been, usually, attributed to photospheric mechanisms (Landstreet & Angel 1977; Coyne & McLean 1979; Boyle et al. 1986). If different temperature zones exist on the stellar surface, possibly arising from non-spherical atmospheric shocks or non-radial pulsations, one would expect changes in polarization across the spectral features, because the net polarization produced at any wavelength as a result of circumstellar grain scattering depends on the distribution of emergent flux across the surface at that wavelength. This may be yet another mechanism which produces polarization changes across spectral features. The large dispersion seen in the ultraviolet region of the normalized $P(\lambda)$ curve of M-type Mira variables has been ascribed to differences in the grain size distributions (Dyck & Sanford 1971). The present calculations show that any change in the brightness distribution of the illuminating star also has larger effects in the ultraviolet region than in the red-infrared region of the normalized $P(\lambda)$ curve. More detailed model calculations are needed along the lines considered here.

VI. CONCLUSIONS

1. Results of the present studies

In the IRAS [12]-[25], [25]-[60] colour-colour diagram, RV Tauri stars populate cooler temperature regions (T < 600 K), distinctly different from that occupied by the oxygen and carbon Miras. Using a model assuming that: (i) the dust envelope is spherically symmetric, (ii) the IR emitting grains are largely of the same kind, and (iii) in the infrared the absorption efficiency $Q_{abs}(\nu) \propto \nu$, it is found that the IRAS fluxes are consistent with the density in the envelope $\rho(r) \propto r^{-2}$, where r is the radial distance. Such a dependence for the density suggests that, most probably, the mass loss rates in RV Tauri stars have not reduced considerably during the recent past, contrary to the suggestion by Jura (1986). In the two-colour diagram, the black-body line and the line corresponding to $\rho(r) \propto r^{-2.2}$ nearly overlap, and the presently available data is insufficient to resolve between the two cases. The latter case is physically more reasonable, however.

The spectroscopic subgroups A and B are well-separated in the IRAS two-colour diagram, with group B objects having systematically cooler dust envelopes. If only the objects detected by the IRAS are considered, it is found that stars belonging to group B show systematically larger excess at L band for a given excess at K. Apparently, there is no correlation between the light curve types (RVa and RVb) and the far infrared behaviour of these objects. It is fairly certain that the physical properties, including the chemical composition, of the embedded stars are directly reflected on those of the dust grains. Most probably, the grain formation processes in RV Tauri stars are continuous and not sporadic as

179

suggested by Goldsmith et al. (1987).

Because of the rather weak wavelength dependence of polarization, the circumstellar grain scattering appears to be the main mechanism responsible for the continuum polarization in the objects considered.

The polarimetric behaviour of the carbon-rich RV Tauri star AR Pup is found to be exceptional in several respects. The observed amplitude of polarization in the U band is ~ 14.6%, the highest so far observed in any late-type star. The polarimetric data when combined with the simultaneous photometry indicates that the observed large time-dependent variations, both in the amount and wavelength dependence of polarization, are cyclic and related to the light variation. The polarization increases largely close to the epochs of light minima, during the ascending branch of the light curve. The wavelength dependence of polarization exhibits a wide range of shapes, and the shape of the $P(\lambda)$ curve apparently depends on the level of polarization itself, such that, as the level of polarization increases, the curve becomes steeper towards ultraviolet.

The most significant result, which would constrain the possible polarization models of AR Pup, is the finding that in the (Q,U) plane the observations in UBVR filter bands, obtained during February-March 1986, lie on separate straight lines. Such a regular behaviour in the polarization and position angle appears to be a result of some very systematic variation in the several parameters that determine the level, direction and wavelength dependence of polarization produced. It is difficult to conceive that the whole extended infrared emitting circumstellar envelope was involved in producing such a regular variation. Most likely, transient localized regions were largely responsible for the polarimetric behaviour. The rapid and regular changes in polarization observed in AR Pup after light minima are, possibly, related to the outward passage of atmospheric shocks directly. The physical conditions existing close to the light minimum may be

180

favouring the formation of more localized condensations which are responsible for the observed polarizations.

In the (Q,U) plane, the RV Tauri stars, in general, show a regular variation during the light cycle, implying a very regular variation in the geometry involved. Hence, it is suggested that the variations in polarization observed in RV Tauri stars during the light cycle are rather caused by changes in asymmetries associated with the pulsation of the star than due to changes in an asymmetric envelope.

The carbon Mira R Lep shows large changes in the normalized wavelength dependence of polarization. It is found that both the amount and position angle of polarization had components which secularly varied since their first measurements in 1966. Circumstantial evidences suggest a possible connection between the largest polarization observed in 1966 and the faintest ever observed light maximum during 1959-60. For a net polarization to appear in integrated light, there should be an overall departure from spherical symmetry. It is proposed that the secularly varied component of polarization seen after 1966 is possibly a result of an episodic asymmetric mass ejection sometime before 1962 and its subsequent dissipation in the circumstellar envelope.

Numerical computations show that the changes in the net polarization produced by an envelope due to changes in the size of a star, as a result of radial pulsation, is not significant. However, in objects that show polarization variation coupled with the pulsation, other effects such as changes in the number and sizes of scattering grains may be occurring as a result of the changes in temperature during the pulsation cycle.

The mean polarimetric behaviour of oxygen-rich stars is found to be consistent with the scattering by grains of dirty silicate than by pure silicate grains. It is also found that the polarimetric behaviour of red carbon stars is inconsistent with the scattering by graphite grains, suggesting the

181

existence of carbon grains in the envelopes around them in some other forms, such as amorphous carbon.

Polarization changes across spectral features, observed in several cool objects, have been attributed to photospheric effects (Landstreet & Angel 1977; Coyne & McLean 1979; Boyle et al. 1986). The present study clearly indicates that circumstellar grain scattering produces not only significant changes in the normalized wavelength dependence of polarization but also polarization changes across spectral features if the illuminating star has a non-uniform surface brightness distribution.

2. Some suggestions for future studies

A polarimetric survey of RV Tauri stars is necessary to see whether the phenomenon seen in AR Pup is more frequent or not. A suitable model to explain such large polarization as observed in AR Pup is also needed. It may be necessary to invoke multiple scattering if grains are spherical, or some mechanism for aligning the grains if they are elongated. The large changes in polarization close to the epochs of light minima indicate the possibility of grain condensation close to those epochs; the formation of polyatomic molecules should precede the dust condensation, and hence a spectroscopic search for such molecules would be highly desirable. Higher resolution infrared spectrophotometry to detect dust features also would be highly desirable.

The rapid increase in polarization and its most likely relation to the passage of atmospheric shocks in RV Tauri stars implies a non-radial propagation for the latter. Multiwavelength observations of a larger sample of RV Tauri stars, belonging to both the oxygen-rich and carbon rich groups, are needed to determine the mean wavelength dependence of polarization, because at low polarization levels (<1.0%) the interstellar component might distort the intrinsic polarization significantly. Grains of large sizes (a $\gg$ 0.1μm)

are required to explain the flat wavelength dependence of polarization observed in carbon-rich RV Tauri stars; but this involves the problem of grain growth to such large sizes. Alternatively, it is possible that the grains are smaller ($a<0.1\mu$m) and the near flat wavelength dependence is a result of illumination by a star with a non-uniform surface brightness which in turn may be a result of non-radial pulsation; quantitative modeling alone can resolve these possibilities.

In the present polarization model calculations, only a simple geometry for the brightness distribution has been considered. Further, it is assumed that the emergent radiation has a blackbody distribution and a cosine law for the limb darkening. Detailed calculations incorporating more realistic atmospheric model parameters are needed to assess the extent of polarization changes across spectral features.

Bujarrabal et al. (1988) have reported the detection of microwave emissions corresponding to the rotational transitions of carbon monoxide, $J=2-1$ (230.54 GHz) and $J=1-0$ (115.27 GHz), from R Sct and AC Her. Any correlation between the CO microwave emissions and the envelope temperatures, if found to exist, would provide valuable information on the production of CO molecules in the circumstellar envelopes. A study of CO emissions, which provides the best estimates of mass loss rates (Zuckerman & Dyck 1986a), from RV Tauri stars, especially those detected by the IRAS, would be highly fruitful. At far IR wavelengths, U Mon has larger fluxes when compared to AC Her, but the CO emissions are very weak (Bujarrabal et al. 1988). Similarly, strong OH maser emissions have been detected from the prototype RV Tau, while no emissions could be detected from AC Her, in spite of it having a much larger flux at 35μm than RV Tau (Fix & Claussen 1984). AC Her is a carbon-rich RV Tauri star, whereas both U Mon and RV Tau are oxygen-rich objects. The other objects in the sample of Bujarrabal et al. (1988) are the oxygen-rich objects AI Sco and RV Tau (R Sct is excluded, since its IR properties

183

deviate considerably from that of the rest of the RV Tauri stars detected by the IRAS). The results obtained by Bujarrabal et al. (1988) and Fix & Claussen (1984) could possibly be due to the difference in the chemical composition of the circumstellar envelopes around oxygen-rich and carbon-rich objects. A systematic study involving a larger number of objects is needed along these lines.

Publications

1. Dramatic changes in the polarization of AR Pup. *Raveendran, A.V., Kameswara Rao, N., Deshpande, M.R., Joshi, U.C. & Kulshrestha, A.K.*, 1985, Inf. Bull Var. Stars, No. 2713.

2. AR Puppis. *Raveendran, A.V., Kameswara Rao, N., Rozario, M.J., Joshi, U.C. & Kulshrestha, A.K.*, 1986, IAU Circ. No. 4188.

3. A d.c. amplifier for photoelectric photometry. *Raveendran, A.V. & Mohin, S.*, 1987, Kodaikanal Obs. Bull. **8**, 13.

4. Polarimetric observations of the RV Tauri star AR Puppis. *Raveendran, A.V. & Kameswara Rao, N.*, 1988, Astron. Astrophys., **192**, 259.

5. Photometric and polarimetric observations of the RV Tauri star AR Puppis. *Raveendran, A.V. & Kameswara Rao, N.*, 1988, Lecture notes in Physics, Vol. 305, p 223, Springer-Verlag, Germany: Proceedings of IAU Colloquium No. 108, Atmospheric diagnostics of stellar evolution : Chemical evolution, Mass Loss and Explosion, ed. K.Nomotto.

6. Polarimetric study of the RV Tauri star AC Herculis. *Raveendran, A.V., Kameswara Rao, N. & Anandaram, M.N.*, 1989, Bull. Astr. Soc. India, **17**, (in press).

7. Long-term polarimetric behaviour of the carbon Mira R Leporis. *Raveendran, A.V. & Kameswara Rao N.*, 1989, Astron. Astrophys., **215**, 63.

8. Dust envelopes around RV Tauri stars. *Raveendran, A.V.*, 1989, Mon. Not. R. astr. Soc., **238**, 945.

9. Polarimetric and photometric study of the RV Tauri star AR
   Puppis. *Raveendran, A.V., Kameswara Rao, N. &*
   Anandaram, M.N., 1989, Mon. Not. R. astr. Soc. (in
   press).

References

Alexander, J.B., Andrews, P.J., Catchpole, R.M., Feast, M.W., Lloyd Evans, T., Menzies, J.W., Wisse, P.N.J. & Wisse, M., 1972. Mon. Not. R. astr. Soc., **158**, 305.

Alksne, Z.K. & Ikaunieks, Ya.Ya., 1981. Carbon Stars, ed. J.H.Baumert, Astronomy and Astrophysics series, Volume 11, Pachart Publishing House, Arizona.

Arp, H., 1962. Astrophys. J., **135**, 971.

Baird, S.R., 1981. Astrophys. J., **245**, 208.

Baird, S.R. & Cardelli, J.A., 1985. Astrophys. J., **290**, 689.

Barnes, T.G. & DuPuy, D.L., 1975. Astrophys. J., **200**, 364.

Bastien, P. & Landstreet, J.D., 1979. Astrophys. J., **229**, L 137.

Beichman, C.A., Neugebauer, G., Habing, H.J., Clegg, P.E. & Chester, T.J., 1985. IRAS Point Source Catalogue, Jet Propulsion Lab.

Beichman, C.A., Neugebauer, G., Habing, H.J., Clegg, P.E. & Chester, T.J., 1985a. IRAS Explanatory Supplement.

Bidelman, W.P., 1956. Vistas in Astronomy, Vol. 2, 1428.

Boyle, R.P., Aspin, C., Coyne, G.V. & McLean, I.S., 1986. Astron. Astrophys., **164**, 310.

Broglia, P., Conconi, P. & Guerrero, G., 1978. Astron. Astropys. Suppl. Ser., **33**, 339.

Bujarrabal, V., Bachiller, R., Alcolea, J. & Martin-Pintado, J, 1988. Astron. Astrophys., **206**, L17.

Cardelli, J.A., 1985. Astron. J., **90**, 1494.

Cottrell, P.L., 1979. Mon. Not. R. astr. Soc., **189**, 13.

Cox, J.P., 1974. Rep. Prog. in Phys., **37**, 563.

Cox, R.E. & Sinnott, R.W., 1977. Sky and Telescope, **54**, 60.

Coyne, G.V., 1974. Astron. J., **79**, 565.

Coyne, G.V., Gehrels, T. & Serkowski, K., 1974. Astron. J., **79**, 581.

Coyne, G.V. & Magalhaes, A.M., 1979. Astron. J., **84**, 1200.

Coyne, G.V. & McLean, I.S., 1979. in IAU Colloquium No. 46, Changing Trends in Variable Star Research, eds. F.M. Bateson, J.Smak, I.H.Urch, p 386.

Crawford, D.L., 1975. Astron. J., **80**, 955.

Czyzak, S.J., Hirth, J.P. & Tabak, R.G., 1982. Vistas in Astronomy, Vol. **25**, 337.

Daniel, J.Y., 1978. Astron. Astrophys., **67**, 345.

Daniel, J.Y., 1980. Astron. Astrophys., **87**, 204.

Daniel, J.Y., 1982. Astron. Astrophys., **111**, 58.

Dawson, D.W., 1979. Astrophys. J. Suppl. Ser., **41**, 97.

DeGioia-Eastwood, K., Hackwell, J.A., Grasdalen, G.L. & Gehrz, R.D., 1981. Astrophys. J., **245**, L75.

Demers, S. & Fernie, J.D., 1966. Astrophys. J., **144**, 440.

Deshpande, M.R., Joshi, U.C., Kulshrestha, A.K., Banshidhar, Vadher, N.M., Mazumdar, H.S., Pradhan, S.N. & Shah, C.R., 1985. Bull. Astron. Soc. India, **13**, 157.

Detre, L., 1966. Inf. Bull. Var. Stars, No. 152.

Doherty, L.R., 1986. Astrophys. J., **307**, 261.

Dyck, H.M., 1968. Astron. J., **73**, 688.

Dyck, H.M. & Sanford, M.T., 1971. Astron. J., **76**, 43.

Dyck, H.M. & Jennings, M.C., 1971. Astron. J., **76**, 431.

Dyck, H.M., Forbes, F.F. & Shawl, S.J., 1971. Astron. J., **76**, 901.

Dyck, H.M., Forrest, W.J., Gillett, F.C., Stein, W.A., Gehrz, R.D., Woolf, N.J. & Shawl, S.J., 1971., Astrophys., J., **165**, 57.

Eggen, O.J., 1986. Astron. J., **91**, 890.

Erleksova, G.E., 1984. Inf. Bull. Var. Stars. No. 2614.

Fernie, J.D., 1963. Astron. J., **68**, 780.

Fix, J.D. & Claussen, M.J., 1984. Astrophys. J., **287**, L35.

Forrest, W.J., Gillett, F.C. & Stein, W.A., 1975. Astrophys. J., **195**, 423.

Frecker, J.E. & Serkowski, K., 1976. Appl. Optics, **15**, 605.

Gaposchkin, S., 1953. Harvard Ann., **113**, 69.

Gauzit, M.J., 1959. Ann. Astrophys., **22**, 781.

Gehrz, R.D. & Woolf, N.J., 1970. Astrophys. J., **161**, L213.

Gehrz, R.D., 1972. Astrophys. J., **178**, 715.

Gehrz, R.D. & Ney, E.P., 1972. Publs. astr. Soc. Pacif., **84**, 768.

Gehrz, R.D. & Hackwell, J.A., 1974. Astrophys. J., **193**, 385.

Gerrard, A. & Burch, J.M., 1975. Introduction to Matrix Methods in Optics, John Wiley & Sons Ltd., London.

Gillett, F.C., Merrill, K.M. & Stein, W.A., 1971. Astrophys. J., **164**, 83.

Gilman, R.C., 1972. Astrophys. J., **178**, 423.

Gingold, R.A., 1974. Astrophys., J., **193**, 177.

Gingold, R.A., 1976. Astrophys., J., **204**, 116.

Goldsmith, M.J., Evans, A., Albinson, J.S. & Bode, M.F., 1987. Mon. Not. R. astr. Soc., **227**, 143.

Hacking, P., Neugebauer, G., Emerson, J., Beichman, G., Chester, T., Gillett, F., Habing, H., Helou, G., Houck, J., Olnon, F., Rowan-Robinson, M., Soifer, B.T., Walker, D., 1985. Publs. astr. Soc. Pacif., **97**, 616.

Hardie, R.H., 1962. in Astronomical Techniques, ed. W.A. Hiltner, The University of Chicago Press, London, p 178.

Harrington, J.P., 1969. Astrophy. Letters, **3**, 165.

Harvey, P.M., Thronson, H.A. & Gatley, I., 1979. Astrophys. J., **231**, 115.

Henden, A.A. & Kaitchuck, R.H., 1982. Astronomical Photometry, Van Nostrand, Reinhold, New York.

Henson, G.D., Kemp, J.C. & Kraus, D.J., 1985. Publs. astr. Soc. Pacif., **97**, 1192.

Hertzsprung, E., 1928. Bull. Astr. Inst. Netherlands, **4**, 153.

Hiltner, W.A., 1962. in Astronomical Techniques, ed. W.A. Hiltner, The University of Chicago Press, London, p 229.

Hoffmeister, C., 1957. Astrophys. J., **125**, 824.

Iben, I.Jr., 1967. Ann. Rev. Astron. Astrophys., **5**, 571.

Iben, I.Jr., 1974. Ann. Rev. Astron. Astrophys., **12**, 215.

Iben, I.Jr., 1977. in Advanced Stages in Stellar Evolution, ed. A.Bouvier, A.Maeder, Geneva: Geneva Obs.

Iben, I.Jr., 1987. in Late Stages of Stellar Evolution, ed. S.Kwok, S.R.Pottasch, Astrophysics and Space Science Library, Volume 132, p 175.

Iben, I.Jr. & Renzini, A., 1983. Ann. Rev. Astron. Astrophys., 21, 271.

Ikaunieks, J., 1975. in Pulsating Stars, ed. B.V.Kukarkin, IPST Astrophysics Library, John Wiley & Sons, New York, p 297.

Iriarte, B., Johnson, H.L., Mitchell, R.I. & Wisniewski, W.K., 1965. Sky and Telescope, 30, 21.

Johnson, H.L., 1963. in Basic Astronomical Data, ed. K.Aa.Strand, The University of Chicago Press, Chicago, p 204.

Jones, T.W. & Merrill, K.M., 1976. Astrophys. J., 209, 509.

Jones, T.W., Ney, E.P. & Stein, W.A., 1981. Astrophys. J., 250, 324.

Jura, M., 1986. Astrophys. J., 309, 732.

Jura, M., 1986a. Astrophys. J., 303, 327.

Kruszewski, A., Gehrels, T. & Serkowski, K., 1968. Astron. J., 73, 677.

Kukarkin, B.V., Kholopov, P.N., Efremov, Yu.N., Kukarkina, N.P., Kurochkin, N.E., Medvedeva, G.I., Perova, N.B., Fedorovich, V.P. & Frolov, M.S., 1969. General Catalogue of Variable Stars, Moscow.

Kukarkin, B.V., 1975. Pulsating Stars, IPST Astrophysics Library, John Wiley & Sons, New York.

Lambert, D.L., 1988. to appear in IAU Colloquim No. 108, The Evolution of Peculiar Red Giants.

Landolt, A.U., 1983. Astron. J., 88, 437.

Landstreet, J.D. & Angel, J.R.P., 1977. Astrophys. J., 211, 825.

Likkel, L., Omont, A., Morris, M. & Forveille, T., 1987. Astron. Astrophys., 173, L11.

Little-Marenin, I.R., 1986. Astrophys. J., 307, L15.

Lloyd Evans, T., Wisse, P.N.J., Wisse, M., 1972. Mon. Not. R. astr. Soc., 159, 67.

Lloyd Evans, T., 1983. Observatory, 103, 276.

Lloyd Evans, T., 1974. Mon. Not. R. astr. Soc., 167, 17p.

Lloyd Evans, T., 1985. Mon. Not. R. astr. Soc., 217, 493.

Low, F.J. et al., 1984. Astrophys. J., 278, L19.

McLaughlin, D.B., 1932. Publs. Univ. Obs. Michigan, **4**, 135.

Magalhaes, A.M., Coyne, G.V., Codina-Landaberry, S.J. & Gneiding, C., 1986. Astron. Astrophys., **154**, 1.

Marcondes-Machado, J.A., 1987. Astron. Astrophys., **188**, 131.

Materne, J., 1976. Astron. Astrophys., **47**, 53.

Mayall, M.W., 1963. J. Roy. Astr. Soc. Canada, **57**, 237.

Mayall, M.W., 1965. J. Roy. Astr. Soc. Canada, **59**, 245.

Mayall, M.W., 1970. The American Association of Variable Star Observers, AAVSO Report 28.

Michalowska-Smak, A. & Smak, J., 1965. Acta. Astronomica, **15**, 333.

Neugebauer, G., Becklin, E. & Hyland, A.R., 1971. Ann. Rev. Astr. Astrophys., **9**, 67.

Nicolet, B., 1978. Astron. Astrophys. Suppl. Ser., **34**, 1.

O'Connell, D.J.K., 1933. Harvard Obs. Bull. No. 893, 14.

O'Connell, D.J.K., 1961. Spec. Vat. Ric. Astr., **6**, 341.

Odenwald, S.F., 1986. Astrophys. J., **307**, 711.

Oke, J.B., 1965. Ann. Rev. Astron. Astrophys., **3**, 23.

Oliver, J.P., 1975. Publs. astr. Soc. Pacif., **87**, 217.

Olnon, F.M. & Raimond, E., 1986. Astron. Astrophys., Suppl. Ser., **65**, 607.

Pancharatnam, S.,1955. Proc. Indian Acad. Sci., **A 41**, 137.

Payne-Gaposchkin, C., 1954. Variable Stars & Galactic Structure, University of London, The Athlone Press.

Payne-Gaposchkin, C. & Gaposchkin, S., 1938. Variable Stars, Harvard Observatory Monographs, No. 5, Published by the Observatory, Cambridge, Massachusetts.

Payne-Gaposchkin, C., Brenton, V.K. & Gaposchkin, S., 1943. Harvard Ann., **113**, 1.

Pickering, E.C., 1912. Harvard Circ., No. 173.

Polyakova, T.A., 1984. Sov. Astron. Lett., **10**, 312.

Preston, G.W., Krzeminski, W., Smak, J. & Williams, J.A., 1963. Astrophys. J., **137**, 401.

Raveendran, A.V., Ashoka, B.N. & Kameswara Rao, N., 1986. in

IAU Colloquium No. 87, Hydrogen deficient stars and related objects, eds. K.Hunger, D.Schonberner, N.Kameswara Rao, p 191.

Rosino, L., 1951. Astrophys. J., 113, 60.

Rosino, L., 1980. Vistas in Astronomy, Vol. 22, 39.

Rowan-Robinson, M. & Harris, S., 1983. Mon. Not. R. atron. Soc., 202, 767.

Rowan-Robinson, M. & Harris, S., 1983a. Mon. Not. R. atron. Soc., 202, 797.

Sandage, A. & Tammann, G.A., 1968. Astrophys. J., 151, 531.

Sanford, R.F., 1928. Astrophys. J., 68, 408.

Schwarzschild, M., 1975. Astrophys. J., 195, 137.

Schwarzschild, M. & Harm, R., 1967. Astrophys. J., 150, 961.

Serkowski, K., 1966. Astrophys. J., 144, 857.

Serkowski, K., 1970. Astrophys. J., 160, 1107.

Serkowski, K., 1971. Kitt Peak Nat. Obs. Contribution No. 554, 107.

Serkowski, K., 1974. in Planets, Stars, and Nebulae Studied with Photopolarimetry, ed. T. Gehrels, The University of Arizona Press, Tucson, Arizona, p 135.

Serkowski. K., Mathewson, D.S., & Ford, V.L., 1975. Astrophys. J., 196, 261.

Shah, G.A., 1977. Kodaikanal Obs. Bull. Ser. A, 2, 42.

Shapley, H., 1914. Astrophys. J., 40, 448.

Shapley, H. & Walton, M.L., 1927. Harvard Circ. 313.

Shapley, H. & Payne, C.H., 1930. Harvard Obs. Bull. No. 872.

Shawl, S.J., 1975. Astron. J., 80, 602.

Shawl, S.J., 1975a. Astron. J., 80, 595.

Shmidt, Th., 1958. Z. Astrophys., 45, 214.

Shmidt, Th., 1958a, Z. Astrophys. 46, 145.

Simmons, J.F.L., 1982. Mon. Not. R. astr. Soc., 200, 91.

Stebbins, J., Whitford, A.E. & Johnson, H.L., 1950. Astrophys. J., 112, 469.

Strohmeier, W., 1972. Variable Stars, Ed. A.J.Meadows, Pergamon Press, Braunschweig.

Treanor, P.J., 1962. in Astronomical Techniques, ed. W.A.Hiltner, The University of Chicago Press, London, p 247.

Tsesevich, V.P., 1975. in Pulsating Stars, ed. B.V.Kukarkin, IPST Astrophysics Library, John Wiley & Sons, New York, p 112.

van der Veen, W.E.C.J. & Habing, H.J., 1988. Astron. Astrophys., **194**, 125.

van de Hulst, H.C., 1957. Light Scattering by Small Particles, John Wiley & Sons, New York.

Wallerstein, G., 1973. Ann. Rev. Astr. Astrophys., **11**, 115.

Wickramasinghe, N.C. & Guillaume, C., 1965. Nature, **207**, 366.

Willems, F.J. & de Jong, T., 1986. Astrophys. J., **309**, L39.

Willems, F.J. & de Jong, T., 1988. Astron. Astrophys., **196**, 173.

Willson, L.A., 1987. in Late Stages of Stellar Evolution, eds. S.Kwok, S.R.Pottasch, Astrophys. Space Science Library Vol. 132, p 253.

Wood, P.R., 1979. in IAU Colloq. No. 46, Changing Trends in Variable Star Research, eds. F.M.Bateson, J.Smak, I.H.Urch, p 163.

Woolf, N.J., 1973. in IAU Colloquium No. 52, Interstellar Dust and Related Topics, eds. J.M.Greenberg, H.C.Van de Hust, p 485.

Young, A.T., 1974. in Methods of Experimental Physics: Astrophysics Volume 12A, ed. N. Carleton, New York, Academic Press, p 52.

Zellner, B., 1971. Astron. J., **76**, 651.

Zuckerman, B., 1980. Ann. Rev. Astron. Astrophys., **18**, 263.

Zuckerman, B. & Dyck, H.M., 1986. Astrophys. J., **311**, 345.

Zuckerman, B. & Dyck, H.M., 1986a. Astrophys. J., **304**, 394.